Electrophysiological Role of Voltage-gated Sodium Channel β2 Subunits in the Heart

by

Yangyang Bao

A dissertation submitted in partial fulfillment
of the requirements for the degree of
Doctor of Philosophy
(Pharmacology)
In the University of Michigan
2015

Doctoral Committee:

Professor Lori L. Isom, Chair
Assistant Professor Justus Mukolu Anumonwo
Associate Professor Anatoli N Lopatin
Assistant Research Scientist Luis Felix Lopez-Santiago
Professor Leslie Satin
Professor Héctor Valdivia

ACKNOWLEDGEMENTS

It is an honor to present the work that I conducted during my PhD training. First, I would like to thank Shanghai JiaoTong University and the University of Michigan, as they provided me a platform, the MD/PhD joint program, for medical and scientific training. I am grateful to all of the students, fellows, faculty, and support staff of the PIBS program and Department of Pharmacology. Second, my thesis committee (Drs. Anumonwo, Lopatin, Lopez-Santiago, Valdivia, Satin and Isom) has provided valuable guidance in my thesis project. Everyone was supportive and helpful in shaping and sharpening my knowledge of cardiac electrophysiology.

Next, all of this work would not have been possible without everything that Dr. Isom has offered. She welcomed me into her laboratory and provided world-class scientific training. She not only equipped me with solid knowledge but also scientific thinking. Dr. Isom taught me how to find the key questions, to figure out a way of testing hypothesis, to collaborate with other world-class experts in the field and train my ability to judge my peer's work. Colleagues in her laboratory are kind and knowledgeable, creating a suitable atmosphere for me to grow. The journey in her laboratory has been memorable and fascinating, exerting impacts on my way of understanding the world into my future life.

Finally, I owe my gratitude to my parents (Guoguang Bao and Xiaoyan Wu) who have stood beside me throughout the entire course of my PhD studies.

TABLE OF CONTENTS

LIST OF FIGURES

LIST OF TABLES

LIST OF ABBREVIATIONS

WT	Wild type
EAD	early afterdepolarization
PVC	premature ventricular complex
AP	action potential
APD	action potential duration
RVOT	right ventricular outflow tract
DF	dominant frequency
AF	atrial fibrillation
BrS	Brugada syndrome
AF/AT	atrial fibrillation/atrial tachyarrhythmia
RV	right ventricle
LV	left ventricle
ECG	electrocardiogram
HR	heart rate
AERP	atrial effective refractory period

CHAPTER I

Introduction: physiology and pathophysiology of voltage-gated sodium channel β subunits in the heart.

Previously published as Bao Y and Isom LL. $Na_V1.5$ and Regulatory β Subunits in Cardiac Sodium Channelopathies. Card Electrophysiol Clin. 2014;6(4):679–694.

Introduction

Voltage-gated sodium channels (VGSCs) are critical for impulse initiation and propagation in excitable cells, including nerve and muscle. The ion-conducting VGSC α subunits are modulated by two β subunits that do not form the pore but play essential roles in electrical signal transduction. VGSC β subunits signal through multiple pathways on multiple time scales *in vivo* and, at least for β1, are essential for life. In addition to regulating sodium current, β subunits associate with potassium channels and play non-conducting roles as cell adhesion molecules (CAMs) that participate in cell-cell coupling and macromolecular complex formation. Mutations in genes encoding VGSC β subunits disrupt both sodium and potassium channel complexes as well as cell-cell communication, leading to heart and brain diseases that can be catastrophic. In this chapter, I will begin with a discussion of β subunit tissue distribution and subcellular localization in the heart, laying the groundwork for a discussion of the anatomical basis

of β subunit-linked cardiac disease. I will provide an overview of β subunit electrophysiological function *in vitro* and *in vivo* in heart and discuss cardiac disease-related β subunit gene mutations, clinical phenotypes, and their implications. Possible mechanisms of β subunit-mediated cardiac arrhythmias will be presented. The pathophysiological implications of simultaneous expression of β subunit gene mutations in heart and brain will be considered.

Topology of VGSC α and β subunits

VGSCs are responsible for the upstroke of the cardiac action potential (AP) and are required for impulse propagation in the heart[1]. Structurally, three different subunits are required to assemble the VGSC complex in brain: one pore-forming α subunit that is both covalently and non-covalently linked to two different β subunits[2]. Because cardiac VGSCs have not been purified, it is assumed, but not proven, that they are also heterotrimers. Five β subunit proteins have been identified in mammals, including β1, β1B, β2, β3 and β4. They are encoded by four genes: *SCN1B-SCN4B*[3–7]. While the pore forming VGSC α subunit is sufficient for ion conduction, at least in heterologous systems, β subunits regulate sodium current (I_{Na}) density, kinetics, voltage-dependence of activation and inactivation as well as surface expression. In addition to I_{Na} modification, β subunits also function as cell adhesion molecules (CAMs)[8], mediating cellular aggregation, neuronal migration, pathfinding, and axonal fasciculation in brain[9]. While our knowledge of β subunit-mediated cell-cell adhesion in heart is not as extensive, we propose that β subunits contribute to cell-cell coupling at the intercalated disk (ID)[10]. With the exception of β1B, all of the VGSC β subunits share similar

topologies, containing a single, heavily glycosylated, immunoglobulin (Ig) fold in the extracellular region, a single transmembrane domain, and an intracellular C-terminus[7]. β1B (originally called β1A[4]), a *SCN1B* splice variant formed through retention of intron 3, contains an Ig loop that is identical to that of β1, but lacks a transmembrane domain and is thus a secreted protein[11]. β1B functions as a soluble CAM ligand in addition to a modulator of I_{Na} [11]. Of the five β subunits, β1B, β1, and β3 are non-covalently linked to VGSC α subunits, while β2 and β4 are covalently linked through disulfide bonds. The residue responsible for the covalent interaction between β2 and α subunit was recently identified as cysteine-26[12]. β4, which shares several similar cysteine sites with β2, is postulated to link to VGSC α subunits through cysteine-28[5].

Localization of VGSC α and β subunits in the heart

Tissue distribution

Importantly, and similar to cardiac potassium channels[13,14], VGSC α and β subunits exhibit gradients of expression throughout the heart. All β subunits, except for β1B, are expressed in mouse sinoatrial (SA) node [15]. The predominant cardiac VGSC α subunit, $Na_V1.5$, is absent from the central region of the SA node but its expression increases in a gradient fashion toward the peripheral SA nodal region[16]. This arrangement is proposed to play a key role in controlling impulse exit from the node[17]. The TTX-sensitive (TTX-S) VGSCs $Na_V1.1$ and $Na_V1.3$ are expressed in the central SA node, with $Na_V1.1$ as the predominant sodium channel in this region. In mouse heart, the SA and atrioventricular (AV) nodal regions have higher expression levels

of *SCN1B* (encoding β1/ β1B) and *SCN3B* (encoding β3) compared to the atrium[18]. *SCN1A* (encoding $Na_V1.1$) and *SCN9A* (encoding $Na_V1.7$) are also highly expressed in AV node[18]. Profiling of ion channel genes in non-diseased human heart revealed that *SCN5A* (encoding $Na_V1.5$) and *SCN9A* transcript levels are higher in left atrium than left ventricle, while *SCN1B* is expressed at a higher level in both left and right atria compared to the two ventricles[19]. *SCN3A* (encoding $Na_V1.3$) is expressed at lower levels in right atrium than right ventricle. Interestingly, the TTX-S VGSC *SCN9A*, which is more often expressed in neurons, is more highly expressed in "neuronal-like" Purkinje fibers compared to right ventricle. Both *SCN5A* and *SCN1B* transcript levels are higher in endocardium than in epicardium. Nevertheless, *SCN2B* (encoding β2) and *SCN3B* appear to be homogeneously distributed throughout the heart[19]. In contrast to findings in human heart, *SCN3B* is highly expressed in the ventricles and Purkinje fibers but not in the atria in sheep heart[20]. β1 expression is higher in the trabeculated myocardium and the bundle branches in postnatal mouse[21]. Taken together, it is clear that a detailed understanding of VGSC subunit localization is critical to understanding the mechanisms of cardiac physiology and pathophysiology.

Subcellular localization

Both TTX-S and TTX-R VGSCs are expressed in cardiac myocytes. TTX-R $Na_V1.5$ co-localizes with tyrosine phosphorylated β1, β2, and β4 at the ID, while non-phosphorylated β1, β2, and β3 co-localize with TTX-S $Na_V1.1$,

$Na_V1.3$ and $Na_V1.6$ at the transverse-tubules (T-tubules) in rodent ventricular myocytes[10,22,23]. A recent study also revealed low-level cell surface expression of $Na_V1.4$ and $Na_V1.6$ in mouse ventricular myocytes[24]. In human atrial myocytes, $Na_V1.2$ is co-localized at IDs with β1 and β3. $Na_V1.4$ and the predominant $Na_V1.5$ channels are co-localized with β2 in a striated pattern. $Na_V1.1$, $Na_V1.3$, and $Na_V1.6$ are located in scattered puncta on the cell surface in a pattern similar to β3 and β4[25]. Because the subcellular distributions of VGSC α and β subunits in human heart appear to be different than in mouse and rat, a more complete study using reliable antibodies will be an important next step in our pursuit of novel therapeutic agents to treat cardiac disease in human patients.

VGSCs exist as macromolecular complexes in heart

Mammalian VGSCs exist as macromolecular complexes *in vivo.* Immunoprecipitation studies showed that $Na_V1.5$, β1, and β2 associate in solubilized rat heart membranes[22]. Phosphorylated β1 (at residue tyrosine-181) co-localizes with connexin-43, N-cadherin, and $Na_V1.5$ at rodent IDs but is not detected at the t-tubules[10]. Co-immunoprecipitation demonstrated that N-cadherin, an adherens junction protein, interacts with phosphorylated β1 in rodent heart membranes as well as in a heterologous system via the β1 extracellular domain. Connexin-43, a gap junction protein that is critical for impulse propagation, associates with the $Na_V1.5$ complex in heart membranes[10]. The cytoskeletal adaptor protein, ankyrin, is a member of the VGSC signaling complex in heart[26]. $Ankyrin_G$ (AnkG), which interacts directly with $Na_V1.5$ at the ID, is required for

$Na_V1.5$ targeting, expression, and biophysical function[27]. Disruption of AnkG-$Na_V1.5$ interactions is associated with Brugada syndrome (BrS)[28]. Plakophilin-2 (a desmosomal protein) interacts with connexin-43, and AnkG at the ID[29]. Thus, desmosomes, gap junctions, and VGSC α and β subunits constitute an interacting network, or "connexome", at the ID, controlling excitability, electrical coupling, and intercellular adhesion in the heart[30]. At T-tubules, another ankyrin isoform, $ankyrin_B$ (AnkB) co-assembles with TTX-S VGSCs by binding to the non-phosphorylated C-terminal region of β1[10]. Mutations in *ANK2*, encoding AnkB, result in ankyrin-B syndrome (formerly LQT4) with a wide spectrum of phenotypes[31,32]. Interestingly, interactions between β1 and ankyrin are abolished in a heterologous system by expression of a β1 construct that mimics phosphorylated β1 (β1Y181E), suggesting that β1 tyrosine phosphorylation is important for ankyrin recruitment and thus VGSC complex formation in heart[33]. These interactions are summarized in Figure 1.

How are cardiac VGSCs modulated *in vitro*?

A conventional method to study ion channels and mutant channels linked to channelopathies is functional expression in heterologous systems. Although far from the native environment, *in vitro* studies are a convenient first approach to gain structure-function information. Co-expression of β subunits with the predominant cardiac VGSC $Na_V1.5$ in heterologous systems has yielded valuable but also confusing information. β1-mediated effects on $Na_V1.5$ are inconsistent between laboratories. Some groups report no effect of β1 on $Na_V1.5$ function[34,35]. Others report that β1 increases $Na_V1.5$ I_{Na}

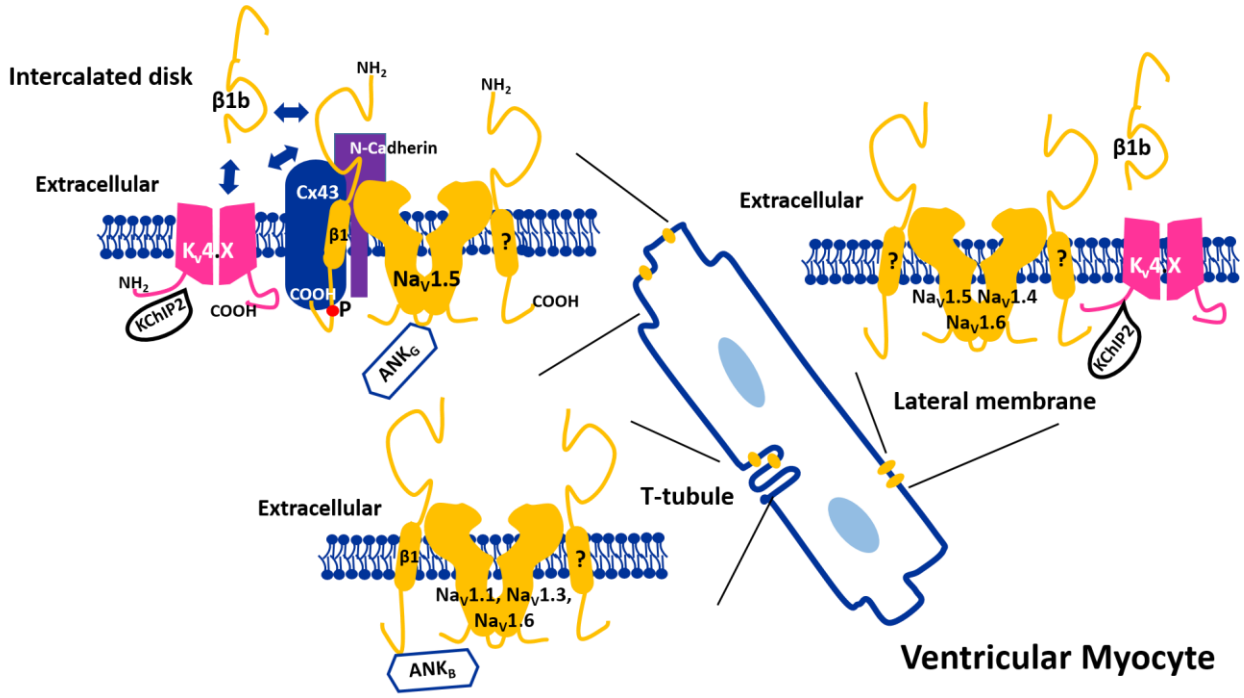

Figure 1 Differential subcellular localization of β1 in rodent ventricular myocytes.

The TTX-R VGSC $Na_V1.5$ co-localizes with $ankyrin_G$, tyrosine-phosphorylated β1, in close association with both N-cadherin and connexin-43, at intercalated disks in ventricular myocytes[10]. Non-phosphorylated β1 and $ankyrin_B$ co-localize with the TTX-S VGSCs $Na_V1.1$, $Na_V1.3$, and $Na_V1.6$ at the t-tubules[10,23]. Although both β1 and β1B have been demonstrated to modulate I_{to}, their spatial relationship to the $K_V4.x$/KChiP2 complex is unknown[36–38]. β2 has been detected at intercalated disks[23] and T-tubules[22] by immunostainings. β3 and β4 are preferentially expressed at T-tubules and intercalated disks respectively[23]. According to cardiac sodium channel "multiple pool" model[39], $Na_V1.5$ is also localized at lateral membrane. Besides, low level of $Na_V1.4$ and $Na_V1.6$ are also detected on cell surface[24]. The β subunit isoform has not been identified and will be an interesting topic for future study.

density without affecting the gating properties[40], that β1 shifts the voltage dependence of inactivation[22,41,42], or that β1 alters the rate of recovery from inactivation[20,42]. This variety of results may stem from differences in cell background, endogenous β subunits, or differential expression of channel interacting proteins[43–46]. Surprisingly, we found that $Na_V1.5$ retains β1B, the secreted splice variant of *Scn1b*, at the cell surface in heterologous cells[11]. β1B co-expression results in increased $Na_V1.5$-mediated I_{Na} density and a hyperpolarized shift in the voltage-dependence of gating[47]. In contrast, β2 co-expression seems to consistently have no effect on $Na_V1.5$ mediated I_{Na} density, kinetics, or gating properties *in vitro*[12,22,48]. In *Xenopus* oocytes, a system in which I_{Na} is considered to be non-physiological, β3 increases $Na_v1.5$ I_{Na} density, shifts the voltage dependence of inactivation in the depolarizing direction, and increases the rate of recovery from inactivation[20]. In Chinese hamster ovary-K1 cells, β3 has no effect on $Na_v1.5$ peak I_{Na} but reduces persistent I_{Na}, shifts the voltage dependence of inactivation in the hyperpolarizing direction, and decelerates the rate of recovery from inactivation[42]. β4, containing a sequence in its intracellular domain (ICD) that causes open channel block, is unique among VGSC β subunits because of its capability of resurgent I_{Na} generation[49] (although *Scn1b* null mice show reduced resurgent I_{Na} current in the cerebellum, also implicating β1/ β1B in this mechanism[50]). β4-mediated resurgent I_{Na} can be recapitulated with $Na_V1.5$ *in vitro*[51]. Compared to $Na_V1.5$ alone, β4 co-expression decreases the slope of both the voltage-dependence of activation and inactivation[52] with a hyperpolarizing shift in inactivation[53], and accelerates recovery from inactivation in HEK293 cells[52].

Taken together, the large variability in functional results obtained for β subunit expression in heterologous systems calls for carefully controlled comparisons of subunit combinations and functions of disease-related mutations with WT controls in the same cell line under the same recording conditions. Better yet, it is critical to move beyond heterologous expression systems and "ask the animal," so to speak, using transgenic models to investigate the functions of these important proteins *in vivo*.

Mutations in genes encoding VGSC β subunit are linked to cardiac disease

Table 1 Human Cardiac Arrhythmia-associated VGSC β-Subunit Mutations

Gene	Affected isoform	Model	Location	Affected AA	Mutation	MAF (%)[a]	Disease	**Functional Alteration (Ref)**
SCN1B	β1, β1b	Human	ECD	R85H	c.254G>A	NA	AF or GEFS+	**Reduced I_{Na}, and altered gating (CHO)[48]**
	β1, β1b		ECD	E87Q	c.259G>C	NA	CCD	**Reduced I_{Na}, altered gating (CHO) [47]**
	β1, β1b		ECD	D153N	c.457G>A	NA	AF	**Reduced I_{Na}, (CHO)[48]**
	β1, β1b		ECD	V138I	c.412G>A	0.0231	SUNDS	**NA**[54]
	β1		TMD	T189M	c.583G>A	NA	SUNDS	**NA**[54]
	β1b			W179X	c.537G>A c.536G>A	NA	CCD, BrS & CCD	**Reduced I_{Na} and altered gating (CHO) [47]**
	β1b			R214Q	c.641G>A	0.3306	BrS, SIDS, AF	**Reduced I_{Na},, Slower recovery**

								from inactivation ; Increased I_{to} decelerated I_{to} decay (tsA 201)[36,55]
	β1b			H162P	c.641G>A	NA	BrS	**Reduced I_{Na} Altered gating; slower recovery from inactivation (CHO-K1)**[56]
	β1, β1b	Mouse		Null			LQT	**Increased $I_{Na\ peak}$ & $I_{Na\ persistent}$, increased APD**[57]
SCN2B	β2	Human	SP	R28W	c.82C>T	0.0077	AF	**Reduced I_{Na}, and altered gating (CHO)**[48]
			SP	R28Q	c.83G>A	NA	AF	**Reduced I_{Na} and altered gating (CHO)**[48]
			ICD	D211G	c.632A>G	NA	BrS	**Reduced I_{Na} (CHO), decreased surface expression**[58]
SCN3B			SP	R6K	c.17G>A	NA	AF	**Altered gating of I_{Na} (CHO-Pro5)**[59]
	β3	Human	SP	L10P	c.29T>C	0.0077	BrS, AF	**Reduced I_{Na}, altered gating, and trafficking defect**

								(tsA201, CHO-Pro5)[59,60]
			ECD	V36M	c.106G>A	NA	SIDS	**Reduced $I_{Na,peak}$, increased $I_{Na,persistent}$ (HEK293)**[53]
			ECD	V54G	c.161A>C	NA	SIDS, IVF	**Reduced I_{Na}, altered gating , and trafficking defect (CHO, HEK293)**[53, 61]
			ECG	A130V	c.389C>T	NA	AF	**Reduced I_{Na} (HEK293)**[62]
			TMD	M161T	c.482T>C	NA	AF	**Reduced I_{Na} (CHO-Pro5)**[59]
			ECM	V110I	c.328G>A	0.0385	BrS	**Reduced I_{Na}, trafficking defect (tsA201)**[71]
			ICD	A195T	c.583G>A	0.0077	SUNDS	**NA**[54]
		Mouse		Null			BrS & Sinus dysfunction	**Reduced I_{Na} and altered gating**[63,64]
SCN4B	β4	Human	TMD	L179F	c.535C>T	NA	LQT & AVB	**Altered gating of I_{Na}, increased INa, persistent (HEK293)**[48]
			ICD	S206L	c.617G>A	0.0154	SIDS	**Increased $I_{Na\ persistent}$ (HEK293 and myocytes), increased APD**

							(myocytes)[53]
		TMD	V162G	c.485T>G	NA	AF	**NA[65]**
		TMD	**I166L**	**c.496A>C**	**NA**	**AF**	**NA[65]**

ECD: extracellular domain; TMD: transmembrane domain; ICD: intracellular domain; SP: signal peptide; AF: atrial fibrillation; GEFS+: Genetic Epilepsy with Febrile Seizure Plus; BrS; Brugada Syndrome; SIDS: Sudden Infant Death Syndrome; LQT: Long QT Syndrome; CCD: Cardiac Conduction Disease; AVB: Atrial-Ventricular Block; SUNDS: Sudden Unexpected Nocturnal Death Syndrome; MAF: Minor Allele Frequency (listed frequency is the frequency in all populations including European American and African American) based on NHLBI GO Exome Sequencing Project (http://evs.gs.washington.edu/EVS/).

Human mutations in *SCN5A* underlie a number of cardiac disorders ranging from arrhythmias to cardiomyopathies. Because β subunits modulate $Na_V1.5$ *in vitro* (at least in some hands), mutations in the genes encoding these subunits were predicted to be associated with a similar spectrum of cardiac diseases. Numerous candidate gene association studies were performed in cohorts of patients with cardiac arrhythmias who were negative for *SCN5A* mutations. Since 2007, a number of mutations in *SCN1B-SCN4B* have been associated with arrhythmias of various etiologies. Table 1 summarizes these results. These can be generally characterized either as resulting in $Na_V1.5$ gain- or loss-of-function. β subunit gene mutations resulting in $Na_V1.5$ gain-of-function are linked to long QT syndrome (LQTS)[52] and sudden infant death syndrome (SIDS)[53]. β subunit gene mutations resulting in $Na_V1.5$ loss-of-function are linked to BrS[47], progressive cardiac conduction disease (CCD)[47], atrial fibrillation (AF)[48], and idiopathic ventricular fibrillation (IVF)[61]. In addition, homozygous *SCN1B* loss of function mutations are linked to Dravet Syndrome (DS), a severe pediatric epileptic encephalopathy with a high risk of Sudden Unexpected Death in Epilepsy or SUDEP[66,67]. We and others have proposed that the expression of *SCN1B* mutations in brain and heart may result in epilepsy and cardiac arrhythmias, setting up a “perfect storm,” so to speak, with a sometimes fatal result[57,68].

SCN1B

Ventricular arrhythmias and cardiac conduction system defects

The first cardiac disease mutations identified in *SCN1B* were associated with BrS (BRGDA5 OMIM 612838) and cardiac conduction defects (OMIM 612838)[47]. In this study, 282 BrS and 44 cardiac conduction disease patients were screened. A missense mutation in *SCN1B*, p.Glu87Gln, predicted to affect both β1 and β1B, was reported in a BrS patient who also manifested conduction abnormalities. These authors also reported a nonsense mutation, predicted to result in truncation of β1B at residue 179, in two bundle branch block patients. Channel function tests performed in a heterologous system co-expressing $Na_V1.5$ with WT vs. mutant β1 or β1B showed that mutations reduce I_{Na} density. In addition, p.Glu87Gln decreases channel availability by shifting the voltage dependence of inactivation in the hyperpolarizing direction. In 2011, a novel variant of β1B, p.R214Q, was described in both BrS and SIDS[36]. This mutation decreases I_{Na} density by 56.5% and decelerates the rate of recovery from inactivation, resulting in loss of $Na_V1.5$ function in a heterologous system. Interestingly, this mutation also increases transient outward potassium current (I_{to}) by 70.6% in tsA201 cells, resulting in a gain of $K_V4.3$ (*KCND3*) channel function. This was the first time that a functional association between β1B and $K_V4.3$ was demonstrated. These findings extend the mechanistic roles of β subunits in arrhythmogenesis and reinforce the mechanism proposed for BrS. It is clear that I_{Na} reduction plays a pivotal role in causing BrS [69]. The repolarization and depolarization hypotheses are two proposed mechanisms, each involving reduced I_{Na}, underlying BrS that are supported by experimental and clinical data[70]. In brief, in the repolarizing hypothesis, AP durations are shorter in the

epicardium, attributed to the more prominent expression of repolarizing I_{to}. Reduction in "opposing" or depolarizing I_{Na} would further shorten epicardial AP durations, resulting in higher heterogeneity of transmural voltage gradients between the right ventricular epicardium and endocardium. Thus, reentrant excitation waves (Phase 2 reentry) between depolarized endocardium and prematurely repolarized epicardium may be facilitated. In the depolarization hypothesis, right ventricular outflow tract activation delay due to preferential conduction slowing would be aggravated by I_{Na} reduction, which could trigger the occurrence of epicardial reentry. In addition to I_{Na} reduction, β1B p.R214Q may cause further augmentation of the transmural voltage gradient due to increased I_{to}. Since both β1 and β1B transcript expression levels are higher in the right *vs* left ventricle[47], *SCN1B* tissue distribution may confer preferential conduction slowing in the right ventricle when defects occur. Thus, the pathogenesis proposed to be associated with β1B p.R214Q fits both hypotheses underlying BrS. This same mutation was later identified in one BrS patient and two early-onset lone AF patients from a different cohort collected in Denmark[55]. Both AF patients presented with incomplete right bundle branch block and a downslope ST segment, suggesting a phenotypic overlap between this *SCN1B* mutation and *SCN5A* loss-of-function mutation related arrhythmias. To discriminate true monogenetic disease-causing variants from low-frequency genetic variants, the β subunit genes *SCN1B* through *SCN4B* were screened for variations in a population of *SCN5A* mutation negative Danish and Iranian BrS patients. This group also re-investigated prior associations using newly released exome data. They identified a new *SCN1B* mutation in β1B, p.H162, which was not present in controls or public databases. However, they also identified p.R214Q in the general

population with 0.4% minor allele frequency (MAF), thus raising doubts about p.R214Q as a causative mutation[71]. Subsequent to these studies, *SCN1B* p.V138I and p.T189M were found to be linked to sudden unexplained nocturnal death syndrome (SUNDS)[54]. Interestingly, SUNDS and BrS are considered by some investigators to be phenotypically similar[72].

Atrial arrhythmias.

Defects in *SCN5A* leading to loss of I_{Na} are involved in the pathogenesis of familial AF[73,74]. Not surprisingly, the same is true for *SCN1B*. In addition to *SCN1B* p.R214Q described above, *SCN1B* p.R85H and p.D153N are associated with familial AF (ATFB 13 OMIM 615377). *SCN1B* p.R85H, located in the Ig loop region, affects both β1 and β1B. In contrast, p.D153N is located in exon 4 of *SCN1B* and thus can only affect β1. Both mutations result in I_{Na} reduction in heterologous expression systems. In addition, p.R85H, which has also been described in a patient with epilepsy[75], shifts both the voltage dependence of activation and inactivation positively. Decreased I_{Na} density may shorten the refractory period and reduce conduction velocity, creating a substrate for re-entry initiation and perpetuation and thereby contributing to AF susceptibility[76].

Animal models of SCN1B mutations.

All of the human patients thus far described with *SCN1B*-linked cardiac disease are heterozygotes. In contrast, epilepsy patients have been identified with both heterozygous and homozygous mutations[66,67], suggesting that homozygous *SCN1B* patients with cardiac disease may also be identified. The majority of these mutations are

located in the extracellular Ig domain, emphasizing the importance of this domain in current modulation and supporting the hypothesis that *SCN1B*-mediated cell-cell adhesion is clinically relevant[77]. To study the physiological roles of *SCN1B* in the heart, we generated *Scn1b* null mice and studied their cardiac phenotype [57,68]. *Scn1b* null mice are models of DS and exhibit severe seizures and SUDEP[68,77]. Interestingly, and consistent with patients with *SCN1B* mutations that affect the heart, we observed both bradycardia and a prolonged QT interval, suggesting VGSC gain-of-function. Indeed, we found a 1.6-fold increase in both peak and persistent I_{Na} density as well as increased AP duration in ventricular cardiac myocytes. These electrophysiological changes could be explained by increases in transcript and protein levels of *Scn5a* and $Na_V1.5$, respectively. Although *Scn1b*$^{+/-}$ mice are closer to the situation in human patients with heterozygous loss-of-function *SCN1B* mutations, the cardiac phenotype of these mice is unremarkable. The reason why the *Scn1b*$^{+/-}$ model fails to recapitulate clinical findings in humans is unknown, although genetic background differences may play a role. Moreover, the atrial phenotype of *Scn1b* null mice has not yet been described. To further separate the role of β1 from β1B in the heart, reintroduction of one splice variant at a time into the *Scn1b* null mice remains under investigation.

SCN2B.

Only three missense mutations have been identified in *SCN2B* to date, two of which result in amino acid substitution at residue 28 in the β2 signal peptide domain, p.R28W and R28Q, as reported in 2009. Both result in loss-of-function in a heterologous system and are linked to paroxysmal AF in human patients. Both AF patients, who were

heterozygous for these mutations, demonstrated saddleback-type ST segment elevation in the right precordial leads and one patient had PR interval prolongation (220ms)[48]. Thus, a BrS like phenotype and conduction abnormalities may be concomitant with an atrial phenotype in a single AF patient. β2 p.D211G, located in the ICD, was discovered in 2013 associated with BrS. This mutation results in reduced $Na_V1.5$ cell surface expression, without affecting single channel conductance, in heterologous cells[58]. Interestingly β2, similar to amyloid precursor protein, can be sequentially cleaved by β and γ secretases[78]. The cleaved ICD of β2 translocates to the nucleus to modulate *Scn1a* transcription in neurons[79]. Although we do not know whether the β2 ICD also exerts transcriptional modulation on *SCN5A* in cardiomyocytes, this might be an alternative explanation for reduced surface expression.

SCN3B

Ventricular arrhythmia.

The first mutation in *SCN3B*, p.L10P, was linked to BrS (BRGDA7 OMIM 613120)[60]. Heterologous expression showed an 82.6% decrease in peak I_{Na} density, an accelerated rate of inactivation, a slowed recovery from inactivation, and a negative 9.6mV shift in the voltage dependence of inactivation. Immunofluorescence revealed that $Na_V1.5$ remained trapped in intracellular organelles when co-expressed with WT *SCN1B* and mutant *SCN3B* p.L10P. Similarly, β3 p.V110I, another trafficking mutation, was found in three Japanese BrS patients from a cohort of 181 individuals[80]. Due to the relative high prevalence of β3 p.V110I in *SCN5A* mutation-negative Japanese BrS patients (10.5% familial cases and 0.6% sporadic cases), a decision was made to begin

testing for *SCN3B* mutations in the Japanese population[81]. Another β3 trafficking mutation, p.V54G, was identified in IVF[61] and SIDS[53]. This mutation did not disrupt the association between α and mutant β subunits, but shifted the voltage dependence of channel gating towards more positive potentials. In the case of IVF, the patient was a 20-year-old male whose positive baseline ECG finding was limited only to epsilon waves, which is often a characteristic manifestation of arrhythmogenic right ventricular dysplasia (ARVD)[82]. However, the T waves were not inverted in the right precordial leads, and there was no other evidence to suggest ARVD. While neither *SCN5A* nor β subunit genes have been implicated in ARVD, a disease more likely caused by defects in desmosomal genes [83,84], VGSCs have been implicated in the connexome and their dysfunction may harm the integrity of this multimolecular complex. Therefore, VGSC subunit mutations may share some clinical features of ARVD[30]. Thus, if a patient presents with ARVD-like symptoms but without mutations in the usual ARVD-linked desmosomal genes, VGSC genes might be good candidates for screening. Finally, β3 p.A195T was detected in a 31-year-old SUNDS patient, although functional studies were not reported.

Atrial arrhythmias

β3 p.A130V was reported in 2010 in a candidate gene association study in a cohort of 477 Chinese AF patients. This mutation results in decreased I_{Na} density and acts as a dominant negative in the presence of WT β3. Interestingly, however, surface biotinylation experiments revealed no changes in cell surface expression level of $Na_V1.5$[62]. Single channel recording of unitary conductance would have been helpful to

further elucidate the I_{Na} reduction mechanism. Later, to increase the probability of screen hits, a cohort was tested with more restricted inclusion criteria in which only early-onset (younger than age of 40) lone AF patients were included[59]. Three mutations, β3 p.R6K, p.L10P, and p.M161T, were identified. β3 p.L10P co-expression with $Na_V1.5$ and WT β1 results in a 45% decrease in peak I_{Na} and a 3.8mV negative shift of voltage dependence of inactivation compared to $Na_V1.5$ co-expressed with WT β1 and β3. p.M161T causes a 57% decrease in peak I_{Na} without observable changes in the voltage dependence of gating. In contrast, p.R6K only shifts the voltage dependence of inactivation by 5mV in the hyperpolarizing direction. Both p.R6K and p.L10P are located in the signal peptide region of β3 while p.M161T is at the border of the transmembrane domain. p.L10P was previously identified in BrS [60]and was shown to interrupt protein trafficking. Overall, additional *in vivo* work will be required to understand the mechanisms of these mutations.

Animal models of SCN3B.

Monomorphic VT can be induced in *Scn3b* null mice, using programmed electrical stimulation, that degenerated to polymorphic VT, suggesting that the ventricles in these animals are prone to arrhythmia[63]. This idea is supported by additional findings, including conduction abnormalities, shorter ventricular effective refractory periods, and a reduction in I_{Na} despite an increase in the expression levels of *Scn5a* mRNA in the right ventricle. The similarity of these electrophysiological features to clinical BrS suggest that *Scn3b* null mice may serve as a BrS model[63]. Shortly after their initial publication, the same group also reported bradycardia, increased P wave duration, prolonged PR

interval, and complete AV block in *Scn3b* null mice, demonstrating electrical abnormalities in the cardiac conduction system and atria. In addition, they found increased SA node recovery times and inducibility of atrial tachycardia and AF by burst pacing, extending the potential use of these animals as models for sick sinus syndrome (SSS) or AF.[64] Interestingly, in contrast to *Scn1b* null mice, no neurological phenotypes were reported, suggesting that the most important functional roles of *Scn3b* may be in the heart. A recent study resolved the crystal structure of the β3 Ig domain, revealing that is assembles as a trimer in the crystal asymmetric unit. Using fluorescence photoactivated localization microscopy, these authors detected full length β3 trimers on the plasma membrane of transfected HEK293 cells[85]. Interestingly, β3 subunits are shown to bind to more than one site on $Na_V1.5$ and induce the formation of α subunit oligomers including trimers. Thus, these results suggest that β3 may participate in cell adhesion *via cis*-homophilic interactions, despite a controversy in the literature regarding the ability of β3 to mediate *trans*-homophilic cell adhesion[86,87]. Furthermore, mutations that perturb the formation of channel trimers are proposed to contribute to arrhythmia [85].

SCN4B.

So far, of the four VGSC β subunit genes, only *SCN4B* is linked to LQTS (LQT10, OMIM 611819)[52]. In addition, *SCN4B* is the only β subunit gene with a mutation that shows complete penetrance in an AF affected family[65]. Similar to *SCN3B*, *SCN4B* is linked to SIDS[53]. β4 p.L179F, identified in a LQTS patient, does not alter I_{Na} density or channel kinetics. Instead, it increases window current through a positive shift in the

voltage dependence of inactivation, widening the voltage range in which I_{Na} may reactivate[88]. More importantly, β4 p.L179F causes a dramatic 8-fold increase in persistent I_{Na} at -60mV. Increased persistent I_{Na} prolongs the AP duration. The resulting delay in repolarization triggers early afterdepolarizations (EADs), which are proposed to induce torsades de pointes[89]. Notably, this LQTS patient also exhibited asymptomatic bradycardia and 2:1 AV block. Intermittent functional 2:1 AV block in the setting of LQTS is usually an isolated disorder[90] with poor prognosis[91]. Based on these data, direct and independent pathological roles of β4 in 2:1 AV block in patients with LQTS were suspected[52]. Although *SCN4B* is not yet associated with conduction disease in humans, *Scn4b* is a genetic modifier of disease severity of cardiac conduction defects in mice[92]. Accordingly, *SCN4B* variants may be considered in risk stratification in LQTS patients. Similar to β4 p.L179F, another gain-of-function mutation, β4 p.S206L identified in SIDS, does not affect peak I_{Na}, but shifts inactivation positively by 7mV, and increases both window current and persistent I_{Na}. To more closely mimic the native environment, functional assays were carried out in rat cardiomyocytes infected with adenovirus[53]. Due to the close proximity of p.S206 to the β4 open-channel blocking sequence, it was postulated that the mutation may enhance the degree of resurgent current. Resurgent I_{Na} -specific protocols in whole-cell patch clamp recordings will be necessary to test this hypothesis. In 2013, two transmembrane domain mutations in β4, p.V162G and p.I166L, were detected in two AF affected Chinese families[65]. Linkage analysis revealed complete penetrance in both pedigrees, although I_{Na} modulation was not tested. Interestingly, in one p.V162G family member, LQTS was also diagnosed, implying gain-of-function. No mutations related to arrhythmia have yet been found in the

extracellular domain of β4, suggesting that, rather than the extracellular Ig loop domain functions being clinically relevant as in β1, malfunction in β4 may be more associated with the transmembrane and intracellular domains. The recent crystallization of the β4 extracellular domain, however, may shed new light on the pathophysiological relevance of this region[93].

Summary

The penetrance of VGSC β subunit gene mutations in human patients is variable. Not all carriers develop arrhythmia and individuals with the same mutation may develop different clinical phenotypes that include epilepsy in addition to cardiac disease[75]. Low penetrance and variable expressivity may stem from epigenetic factors, age, gender, or genetic modifiers. Sporadic occurrence without familial co-segregation and the rarity of these genetic diseases add complexity to understanding the role of mutant VGSC β subunits in arrhythmogenesis. Conclusions of causality have become more difficult to draw in contrast to the rapid growth of genetic information from cohorts of cardiac patients. A practical process of determining potential disease-causing mutations, proposed by Møller *et al*, is recommended here[94]. Regardless of the genetic information, however, there is no substitution for expression studies, especially the generation of transgenic animal models. That said, the cost in time and resources required to perform these experiments necessitate the careful selection of variants to be studied.

β subunits as accomplices of aberrant $Na_V1.5$.

β subunits are not innocent bystanders in *SCN5A*-linked cardiac disease. Instead, they can modify disease severity and, in some cases, their expression is required for pathogenesis. For example, the *SCN5A* LQT mutation, p.D1790G, results in abolishment of α-β1 association and subsequent loss of channel modulation by β1[95]. Functional defects of the BrS-related *SCN5A* mutation p.T1620M are aggravated by co-expression of β1[96]. In another example, reduced expression of β4 in hearts of transgenic mice carrying the BrS- and CCD-related *Scn5a*-1798insD mutation correlates with more severe conduction abnormalities[92]. In a study investigating the mechanism of a BrS-associated trafficking defective mutation, *SCN5A* p.R1432G, a dominant negative effect of the mutant subunit on WT channels could be achieved only in the presence of β1[97], suggesting that β1 is required for mutant-WT $Na_V1.5$ association. In sum, β subunits are actively involved in modulating the severity of *SCN5A*-linked cardiac diseases.

Additional arrhythmogenic roles of β subunit gene mutations.

Thus far we have characterized cardiac β subunit gene mutations relative to their effects on $Na_V1.5$ function. However, these mutations may not contribute to cardiac pathogenesis solely through modulation of $Na_V1.5$. β subunits also associate with and modulate TTX-S VGSCs and K^+ channels in heart[10,37]. As CAMs, β subunits, especially β1, function in cell-cell coupling and serve as adaptor proteins that link cytoskeletal, signaling, and other adhesion molecules to macromolecular ion channel complexes[10].

Thus, β subunit gene mutations can disrupt more than $Na_V1.5$ function to cause cardiac disease.

VGSC α subunits other than $Na_v1.5$ are modulated by β subunits in heart.

Besides $Na_V1.5$, other VGSCs are expressed in the heart and are modulated by β subunits, contributing to the maintenance of normal cardiac function. TTX-S VGSCs in SA node are important contributors to cardiac automaticity. In isolated SA node cells, TTX-S I_{Na} initiates during the late phase of the pacemaker potential. Blockade of TTX-S I_{Na} results in slowed pacemaking in both intact SA node preparations and isolated SA node cells[16]. Similarly, upon perfusion of nanomolar concentrations of TTX into the intact isolated mouse heart, a significant reduction in spontaneous heart rate and markedly greater heart rate variability are observed, similar to SSS in humans[15]. In a volume-overloaded heart failure (HF) rat model, down-regulation of TTX-S $Na_V1.1$ and $Na_V1.6$ expression contributes to HF-induced SA node dysfunction[98]. TTX-S VGSCs in T-tubules of ventricular myocytes play an important role in coupling depolarization of the cell membrane to contraction. Low TTX concentrations reduce left ventricular function[99]. This important role was also confirmed in the rabbit[100]. To understand the role of one of the TTX-S VGSCs in heart, the cardiac phenotype of global *Scn8a* null mice was characterized. Both the PR and QRS intervals were prolonged in this model and Ca^{2+} transients were longer in isolated null myocytes compared to controls. Optical mapping showed that hyperkalemia exaggerates the slowing of conduction velocity in *Scn8a* null mouse hearts, implying that $Na_V1.6$ may serve as a protective functional reserve in maintaining the integrity of AP propagation at relatively depolarized potentials. Thus,

$Na_V1.6$, and possibly other TTX-S VGSCs, may contribute to the maintenance of propagation in the myocardium and to excitation-contraction coupling[101].

It has been well established using heterologous systems that TTX-S VGSCs are modulated by β subunits[3,6,7,11,102]. This also occurs *in vivo*, although the magnitude and direction of the changes vary with cell type. *Scn1b* null ventricular myocytes have increased transient and persistent I_{Na} and a fraction of this is TTX-S[57]. *Scn1b* null hippocampal neurons isolated from the CA3 region express decreased levels of $Na_V1.1$ and increased levels of $Na_V1.3$ without changes in somal I_{Na} density compared to WT[68]. *Scn1b* null cerebellar neurons have altered VGSC localization in the axon initial segment and reduced resurgent I_{Na}[50]. In the peripheral nervous system, the voltage dependence of TTX-S I_{Na} inactivation is shifted in a depolarizing direction in *Scn1b* null small DRG neurons[103]. In *Scn2b* null mice, the loss of β2 results in negative shifts in the voltage dependence of TTX-S I_{Na} inactivation as well as significant decreases in I_{Na} density in acutely dissociated hippocampal neurons. The integral of the compound AP in optic nerve is significantly reduced, and the threshold for AP generation is increased, indicating a reduction in the level of functional plasma membrane VGSCs[104]. In acutely isolated small-fast DRG neurons, *Scn2b* null mice show significant decreases in TTX-S I_{Na} with no detectable changes in the voltage dependence of activation or inactivation. Activation and inactivation kinetics of TTX-S, but not TTX-R, I_{Na} are slower due to *Scn2b* deletion. This selective regulation of TTX-S I_{Na} is supported by reductions in transcript and protein levels of TTX-S *Scn1a*/$Na_V1.1$ and *Scn9a*/$Na_V1.7$[105]. Therefore, β

subunits may also contribute to pathogenesis in cardiac disease by disturbing the regulation of TTX-S I_{Na} in heart as well as in the cardiac innervation.

VGSC β subunits may also contribute to cardiac arrhythmia via neuronal mechanisms that include modulation of *SCN10A*, encoding the TTX-R VGSC $Na_V1.8$, whose association with cardiac conduction was identified by GWAS[106]. This VGSC, originally identified in nociceptors and known to associate with β subunits[107], is also localized to intracardiac neurons, where its blockade markedly reduces AP firing frequency[108]. $Na_V1.8$ current characteristics vary in heterologous systems depending on the type of β subunit expressed[107,109]. In *Scn10a* null mice, the cardiac PR interval is shorter than in WT littermates, with no differences in other ECG parameters or echocardiographic cardiac dimensions and function[106]. In addition to $Na_V1.8$, β subunits associate with a number of peripheral nerve TTX-S VGSCs, including $Na_V1.1$, $Na_V1.2$, and $Na_V1.6$. Thus, through disruptions of some or all of these interactions, β subunit gene mutations may generate arrhythmias via neural mechanisms.

VGSC β subunits modulate K^+ channels.

β1 is a multifunctional molecule that is not specific to VGSC complexes. β1 co-assembles with and modulates the properties of the $K_V4.x$ subfamily of channels that underlie I_{to} in heart and I_A in brain[37,38,110]. I_{to} is an important contributor to AP repolarization in heart[111]. β1 associates with $K_V4.3$, increases the amplitude of the $K_V4.3$ current, and modifies $K_V4.3$ gating [37,38]. The *SCN1B* mutation p.R214Q, which

selectively affects β1B and not β1, is proposed to contribute to the arrhythmogenesis of BrS by concomitantly decreasing I_{Na} and increasing I_{to}[36].

Roles of β subunits in cardiovascular pharmacology and treatment.

β1 expression modulates cardiac VGSC sensitivity to lidocaine block with subtle changes in channel kinetics and gating properties[112]. Flecainide is a class Ic agent that is used in provocation tests to unmask the BrS phenotype[113] and that reduces arrhythmogenesis in patients with LQT3[114]. Quinidine is a class Ia agent which reduces arrhythmogenesis in BrS patients[115] and is reasonable for the treatment of electrical storm in BrS[116]. Flecainide and quinidine are pro-arrhythmic and anti-arrhythmic, respectively, in the *Scn5a*$^{+/-}$ BrS mouse model[117]. In contrast, both flecainide and quinidine exert antiarrhythmic effects in *Scn3b* null hearts through modifying the ventricular effective refractory period rather than changes in AP duration[118]. Although both transgenically engineered mouse lines are VGSC loss-of-function BrS models, their responses to flecainide appear to be different. This genetically specific response to drug was also confirmed in our *Scn1b* null mice, in which carbamazepine, but not lacosamide, failed to block high-frequency firing in nerve[119]. β subunits not only modify the response of $Na_V1.5$ to drug administration, but are also putative drug targets themselves. Late I_{Na} contributes to heart failure (HF) mechanisms. Suppression of late I_{Na} but not transient I_{Na} in failing cardiomyocytes is beneficial[120]. Post-transcriptional silencing of *Scn1b* in a HF canine model results in decreased late I_{Na} without affecting transient I_{Na} [121]. Based on these results, *SCN1B* may prove to be a plausible drug target in HF.

Summary

Considerable advances have been made in understanding the molecular basis of arrhythmia over the past 20 years. From fundamental, single ion channel function under physiological conditions to malfunction of defective channels in pathophysiology, from simple heterologous expression models to integrative animal models, knowledge in pathogenesis of channelopathies is evolving rapidly. Complexities are being added to our previous understanding of monogenic diseases whose etiology clearly cannot be attributed to the effects of single gene mutations alone. Assignment of causation is not a simple task. Common polymorphisms in VGSC α and/or β subunit genes may influence the severity of disease-causing mutations. For example, common *SCN5A* polymorphisms differentially modulate the biophysical effects and expression levels of disease-causing *SCN5A* mutations[122,123]. Expression levels of *Scn4b* modify conduction defect severity caused by a *Scn5a* mutation in mice[92]. Deleterious effects of mutations can be additive. Longer QTc intervals, a higher incidence of arrhythmia, and more severe symptoms are observed in LQTS patients carrying 2 different mutations[124]. Thus, an understanding of a patient's genetic background is required to correctly interpret a disease-causing mutation. Although lacking patient-specific genetic backgrounds, transgenic mouse models allow us to investigate cardiac phenotypes at an integrative level[125] in a relatively "low-noise" genetic background. Thus, in the following chapters, I will discuss how I utilized a transgenic mouse model to investigate electrophysiological consequence of *Scn2b* deletion. The observed cardiac phenotypes, including ventricular and atrial arrhythmia, and insights into their underlying mechanisms will be discussed.

In the future, combining findings from GWAS[126] and patient-specific induced pluripotent stem cell (iPSC) models[127] will allow us to have better insights into genotype-to-phenotype correlations, and provide a basis for more precise risk stratification and prognosis estimation. In addition, patient-specific iPSC models will be invaluable tools for drug screening[128] and the development of individualized therapies.

CHAPTER II

Scn2b deletion in mice leads to ventricular arrhythmia

Work presented here includes collaborative efforts contributed by Dr. B. Cicero Willis and Dr. Xianming Lin from the laboratories of Dr. Jose Jalife at the University of Michigan and Dr. Mario Delmar at New York University, respectively. Dr. B. Cicero Willis and I performed the optical mapping studies together. Dr. Xianming Lin performed super-resolution patch clamp recording. I performed the remainder of the work.

Introduction

As discussed in chapter I, β subunits regulate sodium current (I_{Na}) density, kinetics, voltage dependence of gating, and channel cell surface expression. In addition, β subunits function as cell adhesion molecules (CAMs)[8,9]. Considering their multifunctional roles in channel modulation and cell-cell communication, it is not surprising that mutations in the genes encoding the VGSC β subunits have been implicated in cardiac arrhythmia[129]. Mutations in *SCN2B*, encoding VGSC β2, are associated with atrial fibrillation (AF) and Brugada syndrome (BrS) in human patients[48,130], suggesting that β2 may play important roles in establishing or maintaining normal cardiac electrical activity. β2 is covalently linked to VGSC α subunits via disulfide bonds[12], including the major cardiac VGSC, $Na_v1.5$[7], and is known to enhance

the trafficking of neuronal α subunits (including $Na_V1.1$, $Na_V1.2$, $Na_V1.3$, $Na_V1.6$, and $Na_V1.7$) to the plasma membrane as well as modulate the voltage dependence of channel gating[104,105]. Central neurons isolated from *Scn2b* null mice have reduced cell surface VGSCs and comparably reduced I_{Na} density, altered voltage dependence of inactivation, and increased susceptibility to seizures[104]. Similar changes in I_{Na} have been shown in *Scn2b* null nociceptive neurons[105]. In contrast to neurons, the role of *Scn2b* in heart is not well understood. Co-expression of a *SCN2B* mutant protein linked to AF and BrS with $Na_V1.5$ in a heterologous system revealed a reduction in I_{Na} density compared to expression of $Na_V1.5$ alone, suggesting cardiac VGSC loss-of-function[48,130]. However, the role of β2 in heart has not been explored *in vivo*. Here, I test the hypothesis that β2 plays critical roles in cardiac excitability.

Scn2b deletion results in decreased I_{Na} density in ventricular myocytes.

I compared whole-cell I_{Na} in acutely isolated *Scn2b* null and WT ventricular myocytes. *Scn2b* null myocytes showed a significant reduction in total I_{Na} density (Fig. 2A), a 6.5 mV hyperpolarizing shift in the voltage-dependence of activation, and decreased slope factor (κ) of the activation curve compared to WT (Fig. 2B). There were no observable differences in the voltage-dependence of inactivation (Fig. 2C), or the kinetics of recovery from inactivation between genotypes (Fig. 2D). There were also no observable changes in the level of persistent I_{Na} (Fig. 2E) or the kinetics of inactivation measured at -45 mV (Fig. 2F-G) (Table 2). Taken together, these data indicate that the principal role of VGSC β2 subunits in ventricular myocytes is to regulate I_{Na} density, similar to what we have observed previously in central and peripheral neurons[104,105].

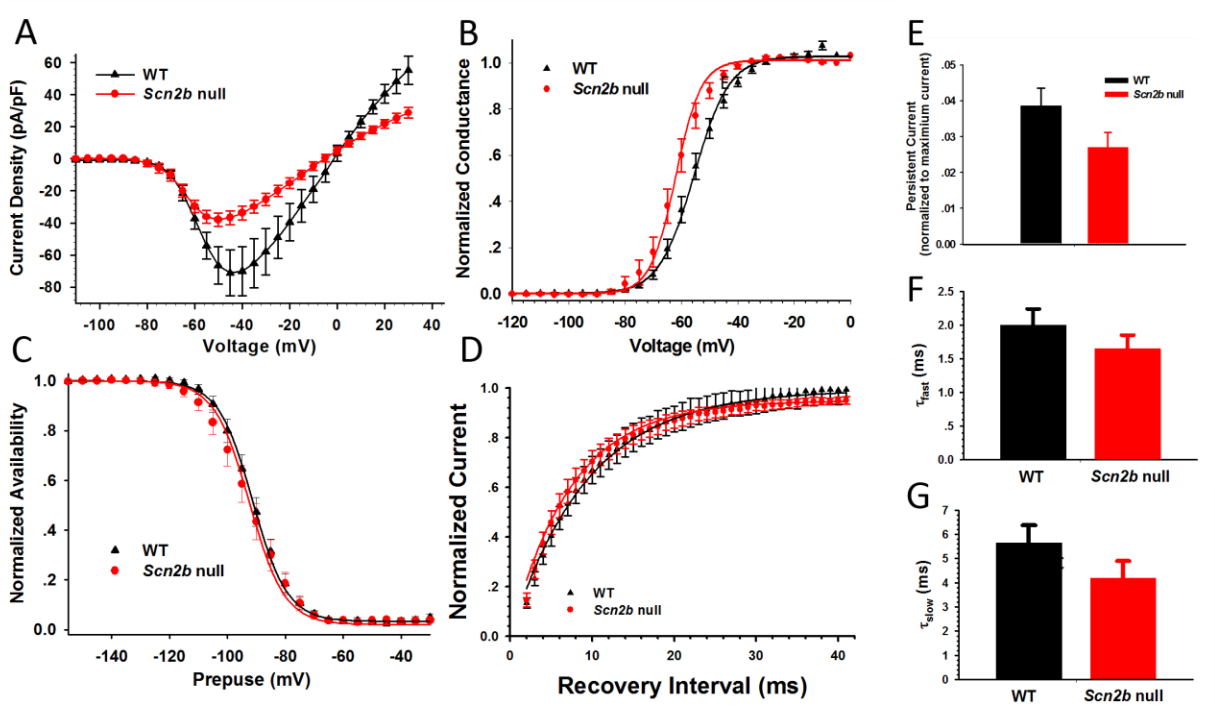

Figure 2 I_{Na} recordings from ventricular cardiomyocytes

A. *Scn2b* null ventricular myocytes have significantly decreased I_{Na} over a voltage range from -50mV to -10mV ($p<0.05$, *Scn2b* null: n=12, N=6; WT: n=9, N=6). B, *Scn2b* deletion shifts the voltage-dependence of activation in the hyperpolarizing direction by 6.5 mV (p=0.019, *Scn2b* null: n=12 N=6; WT: n=9 N=6) and decreases the slope factor κ (p=0.002, *Scn2b* null: n=12 N=6; WT: n=9 N=6). C. There were no differences in steady-state inactivation between wildtype and null cells. D – G. *Scn2b* deletion has no effect on the time dependence of recovery from inactivation, persistent I_{Na}, or the kinetics of inactivation. Significance determined using Student's T test or Mann-Whitney Rank Sum test. N is the number of animal and n is the number of the cell.

Table 2 I_{Na} Biophysical Properties

	WT	*Scn2b* null	p-value
	N=6	N=6	
Voltage dependence of activation			
$V_{1/2}$(mV)	-55.542±1.435	-62.065±1.918	p=0.019
κ	6.201±0.257	4.057±0.361	p=0.002
n	9	12	
Voltage dependence of inactivation			
$V_{1/2}$(mV)	-91.237± 1.611	-92.368± 2.270	p=0.708
κ	-6.004±0.183	-6.129±0.17	p=0.627
C	0.0337± 0.00747	0.0207± 0.0112	p=0.383
n	9	12	
Kinetics of inactivation			
τ_{slow} (ms)	5.650± 0.726	4.184± 0.715	p=0.169
n	9	9	
τ_{fast} (ms)	2.003± 0.24	1.65± 0.204	p=0.276
n	9	12	
Steady-state persistent current			
% of peak current	3.87±0.492	2.7±0.428	p=0.087
n	9	11	
Kinetics of recovery			
τ (ms)	10.359±1.425	8.551±1.166	p=0.336
n	8	10	

Data are mean ± SEM. Kinetics of inactivation were recorded at a test potential of -45 mV. Persistent I_{Na} was recorded at a test potential -45 mV, 50-52 ms after the voltage step. *Significance was determined using Student t-test with $p<0.05$.

No changes in the distribution of sodium channels recorded from T-tubules or crest regions.

VGSCs are differentially localized in the heart. The tetrodotoxin-resistant (TTX-R) channel, $Na_V1.5$, is preferentially localized at the intercalated discs and lateral membrane, while multiple tetrodotoxin-sensitive (TTX-S) VGSCs, including $Na_V1.1$, $Na_V1.3$, and $Na_V1.6$, are localized in the t-tubules[22,131]. β2 subunits have been shown to associate biochemically with $Na_V1.5$[22] and to localize preferentially at intercalated discs[131]. To investigate the whether there is a change of sodium channel redistribution at the subcellular level that may contribute to the current change, we performed super-resolution scanning patch clamp recordings of I_{Na} at the t-tubules and at the cell crests as in[132]. Fig. 3 presents frequency histograms for the number of channels detected within a patch, estimated from the average peak current amplitude (voltage step to −30 mV from a holding potential of −120 mV), and a unitary conductance of 10 pS[133]. The histogram obtained from recordings at the t-tubules showed a Gaussian distribution (Fig.3A), while the data obtained at the cell crest was more bimodal (3B), consistent with previous observations[133]. No difference was apparent between genotypes. Combined with previous finding that subcellular localization of β2 is at the intercalated disc[131], we speculated that sodium current are more affected at the intercalated discs.

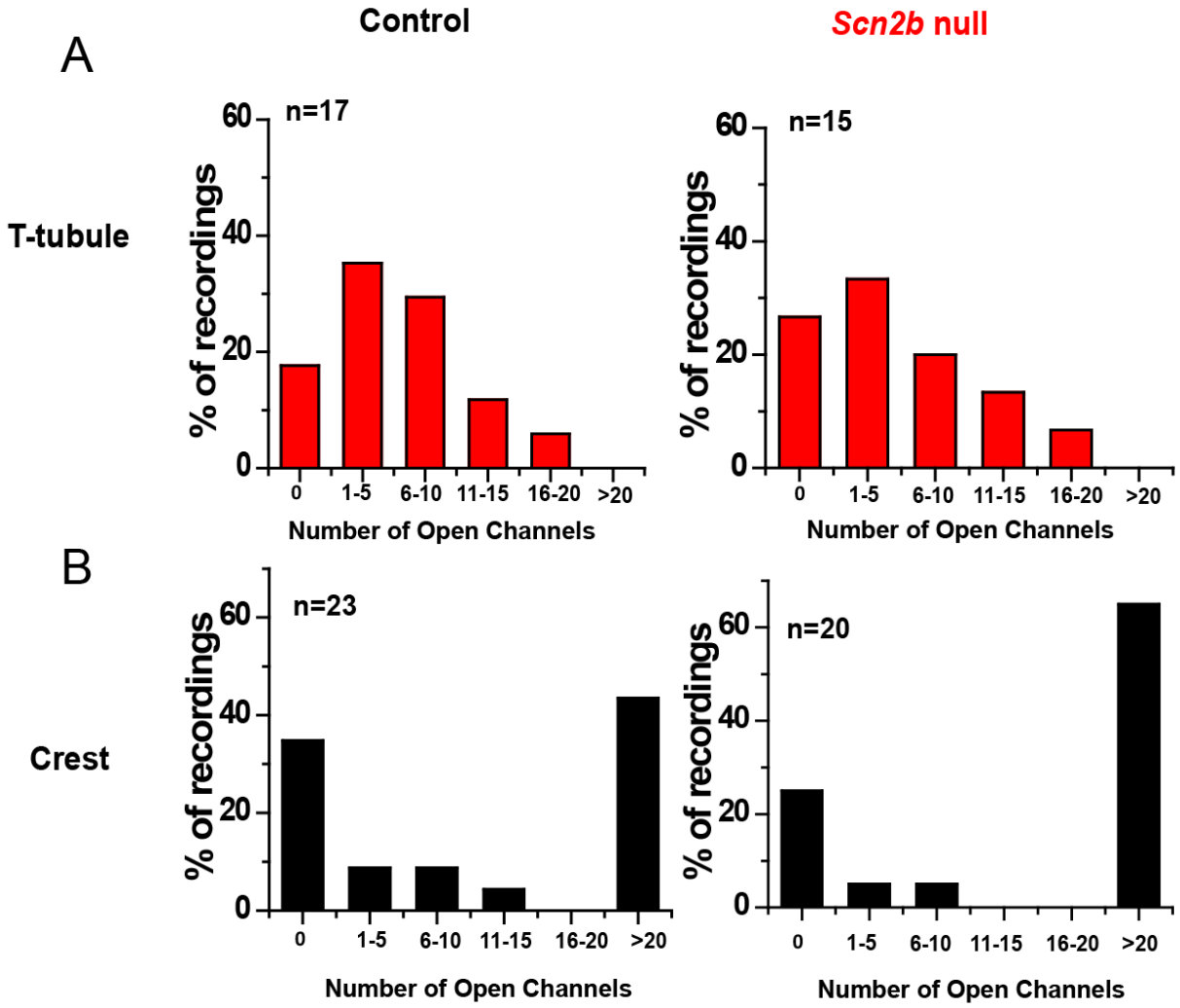

Figure 3 No changes in the distribution of sodium channels recorded from the T-tubules or from the crest regions

Ordinates show percent of recordings (relative to total number of attempts). Abscissae show number of open channels detected. Number of open channels in each recorded patch was estimated from the average peak current amplitude during a voltage step to −30 mV from a holding potential of −120 mV, and an estimated unitary conductance of 10 pS. The number of separate recordings reported in each histogram is indicated in the top left of each panel (WT, N=4; *Scn2b* null, N=3). The pipette was placed on the

opening of the T-tubules (top) or on the crest (bottom). Significance determined using Fisher's exact test. N is the number of mice and n is the number of patch.

Scn2b null hearts have impaired impulse propagation in the right ventricular outflow tract region (RVOT)

To test the hypothesis that cardiac conduction may be compromised due to the loss of I_{Na} in *Scn2b* null ventricle, we performed optical mapping of *ex vivo* Langendorff perfused heart preparations (Fig. 4). Slowed conduction was observed in the *Scn2b* null RVOT, but not the RV, region compared to WT (Fig. 4 A-C). To examine excitability changes in the RVOT region more closely, I performed current clamp recordings of APs in *Scn2b* null myocytes and WT myocytes isolated from the RVOT. While I observed trends toward decreased maximum upstroke velocity at different pacing cycle lengths and depolarized resting membrane potential in *Scn2b* null cells compared to WT cells (Fig. 5B and C), these changes did not reach significance. APDs at early phases (APD_{30}-APD_{50}) were unchanged between genotypes (Fig. 5D). In contrast, late phase APDs (APD_{70}-APD_{90}) were significantly prolonged in *Scn2b* null myocytes compared to WT (Fig. 5E, G). Consistent with this prolonged, late phase APD, we observed a significantly higher incidence of early afterdepolarization (EADs)[134] in *Scn2b* null myocytes (9 out of 21 cells) compared to WT (1 out of 15 cells) (Fig. 5F, $P = 0.024$).

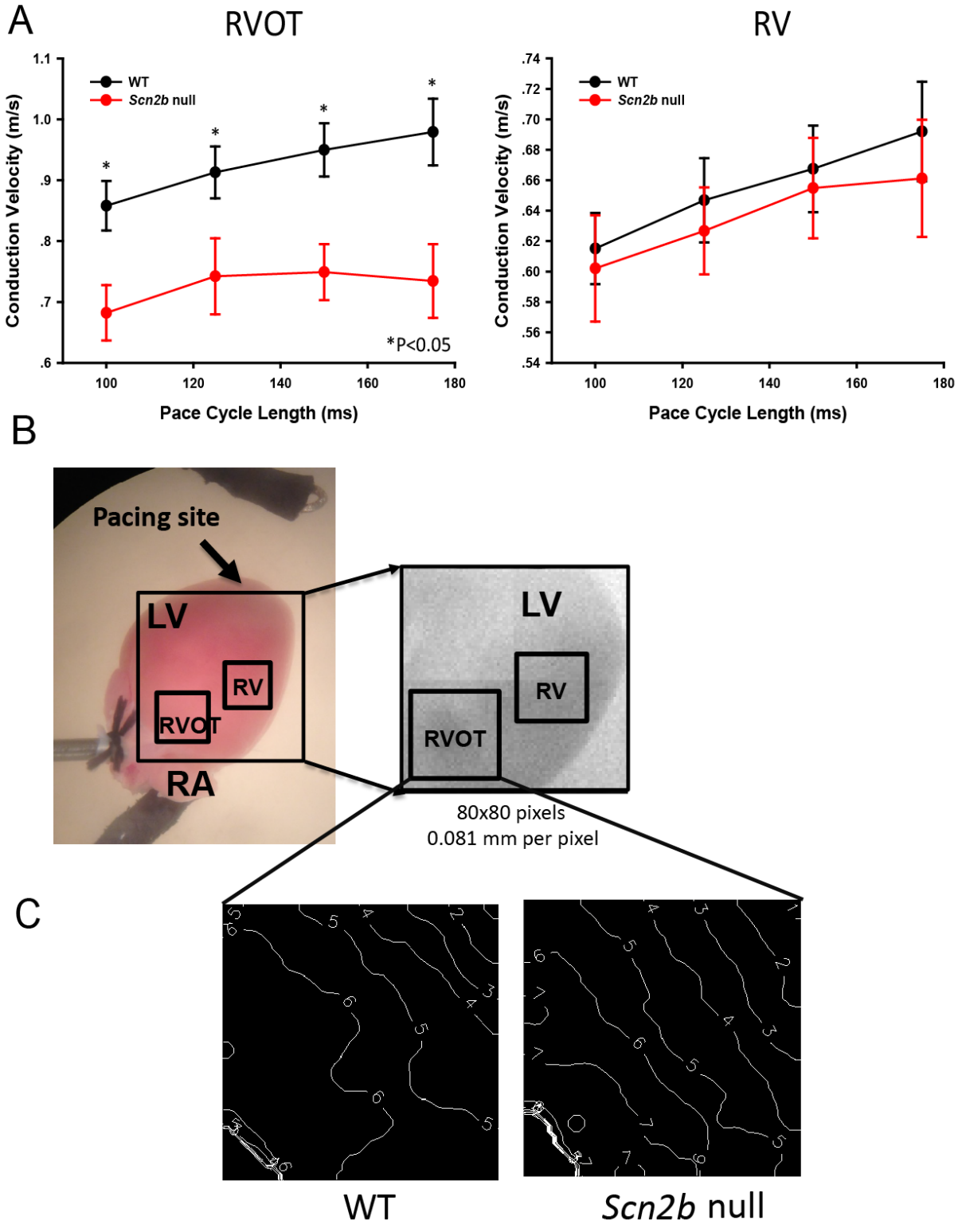
A
RVOT
RV
WT
Scn2b null
Conduction Velocity (m/s)
Pace Cycle Length (ms)
*P<0.05
B
Pacing site
LV
RV
RVOT
RA
80x80 pixels
0.081 mm per pixel
C
WT
Scn2b null

Figure 4 Conduction velocity is decreased in the Scn2b null right ventricular outflow tract (RVOT) region

A. Conduction velocity is significantly decreased in the RVOT region but not right ventricular (RV) free wall (*Scn2b* null: N=9; WT: N=11) paced at various cycle lengths (CL=100ms p=0.011; CL=125ms, p=0.032; CL=150ms *p=0.015; CL=175ms p=0.012; Student's T test, *Mann-Whitney Rank Sum Test where applicable). B. Langendorff heart preparation during optical mapping. Box shows corresponding region for measurement. C. Two representative activation maps from *Scn2b* null and WT preparations at 150 ms pacing cycle length. White lines indicate isochrone lines. Numbers on each line indicate time in msec. Note that isochrone lines are more crowded in *Scn2b* null hearts, indicating conduction slowing in the RVOT.

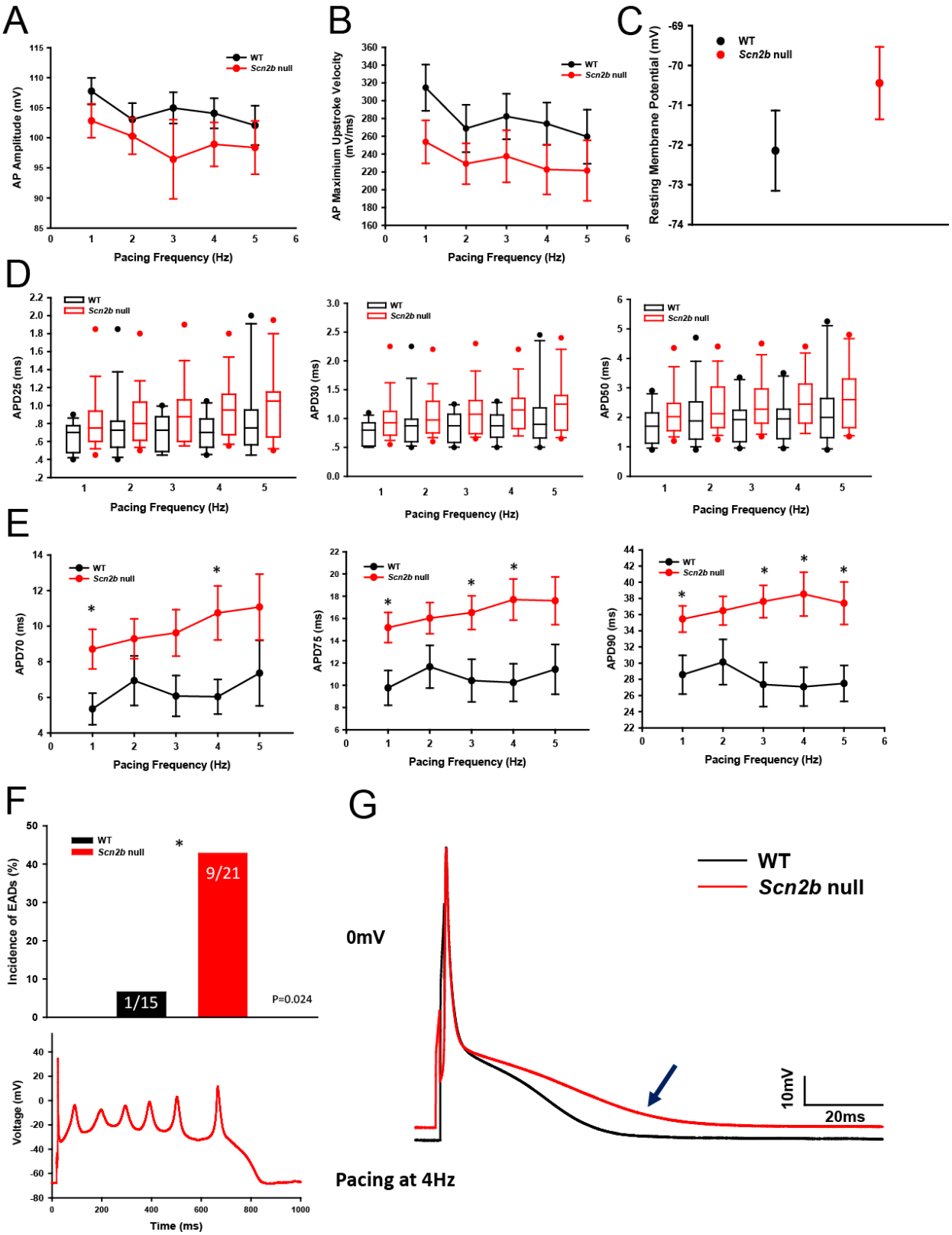

Figure 5 AP recordings from single RVOT myocytes.

A. No differences between genotypes in AP amplitude when paced at 1-5 Hz (WT: N=8, n=10-14; *Scn2b* null: N=5, n=12-16). B. *Scn2b* null hearts exhibited a trend toward decreased AP maximum upstroke velocity (p=0.098-0.418 from 1-5Hz; WT: N=8, n=10-14; *Scn2b* null: N=5, n=11-16). C. *Scn2b* null myocytes showed a slight depolarization in resting membrane potential (p=0.223; WT: N=8, n=14; *Scn2b* null: N=5, n=18). D. Similar time courses of early phase repolarization (APD_{25-50}) between WT and *Scn2b* null myocytes. E. In contrast, the late phase APD values (APD_{70-90}) were significantly prolonged in *Scn2b* nulls (p=0.005-0.021). F. *Scn2b* null myocytes exhibited a higher incidence of early afterdepolarizations (EADs) than WT (p=0.024). A representative *Scn2b* null EAD trace is shown in the lower panel. G. Representative AP traces from each genotype. The final phase of the *Scn2b* null AP is prolonged compared to WT. The trace was paced at 4Hz. Significance was determined using Student's T test, Mann-Whitney Rank Sum Test, or Fisher's exact test where applicable.

Scn2b null ventricles are more arrhythmogenic than WT

To assess the susceptibility of *Scn2b* null ventricles to arrhythmia, we performed optical mapping experiments with simultaneous, volume-conducted ECGs in isolated hearts (Fig. 6). Episodes of spontaneous, non-sustained ventricular tachycardia (NSVT) and premature ventricular complexes (PVCs) were observed in 3 and 4 out of 10 *Scn2b* null hearts, respectively, but not in the 11 WT hearts tested (Fig. 6A). Fig. 6B and C show an anatomical view of the heart under the camera during the optical mapping and epicardial activation during a sinus beat, respectively. As expected from previous studies[135], during the sinus beat, two breakthroughs appeared on the LV and RV free wall close to the apex and then the excitation wavefront propagated towards the base of the heart. All spontaneous aberrant rhythm events appeared with a premature ventricular complex (PVC) within a mean time window of 25-26 min following cannulation and before any pacing or pharmacological maneuvers were performed (Fig. 6D). Episodes of spontaneous NSVT were recorded and phase maps were generated to analyze activation patterns during tachycardia (Fig. 6D-F). Rotors were observed (for example, see Supplemental movie 1), implicating functional re-entry as the underlying mechanism of arrhythmia in *Scn2b* null hearts. Singularity points, the organizing centers of each rotor, were concentrated in the *Scn2b* null RVOT region (Fig. 6E), suggesting that wavebreaks were more likely to occur in this area. Interestingly, rotors were not confined to the RVOT, but were observed to meander to the left and right anterior ventricular free walls over time (Fig. 6F), giving rise to the polymorphic appearance of the ECG (Fig. 6D). Closely coupled PVCs served as triggers for NSVT initiation in *Scn2b* null hearts. Chronological snapshots taken from a phase movie of a *Scn2b* null

heart capturing initiation of an episode of spontaneous polymorphic VT illustrate that the interplay between a PVC and the arrhythmogenic substrate that led to arrhythmia (Fig. 7). During the sinus beat preceding VT, the epicardium was homogeneously activated from apex to base (Fig. 7A). A PVC then emerged (Fig. 7 B-C) as an epicardial breakthrough on the anterior RV free wall near the apex. This premature impulse traveled to the RVOT region and was blocked, likely due to prolonged APD and maintenance of refractoriness (Fig. 7 C-D). The impulse then detoured to the LV, circumventing the RVOT. When the RVOT was finally activated, due to slowed impulse conduction within this region, the rest of the heart had finished repolarizing and was ready for re-excitation. As a result, the excitation wave front turned at the RVOT and initiated a rotor (Fig. 7 E-F).

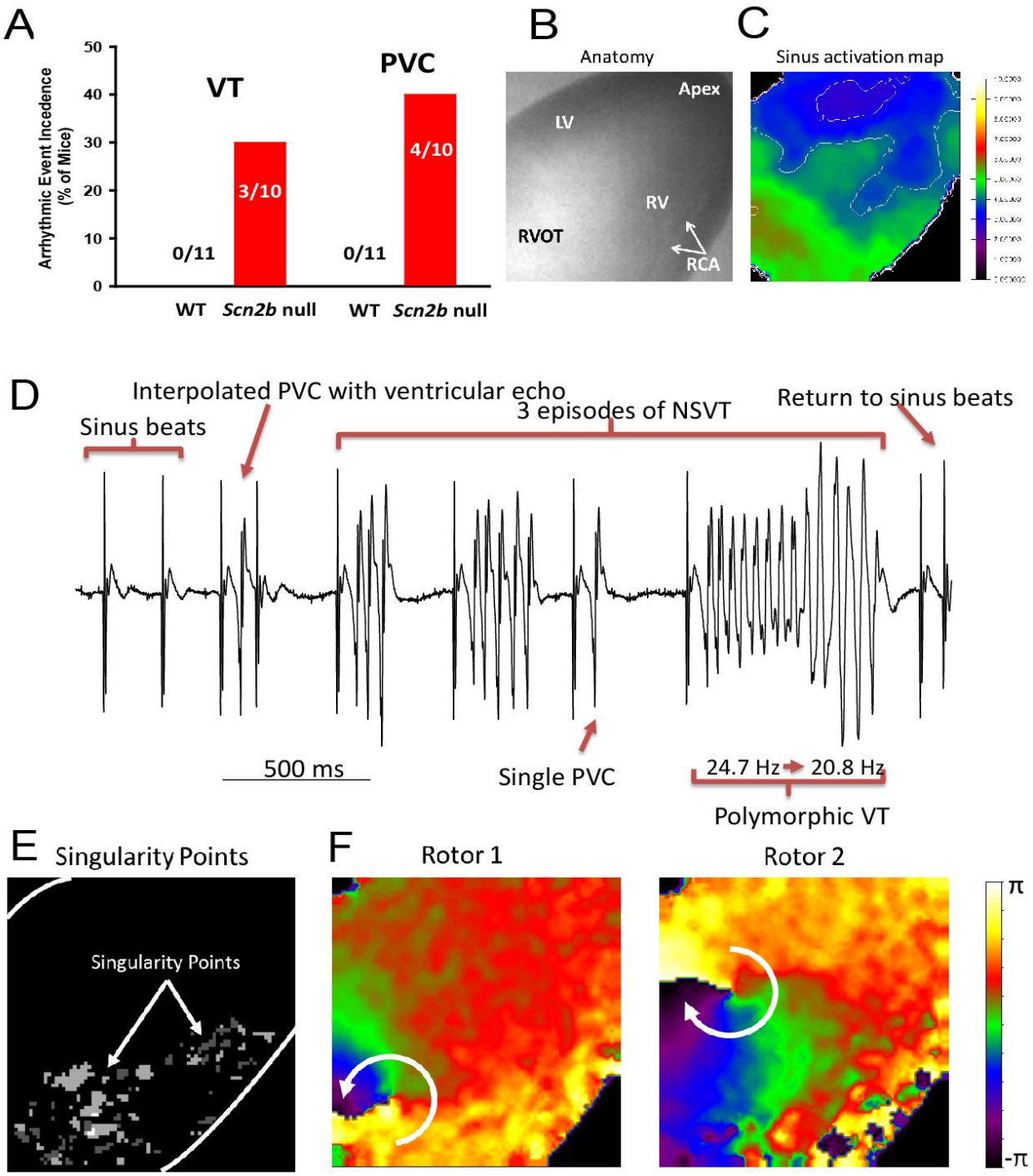

Figure 6 Arrhythmic events captured in Scn2b null hearts by optical mapping.

A. Incidence of PVC and VT in WT (0 out of 11 hearts) *vs Scn2b* null (4 out of 10 and 3 out of 10 hearts, respectively) (p=0.02 and p=0.09, respectively, Fisher's Exact Test). . Anatomical view of the heart under the camera during the optical mapping. LV: left ventricle, RV: right ventricle, RVOT: right ventricular outflow tract, RCA: right coronary artery. C. Activation map of a sinus beat. Normal epicardial activation during the sinus beat had two breakthroughs on the LV and RV free wall close to the apex and then the excitation wavefront propagated towards the base of the heart. White lines are isochrones lines (in msec). D. Volume conductive pseudo ECG (bipolar mode, frontal plane) showed 3 episodes of polymorphic NSVT and PVC. Each episode of VT was triggered by a PVC, sharing the same morphology as a single independent PVC, indicating a focal source of this triggering ectopic beat. The polymorphic VT had a frequency transition from 24.7 Hz to 20.8 Hz. E. Singularity point map. Each singularity point is the organization center where the potential phases merge. Singularity map shows that the location of the rotors (white dots) remained in the RVOT region during most of the recording period. F. Two phase map snapshots of two rotors during VT. Rotors are dynamic, spin in multiple directions, and can meander to other regions, giving rise to the polymorphic appearance of ECG.

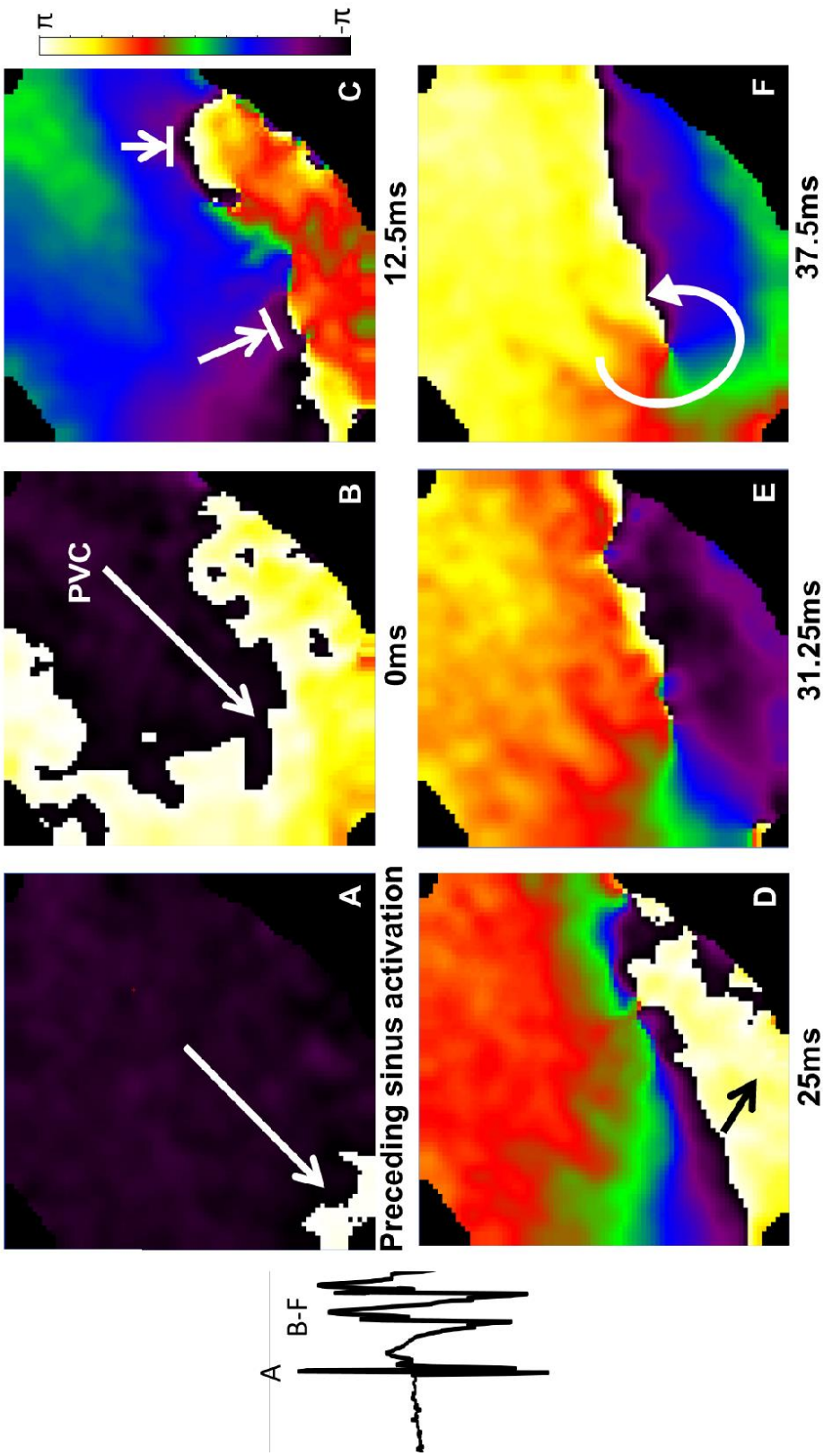

Figure 7 Proposed mechanism of VT initiation and rotor formation.

Chronological snapshots of a phase movie that captured initiation of an episode of spontaneous polymorphic VT illustrate that the interplay between a PVC and the arrhythmogenic substrate of *Scn2b* null hearts leads to arrhythmia. A. During the sinus beat preceding VT, the epicardium was homogeneously activated from apex to base. B and C. A PVC then emerged and resulted in breakthrough to the epicardium in the anterior RV free wall close to apex. C and D. The early impulse traveled to the RVOT region where it was blocked due to prolonged APD and increased refractoriness. E. Thus the impulse detoured to the LV and circumvented the RVOT. When the RVOT was finally activated, due to slowed conduction within this region, the rest of the heart had finished repolarization and was ready for re-excitation. E and F. As a result, the excitation wave front turned around at the RVOT and initiated a rotor. Inset: Corresponding ECG.

Discussion

Scn2b null mice mimic human Brugada syndrome.

BrS is a rare, inherited cardiac disease in structurally normal hearts that results in increased risk of ventricular fibrillation leading to sudden cardiac death[136]. The phenotypic characterization of BrS in human patients is J-point and ST segment elevation in right precordial leads (V1 to V3) with pseudo-right bundle branch block[137]. While only 30–35% of diagnosed BrS cases are attributable to pathogenic variants in known genes, 25–30% of these result from reduction of I_{Na} [138], similar to what we have observed in *Scn2b* null ventricular myocytes. Two hypotheses, focusing on repolarization and depolarization, respectively, have been proposed to explain BrS[70]. Both hypotheses predict that, similar to our mouse model, the RVOT is the most affected region in human heart. Both slowed conduction and prolonged activation-recovery time (ARI) are observed in BrS patients using ECG imaging techniques[139], suggesting that depolarization and repolarization abnormalities may exist in BrS concomitantly.

Mutations in *SCN5A* have been implicated as causal in BrS[140]. Compelling evidence from clinical studies of endocardial[141,142] or epicardial mapping[143,144], shows conduction delay in the RVOT, suggesting that aberrant depolarization underlies BrS[70]. Our data in *Scn2b* null mice demonstrate a reduction in I_{Na} with a corresponding decrease in impulse propagation. Similar to human BrS, the RVOT region is preferentially affected in our model.

Prolongation of repolarization has also been observed in the RVOT region of BrS patients[145 146 139]. This is thought to contribute to QT prolongation in right precordial leads under pharmacological challenge[147]. In addition, an augmented AP notch may reduce the availability of calcium current in human heart, resulting in delay in the second upstroke and the onset of phase 3, resulting in longer AP duration[148,149]. In contrast to humans, the mouse cardiac AP lacks a clear plateau phase, and consequently shows no spike and dome upon I_{Na} reduction[150]. APD shortening, rather than lengthening, was observed in the right epicardium in the murine *Scn5a*$^{+/-}$ model of BrS compared to WT, and was shorter than the corresponding endocardial APD, creating increased right ventricular repolarization gradients[151]. In contrast, a significant prolongation of APD_{90} was observed in the *Scn2b* null model, mimicking clinical findings. Recently, model-independent interactions between I_{K1} and I_{Na} were revealed, implicating reciprocal modulation of expression of Kir2.1 and $Na_V1.5$ within a macromolecular channel complex[152]. Because $Na_v1.5$ and β2 are covalently linked in heart[22], it is likely that β2 subunits also associate with the Kir2.1/$Na_v1.5$ complex at the intercalated disc and that both are down-regulated in *Scn2b* null hearts. Thus, we propose that reduced I_{K1} may contribute to the final AP phase prolongation in *Scn2b* null myocytes.

PVC and arrhythmogenesis in BrS and Scn2b null hearts

Trigger elimination, focal ablation of PVCs originating from the RVOT[153], and substrate modification by epicardial ablation of arrhythmogenic sites in the RVOT anterior free

wall[143] have been demonstrated to be effective in preventing arrhythmic events in human BrS patients. Thus, PVCs are proposed to serve as triggers in arrhythmogenesis. The timing of emergence and spatial orientation of the excitation wavefront of the ectopic beat are key factors in arrhythmia initiation. In animal BrS models, phase 2 re-entry has been proposed as the mechanism of extrasystole, which may further degenerate into ventricular fibrilllation[154]. Accordingly, phase 2 re-enty based PVCs are proposed to originate from the RVOT and be short coupled. Consistent with this, pace mapping shows that PVCs in patients with BrS frequently originate from the free-wall region of the RVOT[155]. However, PVCs that initiate VT are not observed exclusively from the RVOT[156] or with short coupling interval[156,157], indicating high variability in the onset mode of arrhythmia in BrS. More interestingly, when patients carry *SCN5A* mutations, they are less likely to have PVCs from the RVOT[158]. In previous BrS murine model studies, PVCs were demonstrated to play important roles in initiating re-entrant, spontaneous polymorphic ventricular tachycardia[159]. Sites of origin coincided with localized areas of high repolarization heterogeneity. In our *Scn2b* null model, we found that every recorded VT episode occurred following a PVC, suggesting a requirement for PVCs to serve as triggers. In addition, epicardial breakthrough of the initiating PVC was observed to be located at the RV free wall near the apex rather than in the RVOT. We found no differences in the coupling interval between VT-initiating PVCs and PVCs that did not trigger VT (Figure 8). Because the morphologies of these PVC types were similar, we propose that the origins of the PVCs were focal. Thus, the subsequent occurrence of VT was dependent on the repolarizing state of the preceding sinus beat, in which case the repolarization or refractoriness was dynamic. Unlike early

repolarization syndrome, a variant in the J-wave syndrome spectrum often has VF episodes initiated by PVCs with a short-long-short sequence[157], BrS has a more complex and dynamic mode of onset of VT/VF.

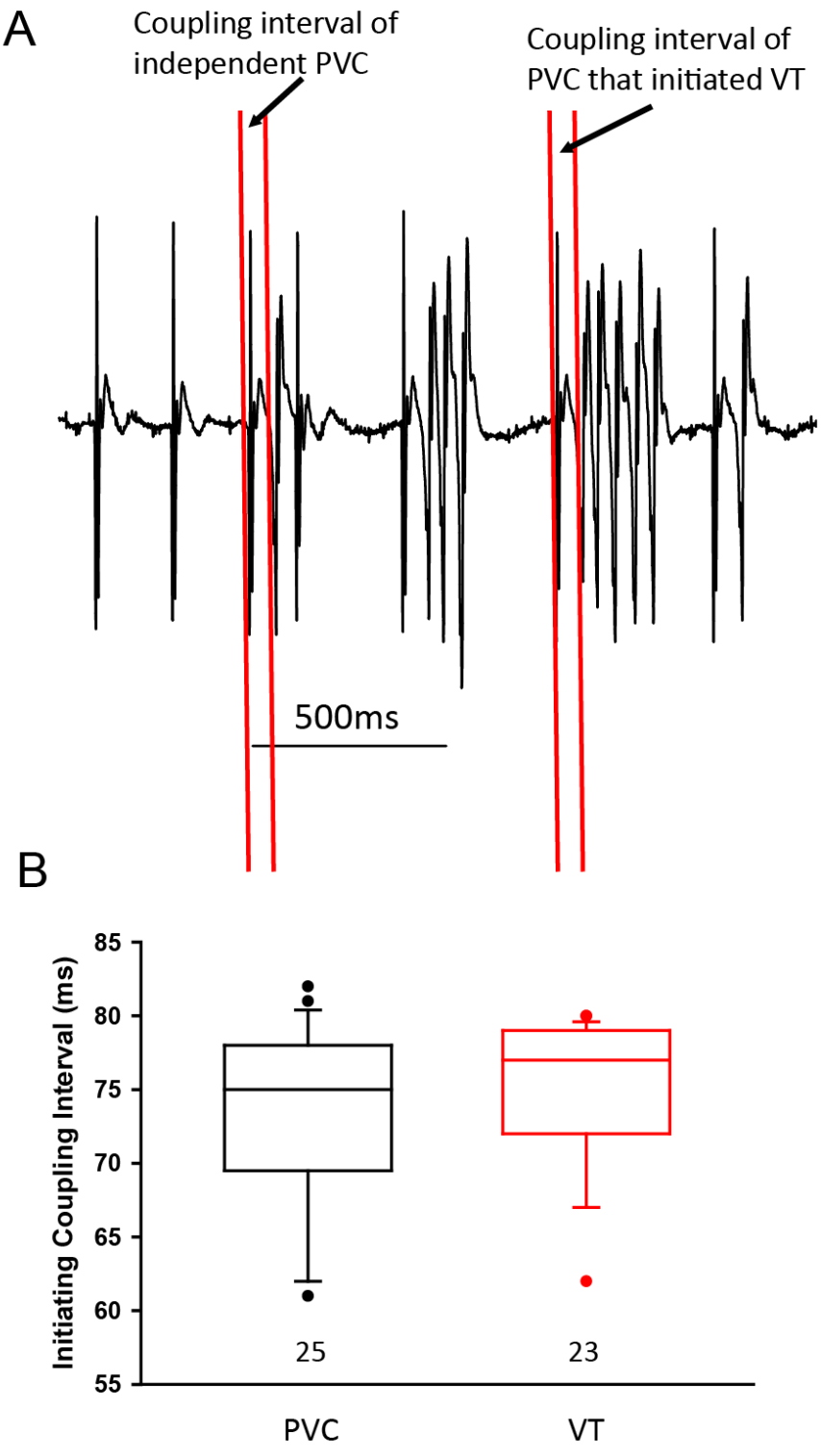

Figure 8 No differences in PVC coupling interval.

A. An independent PVC and a PVC that triggered VT. B. No differences were found in the coupling interval between these two categories in *Scn2b* null heart (p=0.459, Mann-Whitney Rank Sum Test). Numbers below the box plot are the total number of PVCs that were included for analysis in each group.

CHAPTER III

Conduction system is intact in *Scn2b* null mice

Work presented here includes collaborative efforts contributed by Dr. Roberto Ramos Mondragon from the laboratory of Dr. Hector Valdivia at the University of Michigan. Dr. Roberto Ramos and I performed the intracardiac recordings together. I performed the remainder of the work.

Introduction

The cardiac conduction system is specialized myocardium composed of the sino-atrial node, the atrio-ventricular node and the His-Purkinje system, coordinating electrical propagation to allow both sequential and synchronous contraction between and within chambers[160]. Mutations in sodium channel genes including *SCN5A*, *SCN1B* and *SCN10A* have been associated with progressive cardiac conduction disorders (PCCD)[161] and sick sinus syndrome[162], which are characterized by progressive impairment of the conduction system and bradycardia. $Na_V1.5$ are expressed in conduction system and in the regions surrounding the SA and AV node[163]. Since a majority of mutations that associated with PCCD are characterized as sodium channel loss-of-function[164], I proposed that loss of β2 may also affect cardiac conduction system.

To test this hypothesis, I performed body surface ECG and intracardiac recordings from *in vivo* hearts and pseudo-ECG on surgically denervated hearts.

ECGs from *Scn2b* null mice suggest bradycardia

Two sets of animals at different ages, 3 months and 7-9 months, were used for *in vivo* ECG recordings. Reduced heart rate (HR) was observed in *Scn2b* null mice compared to WT in the 3 month-old group (Fig. 9A) with a trend to slowed heart rate in the 7-9 month-old group (Fig. 9B) ($P = 0.025$ and $P = 0.092$, respectively for the groups). In contrast, HRs in denervated *ex vivo Sc2b* null hearts (isolated from 3-6 month old mice) were indistinguishable from that in WT hearts, suggesting altered autonomic control, rather than intrinsic cardiac rhythm alterations in *Scn2b* null mice (Fig. 9C). There were no observable changes in other ECG parameters, including PR interval, P wave duration, QRS duration and QT interval (Table 3). To circumvent known issues in correcting QT intervals for heart rate in mice, we placed an octapolar stimulating/recording catheter into the right heart chamber to directly pace the atrium and entrain the whole heart at a fixed pacing cycle length of 100ms. QT intervals were then measured during pacing and compared between genotypes without correction (Fig. 10). No differences between the two genotypes were found using this method, suggesting that the regional slowed conduction and slight increase in APD observed at the single cell level in *Scn2b* null myocytes were not of sufficient magnitude to be reflected on the ECG (Table 3).

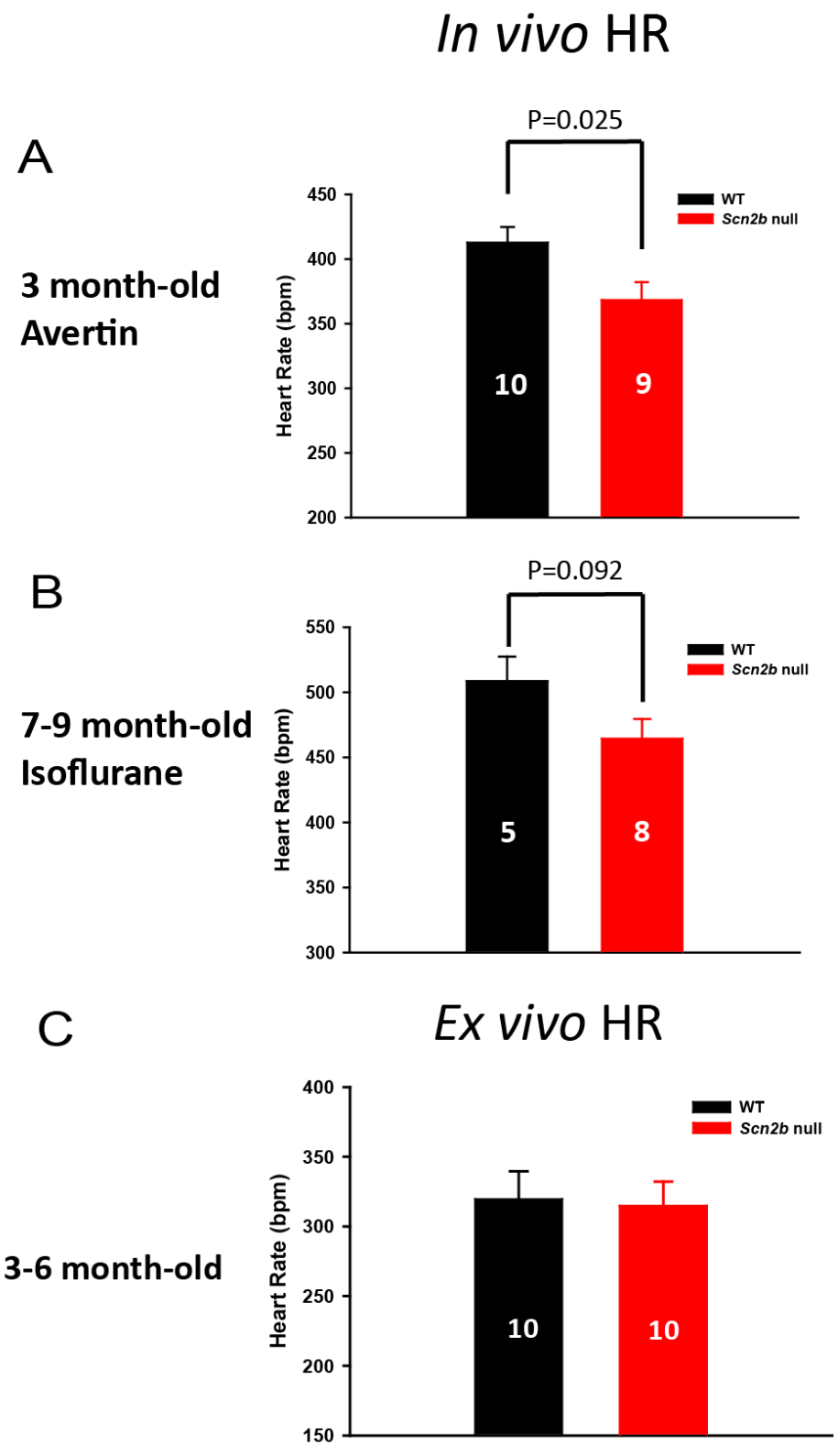

Figure 9 Heart rate was slightly decreased in Scn2b null mice.

A. Decreased HR was observed in Avertin anesthetized 3 month-old *Scn2b* null mice during ECG recordings (p=0.025) . B. A similar trend of HR reduction was observed in 7 – 9 month-old mice anesthetized with Isoflurane (p=0.092). C. There were no differences in HR observed in *ex vivo* hearts (*Scn2b* null: 315±17 bpm; WT: 319±20 bpm) (p=0.863). All panels: Numbers on the bars indicate the number of animals tested. Significance determined with Student's T test.

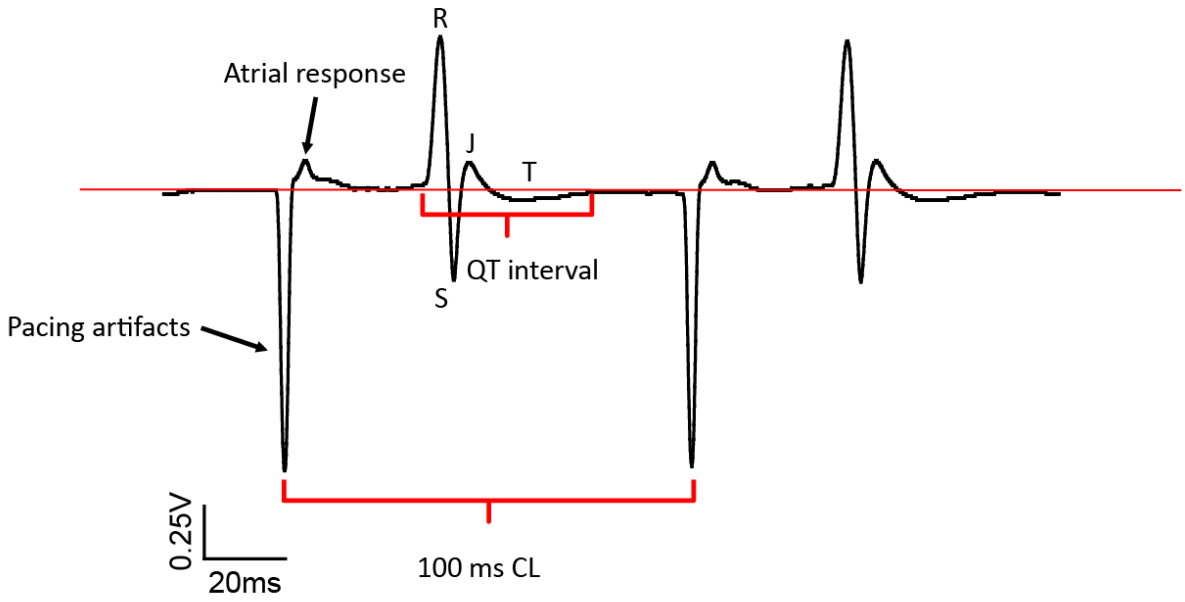

Figure 10 Surface ECG during atrial pacing.

The QT interval was measured when the atrium was paced at a constant cycle length (100ms) to avoid inappropriate correction.

Table 3 ECG Parameters

Age	Anesthetics	Parameter	WT	*Scn2b* null	P-value
2-3 month	**Avertin**	Heart Rate (HR) bpm	413±12	368±14	p=0.025
			N=10	N=9	
		P-wave duration (ms)	10.24±0.71	9.18±0.9	p=0.37
		PR interval (ms)	44.2±1	44.02±1.97	p=0.93
		QRS duration (ms)	11.62±0.47	12.39±0.56	p=0.32
		QT interval (ms)	43.4±0.3	42.5±0.38	p=0.093
			N=7	N=6	
7-9 month	**Isoflurane**	Heart Rate (HR) bpm	509±19	464±15	p=0.092
		P-wave duration (ms)	12.2±0.49	12.82±1.31	p=0.73
		PR interval (ms)	42.89±2.08	39.86±0.93	p=0.157
		QRS duration (ms)	10.25±0.62	9.5±0.29	p=0.239
		QT interval (ms)	42.68±2.46	41.1±1.26	p=0.537
			N=5	N=8	
		Paced QT interval (ms) At 100ms pacing cycle length	44.11±1.7	45.31±1.06	p=0.54
			N=5	N=7	

Data are mean ± SEM. N = number of animals. 1.2% Avertin, 0.23 ml per 10 g of body weight, was administered IP. 1.5% isoflurane was used for acquisition of surface ECGs. Paced QT interval was measured during intracardiac recording with animals maintained under 2% isoflurane. *Significance was determined with Student t-test with P < 0.05.

Scn2b null mice exhibit a normal cardiac conduction system

Loss-of-function mutations in *SCN5A* have been associated with progressive cardiac conduction defects (PCCD)[165]. To assess whether the cardiac conduction system was also affected in *Scn2b* null, we performed intracardiac recordings to measure the conduction time for each segment along the conduction pathway, as well as to assess the electrophysiological properties of the sinoatrial node (SAN) and atrio-ventricular node (AVN). Neither the atrial-His conduction time, His-ventricular conduction time, SAN recovery time, AVN refractoriness, nor Wenckebach periodicity were different from WT mice (Table 4). These data suggest that the cardiac conduction system is intact in the *Scn2b* null heart.

Table 4 Intracardiac electrophysiological values

	WT	***Scn2b* null**	**P value**
AH Interval (ms)	27.2±2	27.8±2.5	p=0.87*
HV Interval (ms)	9.5±0.5	10.4±0.6	p=0.31
	N=5	N=7	
$SNRT_{100}$ (ms)	74.9±11.9	62.4±11	p=0.23*
$SNRT_{90}$ (ms)	106±9.9	83.1±14.3	p=0.22
$AVERP_{100}$ (ms)	47.6±2.6	48.5±2.3	p=0.79
	N=7	N=8	
$AVERP_{80}$ (ms)	58.1±2.2	58.6±2	p=0.89
$AERP_{100}$ (ms)	26.3±2.4	22.3±1.8	p=0.2
$AERP_{80}$ (ms)	19.8±1.1	19.4±1	p=0.78
	N=7	N=7	
WP (ms)	72.6±2.1	73.3±1.1	p=0.77
$WP_{2:1}$ (ms)	53.7±2.1	52.2±1.6	p=0.59
	N=7	N=8	
$VERP_{100}$ (ms)	45.2±2.5	38.7±3	p=0.13
	N=6	N=6	
$VERP_{80}$ (ms)	42.5±3	39.2±3.2	p=0.48
	N=4	N=5	

Values are means ± SE; N, number of mice. AH, interval from atrial to His-signal; HV, interval from His to first QRS- movement in surface-ECG; SNRT, sinus-node recovery-time; AVERP, atrial-ventricular effective refractory

period; AERP, right atrial effective refractory period; WP Wenckebach-periodicity, WP2:1, Wenckebach-periodicity at 2:1 conduction; VERP, right ventricular effective refractory period. Subscripts indicate S1S1 drive cycle lengths. Student t-test and *Mann-Whitney rank sum test.

Discussion

Conduction system and autonomic control in Scn2b null mice

Among murine models that carry sodium channel mutations, *Scn5a* haploinsufficiency[166] and *Scn3b* null mice[63] are most phenotypically similar to our *Scn2b* null mice. Both of the two model human BrS and concomitantly have atrial phenotype including sinus node exit block[17] and AF susceptibility[64]. Since the connection between *SCN5A* and Progressive Cardiac Conduction Defects (PCCD) is well established[165], it is reasonable to expect impairment of conduction system in both *Scn5a*$^{+/-}$ [167,168] and *Scn3b*$^{-/-}$ mice[64]. However, *Scn2b* null mice did not exhibit abnormal conduction, which may attribute to two reasons. Firstly, both *Scn5a* heterozygotes (Hz) and *Scn3b* KO are on the inbred strain of 129SvEv, ours is on C57BL6. Previous study has demonstrated that the severity of conduction defects is strain dependent due to genetic background. *Scn4b* was identified as the responsible gene, which had lower expression in 129P2 than FVB/NJ strain, giving rise to a more severe phenotype[92]. Secondly, the tissue distribution of β subunits may also play a role in contributing to conduction system phenotype. *SCN3B* is highly expressed in the ventricles and Purkinje fibers but not in atrium in sheep heart[20], suggesting its importance in the conduction system. Further investigations are needed to profile tissue distribution of β2 in the heart.

Heart rate was slower in *Scn2b* deficient mice regardless of age and types of anesthetics used, whereas no difference in heart rate were found in pharmacologically denervated heart. Thus altered autonomic control may account for these findings.

Unlike $Na_v1.5$, $\beta 2$ is also extensively expressed in central and peripheral nervous system, modulating other neuronal sodium channels[104,105,169], potentially contributing to autonomic control of the heart.

CHAPTER IV

Higher Susceptibility to Atrial Arrhythmia in *Scn2b* Null Mice

Work presented here includes collaborative efforts contributed by Dr. B. Cicero Willis and Dr. Roberto Romas Mondragon from the laboratories of Dr. Jose Jalife Lab and Dr. Hector Valdivia, respectively. Dr. B. Cicero Willis and I performed the optical mapping together. Dr. Mondragon and I performed intracardiac recordings together. Masson's trichrome staining was performed by Dr. Erby Wilkenson in the ULAM In-Vivo Animal Core as fee-for-service. I performed the remainder of the work.

Introduction

Atrial fibrillation (AF) is the most common sustained arrhythmia disease with a prevalence of 1% to 2% in the US[170]. Mutations that affecting both sodium channel α and β subunits have been linked to AF[171]. Two missense mutations in *SCN2B* have been revealed in human AF patients[48], suggesting an important role of β2 in the heart. To study the role of *Scn2b* in atria, I investigated the atrial phenotype of *Scn2b* null mice using optical mapping and intracardiac recording.

Scn2b null mice have increased susceptibility to atrial fibrillation *in vivo*

Both gain- and loss-of-function mutations in *SCN5A* have been linked to atrial fibrillation[172]. For *SCN5A* loss-of-function mutations, lower conduction velocity and shortened APD give rise to shortened wavelength, facilitating stable re-entry and thus providing a substrate for atrial fibrillation[173]. To test whether *Scn2b* null hearts are also prone to atrial fibrillation, I applied burst pacing to induce atrial tachyarrhythmia before and after carbachol administration. I defined atrial fibrillation/ tachyarrhythmia (AF/AT) as episodes of 1 sec or greater in duration, before or after carbachol administration, during burst pacing or the S1-S2 protocol. Using these criteria, I found that AF/AT susceptibility was significantly higher in *Scn2b* null mice (7 out of 9) compared to WT mice (1 out of 7) ($P = 0.02$, Fig. 11A). The durations of induced AF/AT were variable in *Scn2b* null mice, ranging from just over 1 sec to as long as 11 min (Fig. 11B). In contrast, the majority of AF/AT episodes in WT mice had durations of less than 1 sec. Fig. 11C (center and right panels) shows a representative surface ECG lead-II trace and atrial electrogram acquired during atrial fibrillation and flutter in a *Scn2b* null mouse. This is compared to traces from a WT mouse (left panels) that was resistant to induction of tachyarrhythmia. In the *Scn2b* null example, the atrial electrogram is more complex and fractionated during atrial fibrillation than during atrial flutter, as indicated.

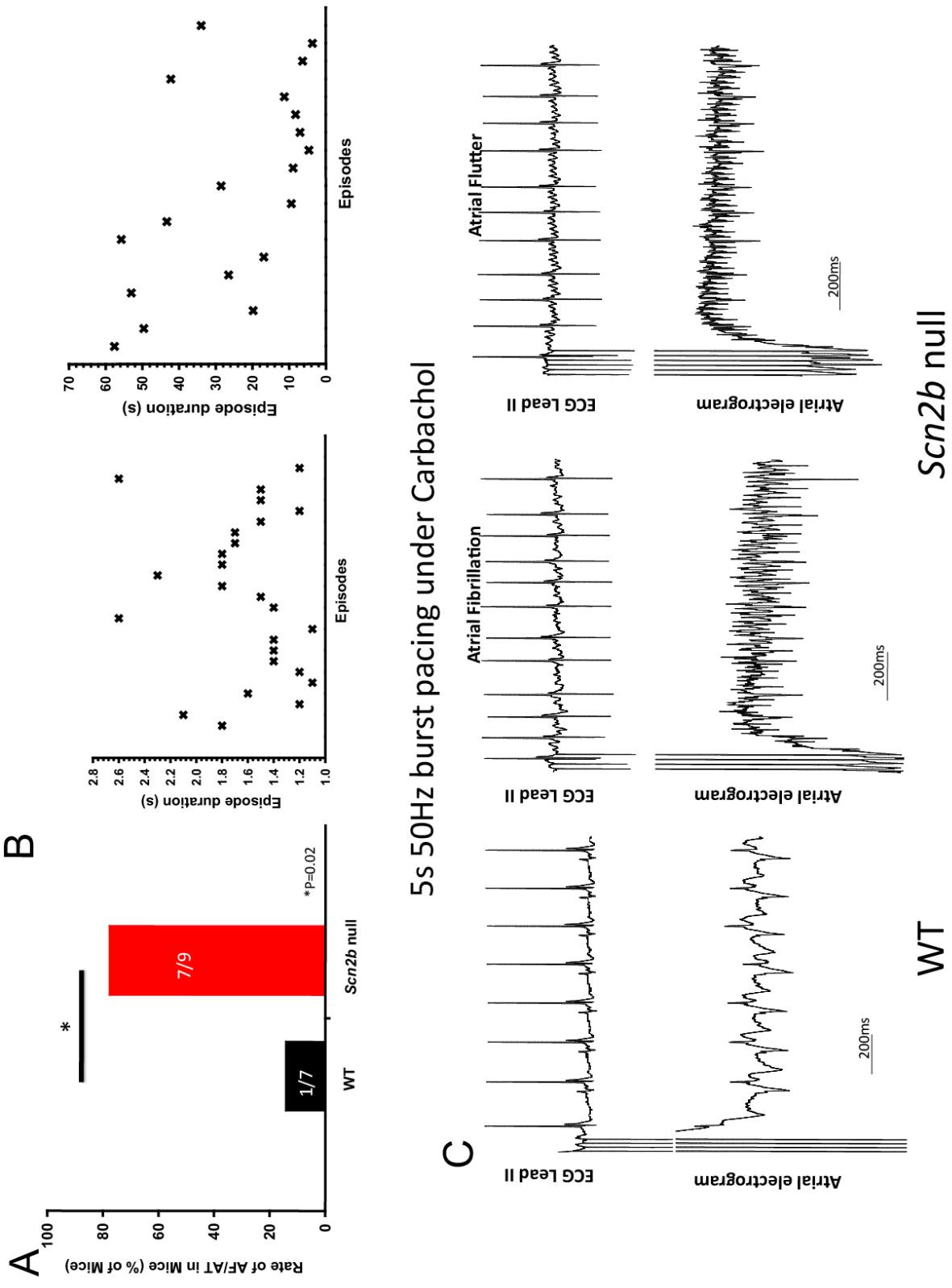

Figure 11 Scn2b null atria are more susceptible to AF.

AF/AT was defined as episodes lasting longer than 1 sec either before or after carbachol administration. Animals that had at least one AF/AT episode that lasted longer than 1 sec were considered to be inducible. A. *Scn2b* null mice (7 out of 9 animals) were more susceptible to atrial arrhythmia than WT mice (1 out of 7 animals) ($p=0.02$, Fisher's exact test, one tailed). B. Distribution of the durations of all AF/AT episodes recorded in *Scn2b* nulls. Most durations ranged from 1.1 sec to 60 sec, with the longest episode lasting 11 min. The majority of episodes recorded in WT were shorter than 1 sec. C. Representative surface ECG and atrial electrogram from each group. Under 5-sec 50 Hz burst pacing with carbachol administration, AF and atrial flutter could be induced in *Scn2b* nulls but not in WT. During AF, the atrial electrogram was more disorganized. Numbers on the bars indicate the number of animals tested.

Re-entry underlies the mechanism of atrial fibrillation in *Scn2b* null atria

To determine the mechanism of atrial arrhythmia in *Scn2b* null hearts, I performed optical mapping in isolated *ex vivo* atrial preparations (Fig. 12A). Consistent with our *in vivo* observations, I was able to induce AF/AT in these preparations by burst pacing in 5 of 11 *Scn2b* null atria compared to 1 of 10 WT atria prior to the application of carbachol (300 nM, P = 0.0725). As expected, carbachol administration increased the level of AF/AT induction in both genotypes (6 of 11 *Scn2b* null *vs.* 3 of 10 WT, P = 0.39). Phase movies recorded during AF/AT in *Scn2b* null atria showed variable forms of rotors, which served as drivers to maintain the atrial arrhythmia. For example, Fig. 12B and Supplemental movie 2 demonstrate AF/AT driven by a single rotor in the right atrium. Fig. 12C and Supplemental movies 3 and 4 show AF/AT driven by two rotors in the figure-of-eight conformation (2 count-rotating rotors share common pathway) in the right atrium prior to carbachol administration and then driven by single rotor in the pulmonary vein (PV) region of the left atrium after carbachol. Fig. 12D and Supplemental movie 5 show AF/AT driven by three independent rotors at different dominant frequencies (17.7 Hz and 26.5 Hz respectively). One rotor was located in the right atrium, while the other two, with figure-of-eight configuration at the higher common frequency, were located in the PV region. In this case, the AF/AT terminated and then was spontaneously re-initiated by a sinus beat due to wavebreak in the right atrium. This re-initiated AF/AT was sustained by a single rotor in the right atrium (Fig. 12D). Spontaneous AF/AT was also observed in one *Scn2b* null atrium but not in any of the WT atrial preparations, suggesting higher atrial arrhythmogenecity in the mutant animals (Fig. 13). Taken together, the dynamic, complex, and non-hierarchical organization of rotors in *Scn2b*

null atria suggest that the substrates for AF/AT may be functionally and anatomically heterogeneous.

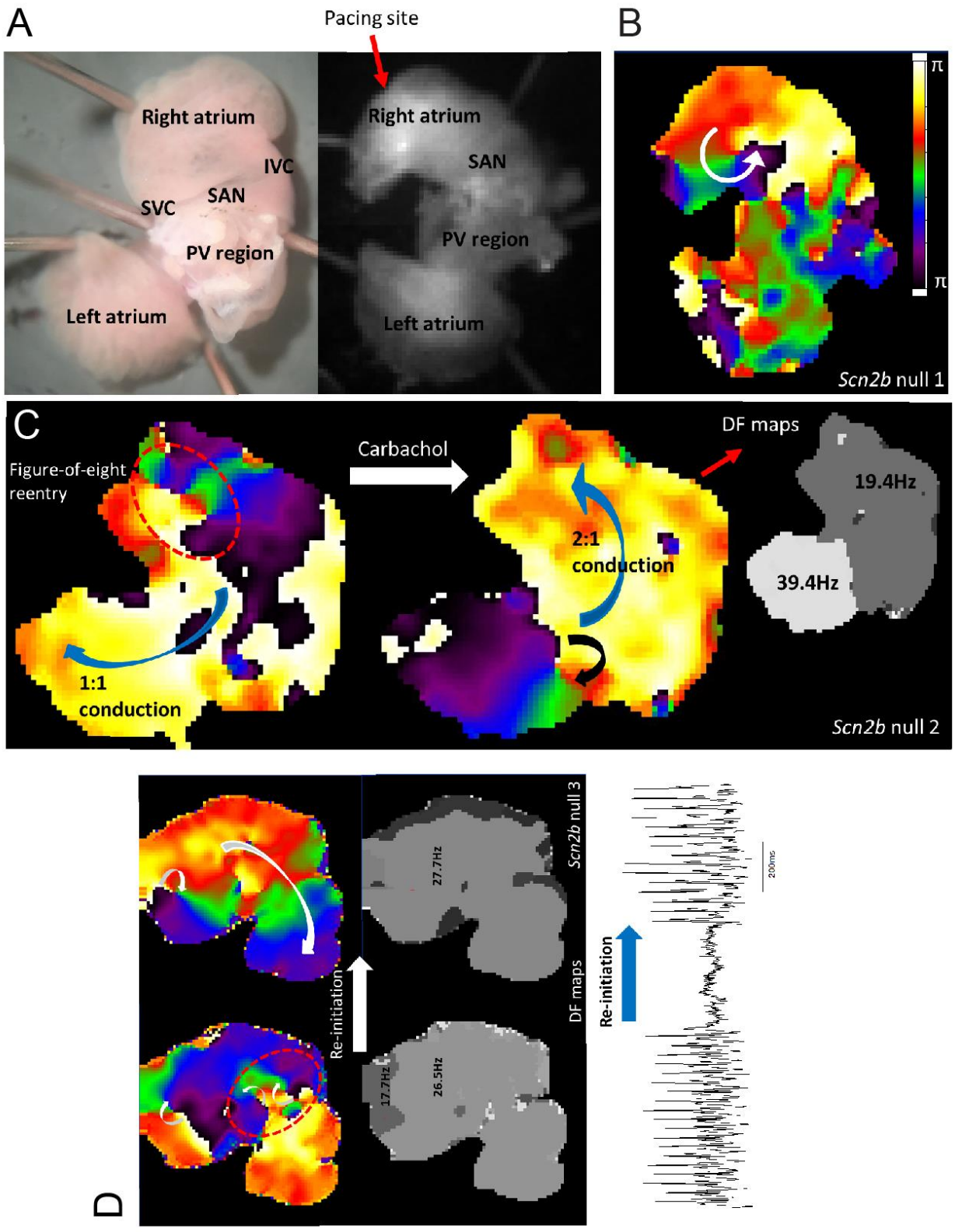
A
Pacing site
Right atrium
IVC
SVC
SAN
PV region
Left atrium
Right atrium
SAN
PV region
Left atrium
B
π
π
Scn2b null 1
C
Figure-of-eight reentry
Carbachol
DF maps
19.4Hz
2:1 conduction
39.4Hz
1:1 conduction
Scn2b null 2
D
Scn2b null 3
27.7Hz
Re-initiation
DF maps
17.7Hz
26.5Hz
Re-initiation
200ms

Figure 12 Complex and dynamic rotors underlie the mechanism of AF in Scn2b null atria.

A. Anatomical view from posterior of the atrial preparation under microscope (left) and camera (right). (SVC: superior vena cava, SAN: sino-atrial node, IVC: inferior vena cava, PV: pulmonary veins) Pacing was at the edge of the right atrium appendage. B. Pacing-induced AF was driven by a single rotor in the right atrium. C. Induced AF was driven by two counter-rotating rotors (figure-of-eight re-enty) with 1:1 conduction to the left side. After carbachol perfusion, AF was driven by a single rotor located in the left atrium PV region with 2:1 conduction to the right side, resulting in twice the dominant frequency in left compared to the right. D. AF was driven by three different rotors spinning at 17.7 Hz and 26.5 Hz in right and left atrium, respectively (upper left and lower left rotors, respectively). After its termination, the AF was spontaneously re-initiated by the wavebreak occurring in the right atrium (upper right and lower right). The resultant single rotor then drove the entire episode at 27.7 Hz in the right atrium with 1:1 conduction to the left. A volume conductive bipolar atrium electrogram showed two corresponding episodes of AF (bottom atrial ECG trace).

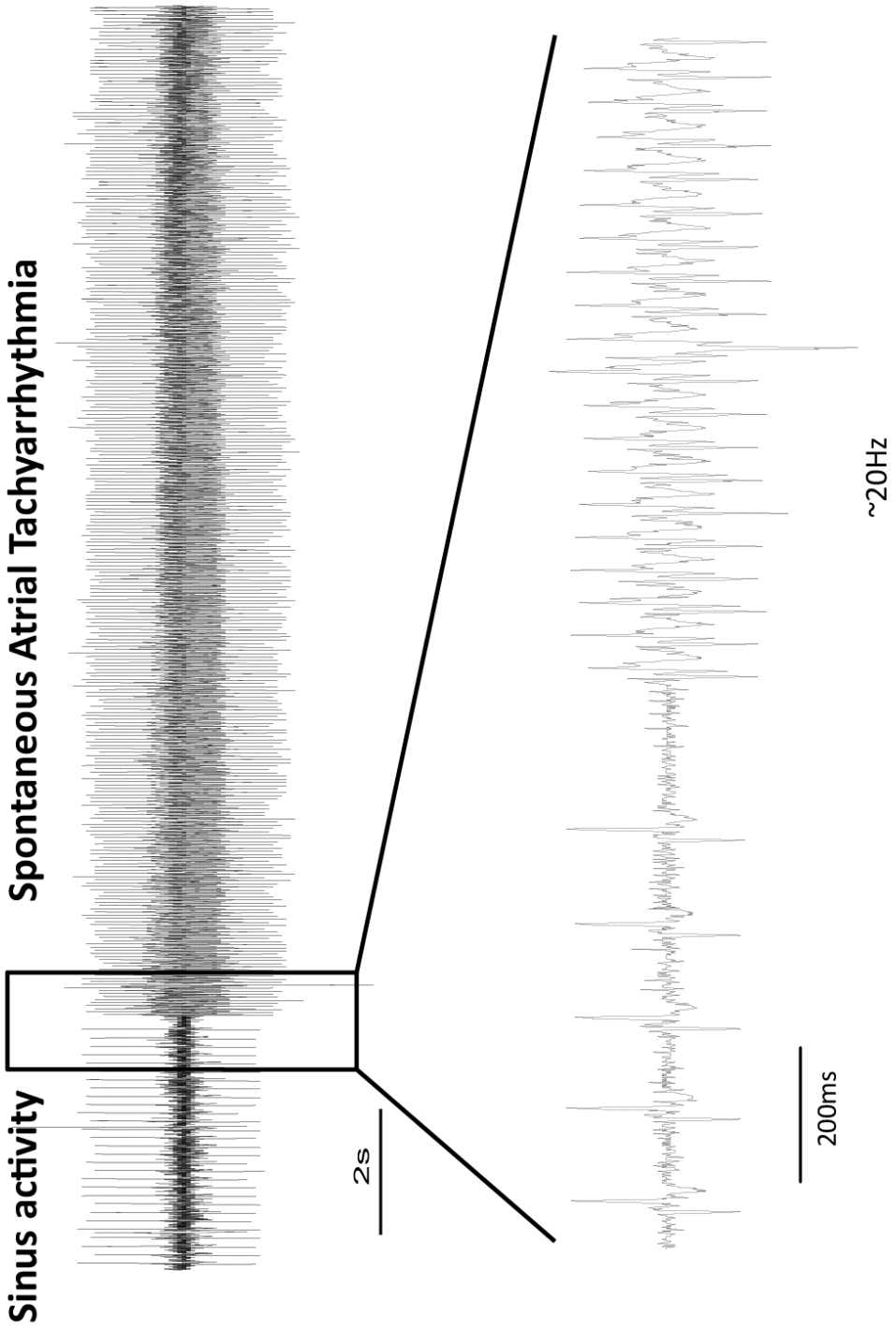

Figure 13 Spontaneous atrial tachyarrhythmia in an ex vivo atrial preparation.

Sudden acceleration of the atrial bipolar electrogram was observed in one of the *Scn2b* null atria but not in WT. No electrical pacing or drug was applied when the atrium developed tachyarrhythmia. Multiple episodes of atrial arrhythmia were observed, the longest episode lasted for 24.5 sec at a frequency of ~20 Hz. The morphology of tachyarrhythmic beats is different from sinus beats, suggesting that this was not simply an acceleration of sinus automaticity.

APD is heterogeneously prolonged in *Scn2b* null atrium

In contrast to the results in the RVOT region, I observed no changes in atrial conduction velocity between genotypes (Fig. 14). AP recordings from single right atrial myocytes showed no differences in amplitude, maximum upstroke velocity, or resting membrane potential between groups (Fig. 15A). While there was a trend toward increased $APD_{25\text{-}30}$, I observed a significant increase in the later phases of the APD ($APD_{50\text{-}90}$) in *Scn2b* null myocytes compared to WT myocytes (Fig. 15B). Fig. 15C presents representative, superimposed AP wave forms from each genotype to illustrate the AP prolongation in *Scn2b* null atrial myocytes compared to WT. In Fig. 15D I plot the range of APD values for ventricular (upper panel) and atrial (lower panel) myocytes of each genotype to illustrate the degree of heterogeneity in the *Scn2b* null atrial data set. I propose that this dispersion of repolarization in individual cells generates functionally heterogeneous substrates in the *Scn2b* null atrium that predispose the tissue to wavebreak during fast pacing.

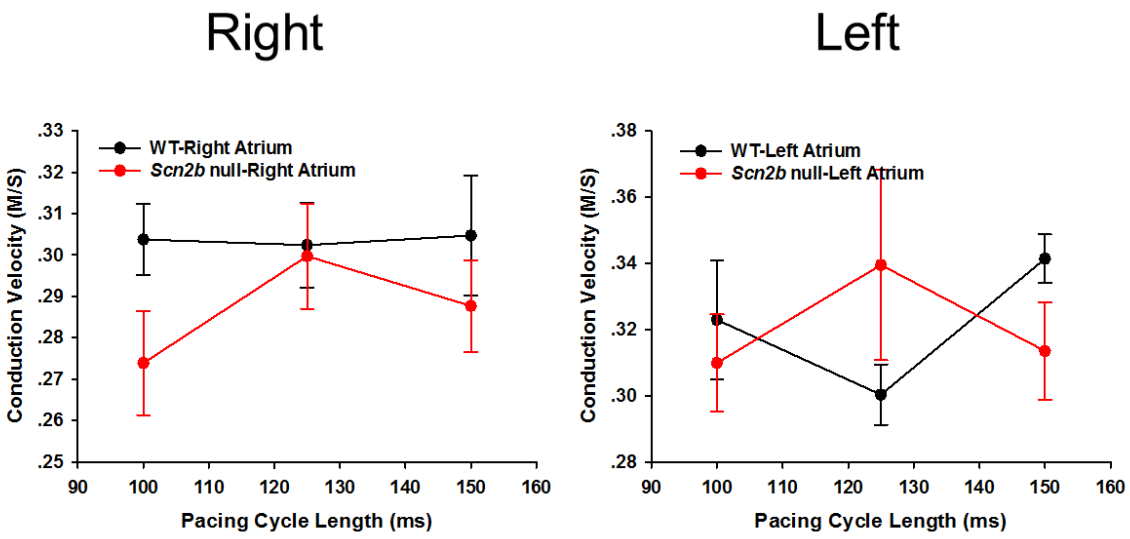

Figure 14 Conduction velocity is not altered in Scn2b null atria.

Right atria, *Scn2b* null: N=9; WT: N=9, Left atria, *Scn2b* null: N=7; WT: N=7.

Significance determined using Student's T test.

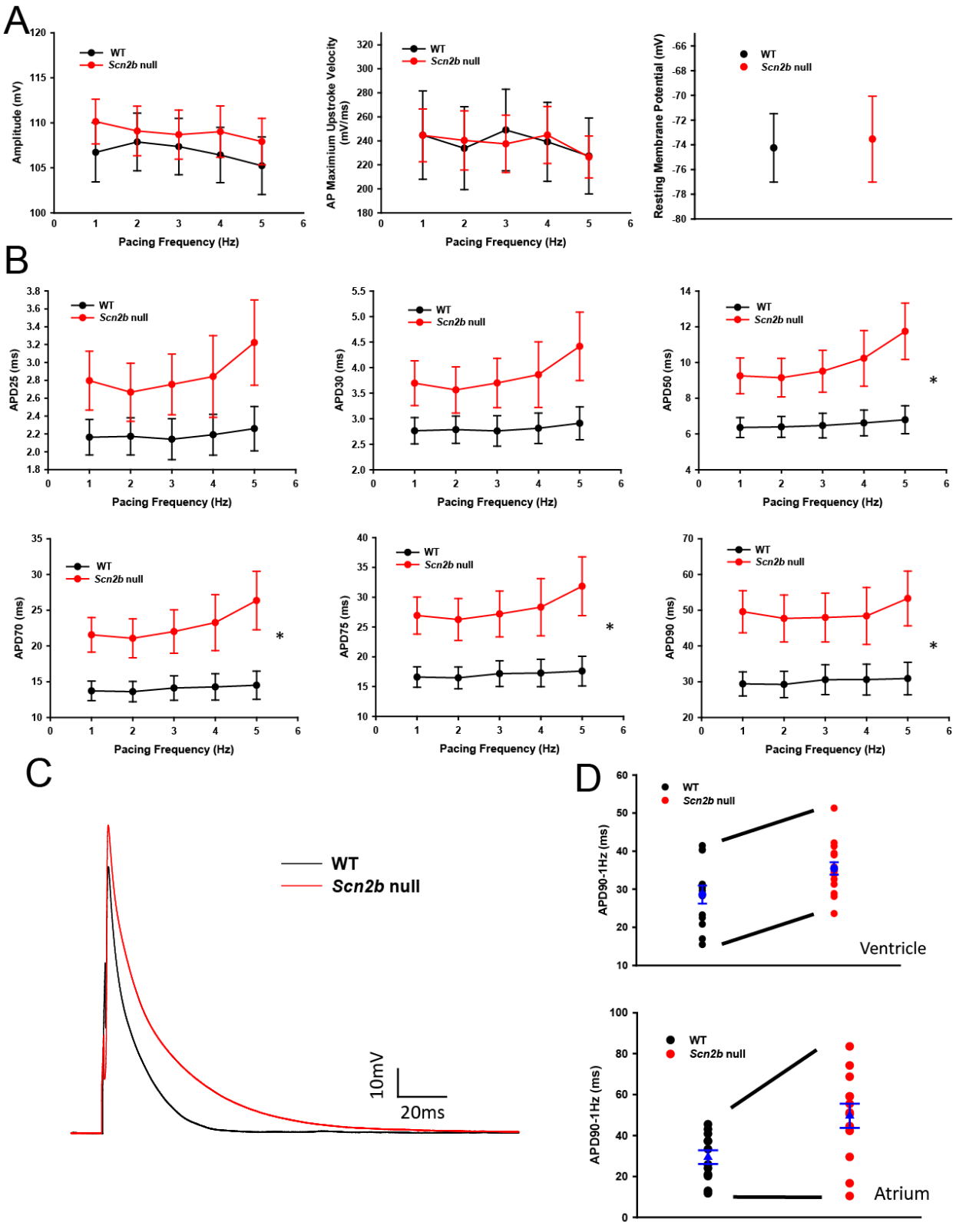

Figure 15 AP recordings from right atrial myocytes.

A. No differences between genotypes were found in AP amplitude, AP maximum upstroke velocity, or resting membrane potential. B. APD_{50-90} were prolonged in the *Scn2b* null group (* $P<0.05$). C. Representative superimposed AP traces from *Scn2b* null and WT myocytes. D. Distribution of the APD_{90} data paced at 1 Hz from ventricular and atrial myocytes. The increase in ventricular APD observed in *Scn2b* nulls is homogenous, shifting the entire data set upward. In contrast, APD lengthening in atrial myocytes is heterogeneous, resulting in a more dispersed distribution of the data set (*Scn2b* null: N=4 mice n=13 cells; WT: N=5 mice n=12 cells, Student's T test).

Increased fibrosis in *Scn2b* null right atrium

Evidence in the literature connects cardiac VGSC dysfunction to fibrosis[174–176]. To assess the level of fibrosis in our *Scn2b* null model, the posterior walls of both right and left atria were sectioned in the coronary plane and stained using Masson's trichrome protocol. I observed an increased level of fibrosis in the right, but not the left *Scn2b* null atria compared to WT (Fig. 16 A-B). I propose that the fibrotic tissue deposited in the *Scn2b* null right atrial interstitial space creates anatomical substrates for wavebreaks as well as anchor points for rotors, and may explain transitions from atrial fibrillation to atrial flutter in the null animals (e.g. Fig. 16C).

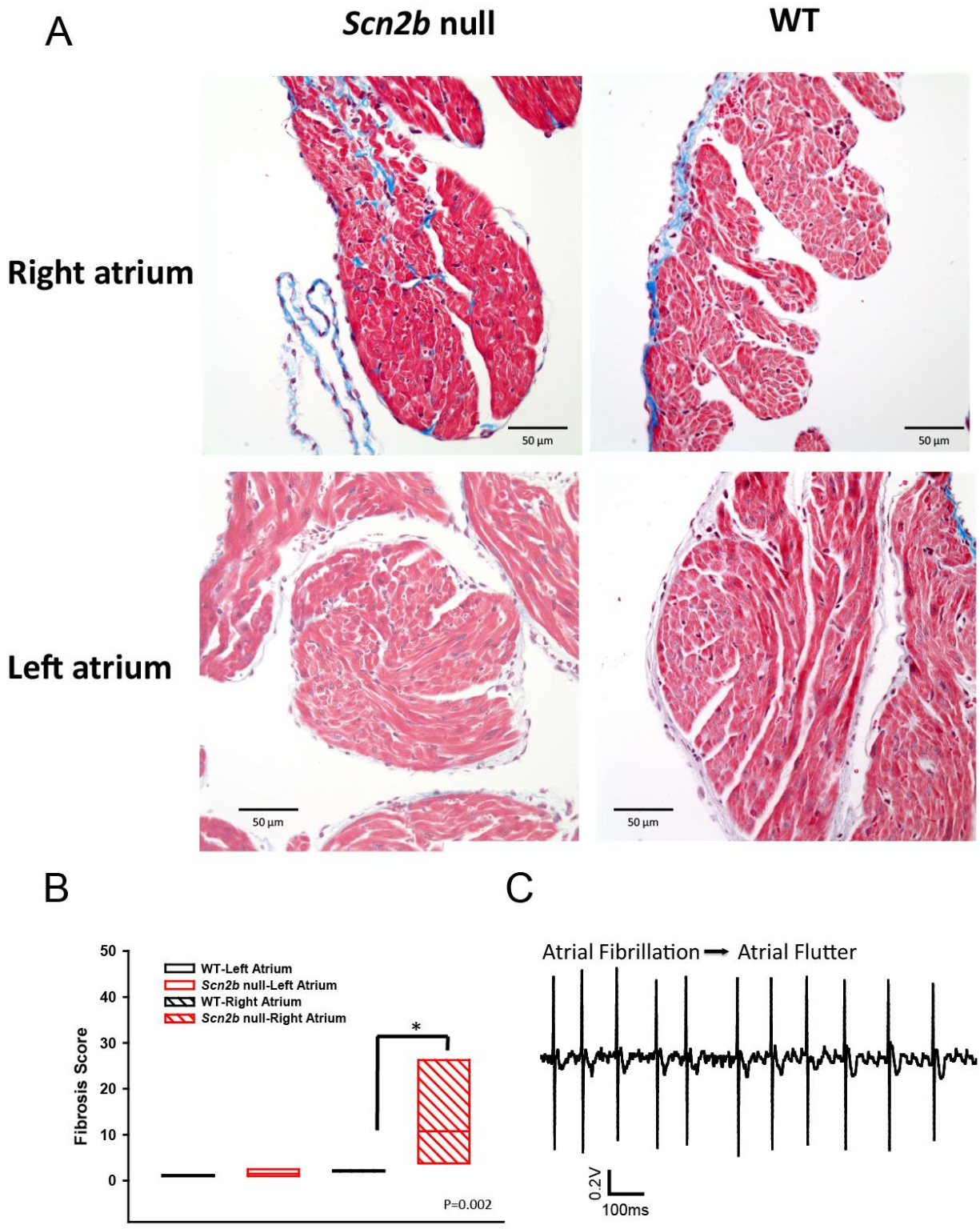

Figure 16 Increased fibrosis in Scn2b null right atrium.

A. Masson's trichrome staining shows increased fibrosis (blue) in *Scn2b* null right atria but not left atria compared to WT. B. Quantification of fibrosis using a scoring system ($p=0.002$, Mann-Whitney Rank Sum Test). Six 8-9 month old animals were included from each genotype. C. Transition of atrial fibrillation to atrial flutter in *Scn2b* null atrium. Increased levels of fibrosis are proposed to provide anchoring points for rotors underlying the transition.

Discussion

AF in BrS

AF is the most prevalent clinical arrhythmia[177], with even higher incidence in BrS patients compared to the general population (5.7%-53% *vs*. 1%-2%, respectively) [178–182]. Both loss- and gain-of-function mutations in *SCN5A* have been linked to familiar AF [172]. The two known AF patients with *SCN2B* mutations exhibited saddleback type ST segment elevation in the right precordial leads, further supporting a close connection between BrS and AF[48]. Loss of *SCN5A* function has been shown to both facilitate and inhibit AF in different BrS patients[183]. Decreased atrial conduction velocity is predicted to favor AF due to shortened wavelength, while concomitant lowered excitability is thought to reduce AF triggers. Thus, *SCN5A*-linked BrS may provide AF substrates rather than increase spontaneous AF occurrence. In line with this hypothesis, the incidence of spontaneous AF does not differ between patients with and without *SCN5A* mutations [181–183]. In contrast, *SCN5A*-linked BrS patients exhibit longer intra-atrial conduction time, increased left atrial volume index, and higher AF inducibility (46.7% *vs* 20.7%) [181,182]. Further, the prevalence of persistent AF is higher in this subgroup of patients[183]. In one of the lone paroxysmal AF patients with a *SCN2B* mutation, left atrial enlargement was identified[48]. Thus, in more advanced AF, which often involves electrical and anatomical remodeling, VGSC α or β subunit gene mutations may facilitate disease progression by providing arrhythmogenic substrates.

I found atrial conduction to be unaltered in *Scn2b* null mice. There were no differences in AP maximum upstroke velocity in single cell recordings, no differences in conduction velocity measured by optical mapping of atrial tissue, and no differences in P wave duration or AH interval acquired in ECG and intracardiac recording. These results suggest that, unlike in the ventricle, atrial I_{Na} is unchanged in response to *Scn2b* deletion. Instead, loss of β2 has extensive effects on AP repolarization and tissue remodeling. The APD was increased in a heterogeneous fashion in *Scn2b* null atrium, resulting in larger repolarization dispersion. In addition, higher levels of fibrosis were found preferentially in *Scn2b* null right atrium. These changes are proposed to provide electrical and anatomical substrates that favor AF, and thus explain the higher susceptibility of *Scn2b* null atrium to AF. The proposed increased heterogeneity of *Scn2b* null atrium is supported by our finding that the number, frequency, location, and organization of rotors are highly dynamic and complex.

Fibrosis in Scn2b null atria

Links between VGSC dysfunction and fibrosis have been demonstrated in the heart. For example, TGF-β1-mediated fibrosis is triggered by *Scn5a* disruption, suggesting a common signaling pathway[176]. In addition, VGSC β2 subunits are substrates for sequential cleavage by BACE-1 and γ-secretase[78]. The cleaved intracellular domain of β2, at least in neurons, translocates to the nucleus to participate in transcriptional regulation of VGSC α subunits and possibly other genes. Thus, the cleaved β2 intracellular domain may normally regulate genes that inhibit fibrosis in the heart. In the absence of β2, fibrotic gene expression may proceed unchecked. Interestingly, fibrosis

is increased in *Scn2b* null right atrium but not in left atrium. This chamber preference was also seen in a TGF- β1 overexpression model of atrial fibrosis and AF[184], implying that the TGF- β1 signaling pathway may also be involved in the mechanism of fibrosis in *Scn2b* null hearts. This question is, however, beyond the scope of the present study.

Role of β2 in cellular electrophysiology

Scn2b deletion results in a ~50% reduction in total I_{Na} density as well as a hyperpolarizing shift and altered slope factor of the voltage-dependence of activation in mouse ventricular myocytes, suggesting that β2 subunits have dramatic effects on ventricular I_{Na} *in vivo*. While heterologous expression studies are a convenient first approach to gain structure-function information[129], co-expression of β2 with $Na_V1.5$ in heterologous cell lines has little to no effect on I_{Na} density, kinetics, or gating properties[12,22,48]. This confusion between *in vivo* and *in vitro* results raises concerns about how to interpret data derived from heterologous systems when modeling electrophysiological properties of myocytes. To add to this complexity, repolarization, rather than depolarization, was more severely affected in *Scn2b* null atrial myocytes compared to *Scn2b* null ventricular cells, implying cell type specific functional roles of β2, possibly through differential multi-protein complex formation or differences in post-transcriptional modification in atrium *vs* ventricle. Solving these important issues will be critical to completely understanding the roles of VGSC α and β subunits in cardiac physiology.

CHARPTER V

Conclusion and Future Directions

Voltage-gated sodium channels (VGSCs) are critical for impulse initiation and propagation in excitable cells, including nerve and muscle. The ion-conducting VGSC α subunits are modulated by two β subunits that do not form the pore but play essential roles in electrical signal transduction. VGSC β subunits signal through multiple pathways on multiple time scales *in vivo* and, at least for β1, are essential for life. In addition to regulating sodium current, β subunits associate with potassium channels and play non-ion-conducting roles as cell adhesion molecules (CAMs) that participate in cell-cell coupling and macromolecular complex formation. Mutations in genes encoding VGSC β subunits disrupt both sodium and potassium channel complexes as well as cell-cell communication, leading to heart and brain diseases that can be catastrophic. In my PhD thesis work, I investigated the physiological roles of VGSC β2 in the heart using the *Scn2b* null mouse model. *Scn2b* deletion results in electrical abnormalities in both atrium and ventricle. Defects in both depolarization and repolarization were observed in the ventricle, similar to human Brugada syndrome (BrS). We also found an increased propensity of the *Scn2b* null atrium to atrial fibrillation (AF), consistent with the higher prevalence of AF in human BrS patients. We conclude that *Scn2b* null mice are a useful new tool for modeling cases of human BrS with susceptibility to atrial arrhythmia. *Scn2b*

null mice also appear to have altered autonomic control, adding neuronal complexity to this unique cardiac arrhythmia model. This study provides insight into the role of VGSC β2 in maintaining normal cardiac electrical activity, introduces a murine model that will be useful in understanding the mechanism of human BrS, and provides a novel perspective on the connection between BrS and atrial fibrillation in patients who carry VGSC gene mutations.

β2 subunits modulate K^+ channels?

Ventricular and atrial APDs were both prolonged in *Scn2b* null myocytes, but in different fashions, raising the possibility that repolarizing currents such as K^+ currents were also modulated by β2. β subunits are multifunctional molecules that are not specific to VGSC complexes. β1 co-assembles with and modulates the properties of the $K_V4.x$ subfamily of channels that underlie I_{to} in heart and I_A in brain[37,38,110]. The *SCN1B* mutation p.R214Q, which selectively affects β1B and not β1, is proposed to contribute to the arrhythmogenesis of BrS by concomitantly decreasing I_{Na} and increasing I_{to}[36]. Thus, profiling ionic currents in *Scn2*b null myocytes will provide important insights into the potential relationship of β2 with other cardiac ion channels. Direct channel modulation, transcriptional modification, trafficking, or compensatory effects are putative mechanisms of how β2 may affect other channels. Filling these knowledge gaps will not only reveal novel functions of β2, but also provide alternative explanations for arrhythmogenesis.

Atrial cardiomyopathy?

Scn2b null atria exhibited higher susceptibility to atrial tachyarrhythmia due to electrical as well as anatomical remodeling. However, I found that these mice had not yet developed spontaneous AF. According to the definition provided in the 2007 ESC statement on classification of cardiomyopathies, cardiomyopathies are defined by structural and functional abnormalities of the ventricular myocardium that are unexplained by flow-limiting coronary artery disease or abnormal loading conditions[185]. Though the definition does not include atria, I propose that the atrial phenotype of *Scn2b* null mice could be practically defined as atrial cardiomyopathy. The difference between AF-induced atrial remodeling and primary atrial cardiomyopathy is that fibrosis in the *Scn2b* null is due to a direct response to gene deletion rather than the auto-reinforcing property of AF. Nevertheless, fibrosis in each scenario may share common signaling pathways. Thus, understanding the role of β2 in fibrosis will be beneficial to developing new therapeutic approaches to the AF. TGF-β1-mediated fibrosis is triggered by *Scn5a* disruption in the heart, suggesting links between VGSC dysfunction and fibrosis[176]. The TGF-β1/SMAD pathway is also involved in structural remodeling in AF[186]. Fibrosis promotes AF by interrupting fiber continuity and interacting with myocytes[187]. Novel upstream approaches such as interfering with the TGF-β1 signaling pathway may prevent atrial fibrillation progression[188], in which case, VGSC β2 could be a putative target.

Role of β2 in the autonomic nervous system?

Altered autonomic control was implied in *Scn2b* null mice. We showed previously that β2 is extensively expressed in the central and peripheral nervous systems, where it modulates neuronal sodium channels[104,105,169], and potentially contributes to autonomic control of the heart. The autonomic nervous system plays an important role in the modulation of cardiac electrophysiology and arrhythmogenesis[189]. A detailed investigation of the role of β2 in autonomic regulation will be essential for us to have a full picture of arrhythmogenesis in patients who carry *SCN2B* mutations.

Large-animal models are a better alternative for arrhythmia studies

Although *Scn2b* null mice recapitulated the pathophysiology of BrS and allowed us to have greater insight into the mechanism of this disease, mice cannot phenocopy human BrS ECG manifestations due to poorly defined J-points and lack of ST segments. These disparities in ECG waveforms result from distinct action potential morphologies between human and mouse myocytes[150]. The J-point in human ECGs is postulated to be equivalent to the end of J wave in the mouse ECG, corresponding to the moment when the potential is equal throughout the heart in the frontal plane, according to a study by Boukens *et al* at under baseline conditions[190]. However, in mice carrying *Scn5a* BrS mutatiosn or challenged by the VGSC blocker, ajmaline, the QRS is no longer an accurate measure of conduction time. Subsequently, the end of the J wave no longer represents the moment of baseline condition. Thus, genetically manipulated larger animal models, which share more common features with humans including heart size and cardiac electrophysiology, should be the focus of future studies. For example,

transgenic rabbits that carry loss-of function mutations in HERG potassium channels successfully model human Long QT syndrome type 2 (LQT2)[191]. Genetically engineered pig hearts carrying a BrS-associated *SCN5A* nonsense mutation (*SCN5A*$^{E558X/+}$) exhibited conduction defects and arrhythmias[192], phenocopying many aspects of human BrS. So far, all human cardiac arrhythmia associated *SCN2B* mutations are heterozygous, thus, investigating large-animal hearts carrying one *SCN2B* mutant allele will allow electrophysiological and molecular studies of arrhythmic mechanisms.

iPSC-CM as cellular models for ion channel mutation study

As discussed in Chapters I and IV, there are critical limitations to using heterologous expression systems as cellular *in vitro* models of arrhythmia. Results from these experiments may misguide us in attributing molecular mechanism of arrhythmia to channel electrophysiological alterations that are only observable in heterologous systems. Besides, low penetrance and variable expressivity of ion channel mutations, which may stem from epigenetic factors, age, gender, or genetic modifiers, add complexity in understanding pathogenesis. Thus, utilizing a cellular model that can recapitulate a patient's unique genetic background as well as maintain all interacting proteins, such as human induced pluripotent stem cell derived cardiomyocytes (iPSC-CMs) will be valuable to future work[127]. In addition, patient-specific iPSC models will be invaluable tools for drug screening[128] and the development of individualized therapies. An important next step to continue my *SCN2B* work would be to collect human skin biopsy samples from diseased *SCN2B* mutation carriers, reprogram them to pluripotency, and then differentiate them to cardiomyocytes for functional assessment.

A better knowledge of genotype-to-phenotype correlations will necessarily become the basis not only for mechanistic studies but also for more precise risk stratification and prognosis estimation for specific patients.

β2: A future therapeutic target for BrS?

The implantation of an ICD is the only proven effective therapeutic strategy for the prevention of sudden cardiac death (SCD) in BrS patients[193]. However, this therapy has a high complication rate, in which the major difficulty is inappropriate shocks[194–196]. If a BrS patient concomitantly has atrial arrhythmia, this can be an important cause of inappropriate ICD shocks[197]. Moreover, patients who receive ICD shocks may also develop psychological distress and have reduced quality of life (QoL)[198]. Thus, gene therapy may potentially be the ultimate solution to provide long term relief to channelopathy patients. Recently, single delivery of an Adeno-Associated Viral (AAV) construct to transfer the *CASQ2* gene to knock-in mice affected by catecholaminergic polymorphic ventricular tachycardia was demonstrated to cure the disease from birth to advanced age[199]. Similarly, as an important multi-functional modulatory molecule in ion channel macromolecular complexes, gene transfer of WT *SCN2B* may be efficacious to BrS patients who carry VGSC loss-of-function mutations.

Summary

Work presented here provides a broad view of the electrophysiological roles of β2 in the heart as well as mechanistic insights into ventricular and atrial arrhythmogenesis,

bridging molecular findings with clinical consequences in a murine model. My work highlights the importance of this multi-functional molecule and lays the groundwork for subsequent studies in large animal models and patient-derived iPSC-CMs. Future studies should include investigating the impact of β2 on other cardiac and autonomic nervous system ion channels, using novel animal and cellular models, elucidating the role of β2 in fibrosis, and developing gene therapy for primary cardiac arrhythmia. Elucidating the multi-faceted functions of β2 in the heart not only advances our understanding of the mechanism of arrhythmia, but also advances personalized therapy for arrhythmia in the new era of precision medicine.

CHAPTER VI

Methods

Animals

Male and female *Scn2b* null mice, congenic on the C57BL/6J background for over 20 generations, were used at the ages indicated in the figure legends. Mouse genotyping was described previously[104].

Ethics statement

This study was carried out in accordance with the recommendations in the Guide for the Care and Use of Laboratory Animals of the National Institutes of Health. The protocol was approved by the University Committee on the Use and Care of Animals at the University of Michigan. All efforts were made to minimize animal suffering.

Cell isolation

Ventricular myocyte isolation for I_{Na} recording

WT and *Scn2b* null cardiac myocytes were acutely isolated from 2-3 month old mice of both genders using a protocol described in Auerbach et al[200]. In brief, hearts were

isolated and were cannulated with perfusion buffer (37°C, 3 ml/min). After blood was cleared out, Type-II collagenase (0.87 mg/ml, Worthington Biochemical), trypsin (0.14 mg/ml), and 12 μM $CaCl_2$ were added to the perfusion buffer for digestion. The digestion time last for 3-4 min. The lower two-thirds of the ventricles (including both left and right ventricle) were isolated and minced in the digestion buffer into small pieces. Reaction was then stopped by stopping buffer, which included perfusion buffer plus 10% fetal bovine serum and 12.5 μM $CaCl_2$. Ca^{2+} concentration was finally increased to 1mM incrementally by 5-step addition of $CaCl_2$ at 37 °C. Only quiescent myocytes were chosen for electrophysiological recordings.

Right ventricular outflow track (RVOT) myocyte isolation

RVOT myocyte isolation was similar to that described above. However, instead of isolating the lower two-thirds of the heart, the RVOT anterior free wall corresponding to the slowed conduction area in optical mapping (see below), were cut from 2-4 month old male mice. Tissues were minced in digestion buffer followed by steps similar to those described above.

Isolation of atrial myocytes

This procedure was similar to the ventricular myocyte isolation described above but with the following changes: 1.25g/25ml Liberase TM (Roche) was added to the digestion buffer during perfusion. Digestion time was modified to 12-18 min. 2-3 month old mice of both genders were used. To minimize the known AP heterogeneity between left and right atria[201], only the right atrial region to the right of the crista terminalis was isolated.

Single Cell Electrophysiology

Standard voltage and current clamp techniques were used to assess the effects of *Scn2b* deletion on cardiac I_{Na} and AP properties, respectively. Borosilicate glass pipettes with resistance of <3MΩ for I_{Na} and 3-5 MΩ for AP recordings were used. Data were acquired using an Axopatch 200B amplifier and Axopatch 700B (Molecular Devices, USA). The data were analyzed using pCLAMP9-10 (Molecular Devices, USA) and custom AP analysis software (National Instruments LabView, USA)

Voltage Clamp Recordings

Voltage clamp I_{Na} recordings were performed at room temperature (21–22°C). The extracellular solution contained (in mM): 5 NaCl, 1 $MgCl_2$, 1 $CaCl_2$, 0.1 $CdCl_2$, 11 Glucose, 132.5 CsCl, and 20 HEPES. The filling solution contained (in mM): 5 NaCl, 135 CsF, 10 EGTA, 5 MgATP, and 5 HEPES. After sealing and breaking into the cells, series resistance compensation (prediction and correction <75%) and leak subtraction were applied. Transient and persistent I_{Na} density, I_{Na} inactivation time, and the voltage dependence of I_{Na} conductance were obtained at voltage between -100 and +30 mV using a holding potential of -120 mV. Every step last for 200 ms, with 2800 ms interpulse time. The voltage dependence of I_{Na} availability was determined by holding at various voltages (-160 mV to 0 mV, 5 mV increments, 200 ms duration) and stepping to -40 mV (30 ms), with 2770 ms interpulse intervals at -120 mV. Boltzmann function was fitted to gain the normalized voltage dependence of I_{Na} availability. And then differences in the $V_{½}$ and slope factor were compared between groups. The time dependence of I_{Na}

recovery was assessed by using two evoking pulse (P1 and P2) at -30mV with various interpulse interval. Holding potential was at -120 mV. The time dependence of I_{Na} recovery was calculated by P2/P1 at each time point, and these results were fit to a single exponential function. The rate of I_{Na} inactivation was fit to a double exponential function. Persistent I_{Na}, measured 50-52 ms after the voltage step, when the current amplitude was stable.

Current Clamp Recordings

Current clamp recordings of APs were acquired at 37°C in standard Tyrode solution (in mM): 148 NaCl, 0.4 NaH_2PO4, 1 $MgCl_2$, 5.4 KCl, 1 $CaCl_2$, 5.5 glucose, 15 HEPES. The internal solution included (in mM): 140 KCl, 5 EGTA-KOH, 10 HEPES. Incremental amounts of current (100 pA steps, 1 ms) were used to map the threshold of current to evoke an AP. Then, 1.5-fold of that current was used for AP recordings at different pacing cycle lengths (200-1000 ms). Only cells with a diastolic membrane potential more negative than -65 mV were included.

Super-resolution scanning patch clamp

This method combined scanning ion conductance microscopy (SICM) with cell-attached patch clamp technology for recording of ion channels at a particular subcellular location. A detailed description of this technique can be found in the previous work of Bhargava *et al*[132]. Briefly, after mapping the topography of the cardiomyocyte surface with SICM, the pipette tip was clipped against the bottom of the dish until appropriate resistence was reached. Then the pipette was repositioned to spatial coordinates that were

selected based on the topography image recorded. Pipette was lowered to the selected location to record sodium channels in the cell-attached configuration.

Optical Mapping

Ventricular mapping

3-6 month old male mice were heparinized (0.5 U/g i.p.) and then euthanized. The heart was excised and placed in ice-cold cardioplegic solution, then it was cannulated and retrogradely perfused through the aorta with warm (36.8 ± 0.3 °C), oxygenated (100% O_2) Tyrodes solution containing (in mM) 130 NaCl, 1.2 NaH_2PO_4, 1.0 $MgCl_2$, 4.0 KCl,1.8 $CaCl_2$, 5.6 glucose, and 25.0 HEPES, pH 7.4. 20-30 min The preparation was equilibrated for 20-30min before any pacing maneuver. Volume-conducted ECGs were acquired in pseudo lead 2 configuration and digitized at 1 KHz (MiniDigi1A digitizer and AxoScope software; Axon Instruments). The preparation was then perfused with 7 μM Blebbistatin (Cayman Chemical), a mechanical uncoupler, to immobilize the heart. A voltage-sensitive fluorescent dye, 100 μM Di-4-ANEPPS (Life Technologies), was used to stain the heart. A CCD camera with 80 × 80 pixel (SciMeasure) was anchored to a SMZ-1000 dissection microscope (Nikon). This high-resolution image system can image a 6.4 × 6.4-mm area at 800 frames per second, which providing a spatial resolution of 80 μm per pixel. The heart was positioned under the microscope allowing the camera to capture the anterior ventricular epicardium including left ventricle, right ventricle, and apex. Optical movies (4 s) were acquired under 532-nm fluorescence excitation (argon laser, 1 W) and 640 ± 20 nm emission. Optical movies were recorded at baseline and at RV apex pacing. The pacing cycle lengths was175 ms to 100 ms. Analysis was

performed using custom-made software. To visualize arrhythmia, phase maps were generated as described elsewhere[101].

Atrial Mapping

This procedure was similar to ventricular mapping. 8-9 month old mice of both genders were used. Instead of cannulation, we excised the whole atrium along the AV rings (mitral and tricuspid), pinned the preparation to a sylgard gel coated dish and superfused the tissue with warm (36.8 ± 0.3 °C), oxygenated (100% O2) Tyrodes solution. The CCD camera was positioned to face the posterior wall of both atria. Optical movies were recorded at baseline and at progressively shorter basic cycle lengths (125 ms to 100 ms) during right atrium appendage pacing. Arrhythmia inducibility was assessed by applying 2 atrial electric stimulations (bursting pacing at 66.67 HZ for 5 or 10 seconds) before and after the carbachol (Cch, 300 nM) administration.

ECG and intracardiac recording

In vivo studies were performed in two sets of mice. One set included 2-3 month old mice and were anesthetized by Avertin (1.2%, 0.23ml/10g i.p. prepared from 2,2,2-tribromoethanol and 2-methyl-2-butanol, Sigma). The other set included 7-9 month old mice that were anesthetized with isofluorane (induction period 5.0% vol. maintenance, 2.0% vol. isofluorane in 70%N_2/30%O_2 for further intracardiac recording). Following the achievement of surgical anesthesia, mice were placed onto a temperature-regulated operating table. Platinum electrodes (Natus Neurology) were inserted subcutaneously in

the limbs and connected to a DSI digital communication module and then to the DSI ACQ-7700 - acquisition interface (Data Sciences International) for a standard lead-II ECG. Standard ECG parameters (HR, P wave duration and PR interval, QRS duration, QT interval) were analyzed under stable baseline conditions with 1.5% vol. isofluorane. A 1.1 French octapolar stimulation-recording catheter (FTS-1113A-0518, Science) was inserted through the jugular vein and advanced into the right atrium and ventricle. Programmed electrical stimulation was assessed to determine the basal sinus node recovery time (SNRT) by applying S1S1 protocol at 120 ms and 90 ms of cycle length (CL), while the atrial refractory period (AERP), atrio-ventricular nodal effective refractory period (AVERP), and ventricular refractory period (VERP) were estimated by delivery of a S1-S1-S2 protocol with a fixed S1 (100ms and 80ms CL) and reducing S2 every 2 ms. Arrhythmia inducibility was assessed by apply 12-18 atrial bursts of pacing (50 HZ for 2 or 5 sec) before and after the i.p. carbachol (Cch, 50 ng/g) application. AF was defined as the occurrence of rapid and fragmented atrial electrograms (lack of regular P waves) with irregular AV-nodal conduction and ventricular rhythm lasting at least 1 sec. The entire procedure was completed in less than 2 h.

Assessment of Fibrosis

Atria from 8-9 month old mice of each gender were collected for histology. Only posterior walls of each side were collected. For the right atrium, tissue that was to the right of the crista terminalis was excised to eliminate collection of SA nodal tissue. Tissues were fixed in 10% formalin and submitted to the University of Michigan Unit for Laboratory Animal Medicine In-vivo Animal Core facility for sectioning and further

analysis using Masson's Trichrome staining. Tissue sections were analyzed for the degree of fibrosis using Aperio© software. The color deconvolution algorithm was used to quantify the connective tissue component of each section. The slides were viewed on ImageScope©. The intensity of the blue staining was measured in areas outlined by a veterinary pathologist. The area and intensity of the staining were scored as weak, medium, or dark according to windows set by calibration of the slides using the algorithm. To account for differences in staining intensity and distribution between slides, a total score was derived from (3 x strong) + (2 x medium) + (1 x week) intensity, as recommended by the software manufacturer.

Statistics

Results are expressed as mean ± SEM. Statistical significance was evaluated using t test, Mann-Whitney rank sum test, or Fisher's exact test, as indicated in the figure legends. $P<0.05$ was considered statistically significant. All calculations were performed using SigmaPlot 11.2 (Systat Software Inc, San Jose California USA).

BIBLIOGRAPHY

1. Veeraraghavan R, Gourdie R, Poelzing S. Mechanisms of Cardiac Conduction: A History of Revisions. *Am J Physiol Heart Circ Physiol*. 2014;(540):1–40. doi:10.1152/ajpheart.00760.2013.

2. Catterall W a. Voltage-gated sodium channels at 60: structure, function and pathophysiology. *J Physiol*. 2012;590(Pt 11):2577–89. doi:10.1113/jphysiol.2011.224204.

3. Morgan K, Stevens EB, Shah B, et al. β3: An additional auxiliary subunit of the voltage-sensitive sodium channel that modulates channel gating with distinct kinetics. *Proc Natl Acad Sci*. 2000;97(5):2308–2313. doi:10.1073/pnas.030362197.

4. Kazen-Gillespie KA, Ragsdale DS, D'Andrea MR, Mattei LN, Rogers KE, Isom LL. Cloning, Localization, and Functional Expression of Sodium Channel β1A Subunits. *J Biol Chem*. 2000;275(2):1079–1088. doi:10.1074/jbc.275.2.1079.

5. Yu FH, Westenbroek RE, Silos-Santiago I, et al. Sodium Channel β4, a New Disulfide-Linked Auxiliary Subunit with Similarity to β2. *J Neurosci*. 2003;23(20):7577–7585. Available at: http://www.jneurosci.org/content/23/20/7577.abstract.

6. Isom LL, De Jongh KS, Patton DE, et al. Primary structure and functional expression of the β1 subunit of the rat brain sodium channel. *Science*. 1992;256(5058):839–42. Available at: http://www.jstor.org/stable/2877043. Accessed February 23, 2014.

7. Isom LL, Ragsdale DS, De Jongh KS, et al. Structure and function of the β2 subunit of brain sodium channels, a transmembrane glycoprotein with a CAM motif. *Cell*. 1995;83(3):433–442. doi:10.1016/0092-8674(95)90121-3.

8. Isom LL. The role of sodium channels in cell adhesion. *Front Biosci*. 2002;7:12–23.

9. Brackenbury WJ, Isom LL. Na Channel β Subunits: Overachievers of the Ion Channel Family. *Front Pharmacol*. 2011;2:53. doi:10.3389/fphar.2011.00053.

10. Malhotra JD, Thyagarajan V, Chen C, Isom LL. Tyrosine-phosphorylated and nonphosphorylated sodium channel β1 subunits are differentially localized in cardiac myocytes. *J Biol Chem*. 2004;279(39):40748–40754. doi:10.1074/jbc.M407243200.

11. Patino GA, Brackenbury WJ, Bao Y, et al. Voltage-Gated Na^+ Channel β1B: A Secreted Cell Adhesion Molecule Involved in Human Epilepsy. *J Neurosci*. 2011;31(41):14577–14591. doi:10.1523/jneurosci.0361-11.2011.

12. Chen C, Calhoun JD, Zhang Y, et al. Identification of the cysteine residue responsible for disulfide linkage of Na^+ channel α and β2 subunits. *J Biol Chem*. 2012;287(46):39061–9. doi:10.1074/jbc.M112.397646.

13. Rosati B, Pan Z, Lypen S, et al. Regulation of KChIP2 potassium channel β subunit gene expression underlies the gradient of transient outward current in canine and human ventricle. *J Physiol*. 2001;533(Pt 1):119–25. Available at: http://www.pubmedcentral.nih.gov/articlerender.fcgi?artid=2278594&tool=pmcentrez&rendertype=abstract. Accessed February 27, 2014.

14. Dixon JE, McKinnon D. Quantitative analysis of potassium channel mRNA expression in atrial and ventricular muscle of rats. *Circ Res*. 1994;75(2):252–60. Available at: http://www.ncbi.nlm.nih.gov/pubmed/8033339. Accessed February 27, 2014.

15. Maier SK, Westenbroek RE, Yamanushi TT, et al. An unexpected requirement for brain-type sodium channels for control of heart rate in the mouse sinoatrial node. *Proc Natl Acad Sci U S A*. 2003;100(6):3507–3512. doi:10.1073/pnas.2627986100.

16. Lei M, Jones SA, Liu J, et al. Requirement of neuronal- and cardiac-type sodium channels for murine sinoatrial node pacemaking. *J Physiol*. 2004;559(3):835–848. doi:10.1113/jphysiol.2004.068643.

17. Lei M, Goddard C, Liu J, et al. Sinus node dysfunction following targeted disruption of the murine cardiac sodium channel gene *Scn5a*. *J Physiol*. 2005;567(2):387–400. doi:10.1113/jphysiol.2005.083188.

18. Marionneau C, Couette B, Liu J, et al. Specific pattern of ionic channel gene expression associated with pacemaker activity in the mouse heart. *J Physiol*. 2005;562(Pt 1):223–34. doi:10.1113/jphysiol.2004.074047.

19. Gaborit N, Le Bouter S, Szuts V, et al. Regional and tissue specific transcript signatures of ion channel genes in the non-diseased human heart. *J Physiol*. 2007;582(Pt 2):675–93. doi:10.1113/jphysiol.2006.126714.

20. Fahmi AI, Patel M, Stevens EB, et al. The sodium channel β-subunit *SCN3b* modulates the kinetics of *SCN5a* and is expressed heterogeneously in sheep heart. *J Physiol*. 2001;537(Pt 3):693–700. Available at: http://www.pubmedcentral.nih.gov/articlerender.fcgi?artid=2278985&tool=pmcentrez&rendertype=abstract. Accessed February 20, 2014.

21. Dominguez JN, Navarro F, Franco D, Thompson RP, Aranega AE. Temporal and spatial expression pattern of β1 sodium channel subunit during

heart development. *Cardiovasc Res*. 2005;65(4):842–850. doi:10.1016/j.cardiores.2004.11.028.

22. Malhotra JD, Chen C, Rivolta I, et al. Characterization of Sodium Channel α- and ß-Subunits in Rat and Mouse Cardiac Myocytes. *Circulation*. 2001;103(9):1303–1310. doi:10.1161/01.cir.103.9.1303.

23. Maier SKG, Westenbroek RE, McCormick KA, Curtis R, Scheuer T, Catterall WA. Distinct subcellular localization of different sodium channel alpha and β subunits in single ventricular myocytes from mouse heart. *Circulation*. 2004;109(11):1421–7. doi:10.1161/01.CIR.0000121421.61896.24.

24. Westenbroek RE, Bischoff S, Fu Y, Maier SKG, Catterall WA, Scheuer T. Localization of sodium channel subtypes in mouse ventricular myocytes using quantitative immunocytochemistry. *J Mol Cell Cardiol*. 2013;64:69–78. doi:10.1016/j.yjmcc.2013.08.004.

25. Kaufmann SG, Westenbroek RE, Maass AH, et al. Distribution and function of sodium channel subtypes in human atrial myocardium. *J Mol Cell Cardiol*. 2013;61:133–41. doi:10.1016/j.yjmcc.2013.05.006.

26. Hashemi SM, Hund TJ, Mohler PJ. Cardiac ankyrins in health and disease. *J Mol Cell Cardiol*. 2009;47(2):203–9. doi:10.1016/j.yjmcc.2009.04.010.

27. Lowe JS, Palygin O, Bhasin N, et al. Voltage-gated Na_v channel targeting in the heart requires an ankyrin-G dependent cellular pathway. *J Cell Biol*. 2008;180(1):173–86. doi:10.1083/jcb.200710107.

28. Mohler PJ, Rivolta I, Napolitano C, et al. $Na_v1.5$ E1053K mutation causing Brugada syndrome blocks binding to ankyrin-G and expression of $Na_v1.5$ on the surface of cardiomyocytes. *Proc Natl Acad Sci U S A*. 2004;101(50):17533–17538. doi:10.1073/pnas.0403711101.

29. Sato PY, Coombs W, Lin X, et al. Interactions between ankyrin-G, Plakophilin-2, and Connexin43 at the cardiac intercalated disc. *Circ Res*. 2011;109(2):193–201. doi:10.1161/CIRCRESAHA.111.247023.

30. Agullo-Pascual E, Cerrone M, Delmar M. Arrhythmogenic Cardiomyopathy and Brugada Syndrome: Diseases of the connexome. *FEBS Lett*. 2014. doi:10.1016/j.febslet.2014.02.008.

31. Mohler PJ, Schott J-J, Gramolini AO, et al. Ankyrin-B mutation causes type 4 long-QT cardiac arrhythmia and sudden cardiac death. *Nature*. 2003;421(6923):634–9. doi:10.1038/nature01335.

32. Le Scouarnec S, Bhasin N, Vieyres C, et al. Dysfunction in ankyrin-B-dependent ion channel and transporter targeting causes human sinus node

disease. *Proc Natl Acad Sci U S A*. 2008;105(40):15617–22. doi:10.1073/pnas.0805500105.

33. Malhotra JD, Koopmann MC, Kazen-Gillespie KA, Fettman N, Hortsch M, Isom LL. Structural requirements for interaction of sodium channel β1 subunits with ankyrin. *J Biol Chem*. 2002;277(29):26681–8. doi:10.1074/jbc.M202354200.

34. Yang JS, Bennett PB, Makita N, George AL, Barchi RL. Expression of the sodium channel β1 subunit in rat skeletal muscle is selectively associated with the tetrodotoxin-sensitive α subunit isoform. *Neuron*. 1993;11(5):915–922. doi:10.1016/0896-6273(93)90121-7.

35. Makita N, Bennett PB, George AL. Voltage-gated Na^+ channel β1 subunit mRNA expressed in adult human skeletal muscle, heart, and brain is encoded by a single gene. *J Biol Chem*. 1994;269(10):7571–7578. Available at: http://www.jbc.org/content/269/10/7571.abstract.

36. Hu D, Barajas-Martínez H, Medeiros-Domingo A, et al. A novel rare variant in *SCN1Bb* linked to Brugada syndrome and SIDS by combined modulation of $Na_v1.5$ and Kv4.3 channel currents. *Hear Rhythm*. (0). doi:10.1016/j.hrthm.2011.12.006.

37. Deschênes I, Armoundas AA, Jones SP, Tomaselli GF. Post-transcriptional gene silencing of KChIP2 and Na_v β1 in neonatal rat cardiac myocytes reveals a functional association between Na and Ito currents. *J Mol Cell Cardiol*. 2008;45(3):336–46. doi:10.1016/j.yjmcc.2008.05.001.

38. Deschênes I, Tomaselli GF. Modulation of Kv4.3 current by accessory subunits. *FEBS Lett*. 2002;528(1-3):183–8. Available at: http://www.ncbi.nlm.nih.gov/pubmed/12297301.

39. Shy D, Gillet L, Abriel H. Cardiac Sodium Channel Na(V)1.5 Distribution in Myocytes via Interacting Proteins: The Multiple Pool Model. *Biochim Biophys Acta*. 2012. doi:10.1016/j.bbamcr.2012.10.026.

40. Qu Y, Isom LL, Westenbroek RE, et al. Modulation of Cardiac Na^+ Channel Expression in Xenopus Oocytes by β1 Subunits. *J Biol Chem*. 1995;270(43):25696–25701. doi:10.1074/jbc.270.43.25696.

41. An RH, Wang XL, Kerem B, et al. Novel LQT-3 mutation affects Na^+ channel activity through interactions between alpha- and β1-subunits. *Circ Res*. 1998;83(2):141–6. Available at: http://www.ncbi.nlm.nih.gov/pubmed/9686753. Accessed February 23, 2014.

42. Ko S-H, Lenkowski PW, Lee HC, Mounsey JP, Patel MK. Modulation of $Na_V1.5$ by β1 and β3 subunit co-expression in mammalian cells. *Pflugers Arch*. 2005;449(4):403–12. doi:10.1007/s00424-004-1348-4.

43. Moran O, Nizzari M, Conti F. Endogenous expression of the β1A sodium channel subunit in HEK-293 cells. *FEBS Lett*. 2000;473(2):132–134. doi:10.1016/s0014-5793(00)01518-0.

44. Moran O, Conti F, Tammaro P. Sodium channel heterologous expression in mammalian cells and the role of the endogenous β1-subunits. *Neurosci Lett*. 2003;336(3):175–179. doi:10.1016/s0304-3940(02)01284-3.

45. Moran O, Tammaro P, Nizzari M, Conti F. Functional Properties of Sodium Channels Do Not Depend on the Cytoskeleton Integrity. *Biochem Biophys Res Commun*. 2000;276(1):204–209. doi:10.1006/bbrc.2000.3463.

46. Meadows LS, Isom LL. Sodium channels as macromolecular complexes: implications for inherited arrhythmia syndromes. *Cardiovasc Res*. 2005;67(3):448–458. doi:10.1016/j.cardiores.2005.04.003.

47. Watanabe H, Koopmann TT, Le Scouarnec S, et al. Sodium channel β1 subunit mutations associated with Brugada syndrome and cardiac conduction disease in humans. *J Clin Invest*. 2008;118(6):2260–2268. doi:10.1172/JCI33891.

48. Watanabe H, Darbar D, Kaiser DW, et al. Mutations in sodium channel β1- and β2-subunits associated with atrial fibrillation. *Circ Arrhythm Electrophysiol*. 2009;2(3):268–275. doi:10.1161/CIRCEP.108.779181.

49. Grieco TM, Malhotra JD, Chen C, Isom LL, Raman IM. Open-Channel Block by the Cytoplasmic Tail of Sodium Channel β4 as a Mechanism for Resurgent Sodium Current. *Neuron*. 2005;45(2):233–244. doi:10.1016/j.neuron.2004.12.035.

50. Brackenbury WJ, Calhoun JD, Chen C, et al. Functional reciprocity between Na^+ channel $Na_v1.6$ and β1 subunits in the coordinated regulation of excitability and neurite outgrowth. *Proc Natl Acad Sci U S A*. 2010;107(5):2283–8. doi:10.1073/pnas.0909434107.

51. Wang GK, Edrich T, Wang S-Y. Time-Dependent Block and Resurgent Tail Currents Induced by Mouse β4154–167 Peptide in Cardiac Na^+ Channels. *J Gen Physiol*. 2006;127(3):277–289. doi:10.1085/jgp.200509399.

52. Medeiros-Domingo A, Kaku T, Tester DJ, et al. *SCN4B*-Encoded Sodium Channel β4 Subunit in Congenital Long-QT Syndrome. *Circulation*. 2007;116(2):134–142. doi:10.1161/circulationaha.106.659086.

53. Tan B-H, Pundi KN, Van Norstrand DW, et al. Sudden infant death syndrome–associated mutations in the sodium channel β subunits. *Hear Rhythm*. 2010;7(6):771–778. doi:10.1016/j.hrthm.2010.01.032.

54. Liu C, Tester DJ, Hou Y, et al. Is sudden unexplained nocturnal death syndrome in Southern China a cardiac sodium channel dysfunction disorder? *Forensic Sci Int*. 2014;236C:38–45. doi:10.1016/j.forsciint.2013.12.033.

55. Olesen MS, Holst AG, Svendsen JH, Haunsø S, Tfelt-Hansen J. *SCN1Bb* R214Q found in 3 patients: 1 with Brugada syndrome and 2 with lone atrial fibrillation. *Hear Rhythm*. 2012;9(5):770–773. doi:10.1016/j.hrthm.2011.12.005.

56. Yuan L, Koivumaki J, Liang B, et al. Investigations of the Na_v β1b sodium channel subunit in human ventricle; functional characterization of the H162P Brugada Syndrome mutant. *Am J Physiol Heart Circ Physiol*. 2014. doi:10.1152/ajpheart.00405.2013.

57. Lopez-Santiago LF, Meadows LS, Ernst SJ, et al. Sodium channel *Scn1b* null mice exhibit prolonged QT and RR intervals. *J Mol Cell Cardiol*. 2007;43(5):636–647. doi:10.1016/j.yjmcc.2007.07.062.

58. Riuró H, Beltran-Alvarez P, Tarradas A, et al. A missense mutation in the sodium channel β2 subunit reveals *SCN2B* as a new candidate gene for Brugada syndrome. *Hum Mutat*. 2013;34(7):961–6. doi:10.1002/humu.22328.

59. Olesen MS, Jespersen T, Nielsen JB, et al. Mutations in sodium channel β-subunit *SCN3B* are associated with early-onset lone atrial fibrillation. *Cardiovasc Res*. 2011;89(4):786–793. doi:10.1093/cvr/cvq348.

60. Hu D, Barajas-Martinez H, Burashnikov E, et al. A Mutation in the β3 Subunit of the Cardiac Sodium Channel Associated With Brugada ECG Phenotype / CLINICAL PERSPECTIVE. *Circ Cardiovasc Genet*. 2009;2(3):270–278. doi:10.1161/circgenetics.108.829192.

61. Valdivia CR, Medeiros-Domingo A, Ye B, et al. Loss-of-function mutation of the *SCN3B*-encoded sodium channel β3 subunit associated with a case of idiopathic ventricular fibrillation. *Cardiovasc Res*. 2010;86(3):392–400. doi:10.1093/cvr/cvp417.

62. Wang P, Yang Q, Wu X, et al. Functional dominant-negative mutation of sodium channel subunit gene *SCN3B* associated with atrial fibrillation in a Chinese GeneID population. *Biochem Biophys Res Commun*. 2010;398(1):98–104. doi:10.1016/j.bbrc.2010.06.042.

63. Hakim P, Gurung IS, Pedersen TH, et al. *Scn3b* knockout mice exhibit abnormal ventricular electrophysiological properties. *Prog Biophys Mol Biol*. 2008;98(2–3):251–266. doi:10.1016/j.pbiomolbio.2009.01.005.

64. Hakim P, Brice N, Thresher R, et al. *Scn3b* knockout mice exhibit abnormal sino-atrial and cardiac conduction properties. *Acta Physiol*. 2010;198(1):47–59. doi:10.1111/j.1748-1716.2009.02048.x.

65. Li R-G, Wang Q, Xu Y-J, et al. Mutations of the *SCN4B*-encoded sodium channel β4 subunit in familial atrial fibrillation. *Int J Mol Med*. 2013;32(1):144–50. doi:10.3892/ijmm.2013.1355.

66. Patino GA, Claes LRF, Lopez-Santiago LF, et al. A functional null mutation of *SCN1B* in a patient with Dravet syndrome. *J Neurosci*. 2009;29(34):10764–78. doi:10.1523/JNEUROSCI.2475-09.2009.

67. Ogiwara I, Nakayama T, Yamagata T, et al. A homozygous mutation of voltage-gated sodium channel β(I) gene *SCN1B* in a patient with Dravet syndrome. *Epilepsia*. 2012;53(12):e200–3. doi:10.1111/epi.12040.

68. Chen C, Westenbroek RE, Xu X, et al. Mice Lacking Sodium Channel β1 Subunits Display Defects in Neuronal Excitability, Sodium Channel Expression, and Nodal Architecture. *J Neurosci*. 2004;24(16):4030–4042. doi:10.1523/jneurosci.4139-03.2004.

69. Li A, Behr ER. Brugada syndrome: an update. *Future Cardiol*. 2013;9(2):253–71. doi:10.2217/fca.12.82.

70. Meregalli PG, Wilde A a M, Tan HL. Pathophysiological mechanisms of Brugada syndrome: depolarization disorder, repolarization disorder, or more? *Cardiovasc Res*. 2005;67(3):367–78. doi:10.1016/j.cardiores.2005.03.005.

71. Holst AG, Saber S, Houshmand M, et al. Sodium Current and Potassium Transient Outward Current Genes in Brugada Syndrome: Screening and Bioinformatics. *Can J Cardiol*. (0). doi:10.1016/j.cjca.2011.11.011.

72. Vatta M, Dumaine R, Varghese G, et al. Genetic and biophysical basis of sudden unexplained nocturnal death syndrome (SUNDS), a disease allelic to Brugada syndrome. *Hum Mol Genet*. 2002;11(3):337–45. Available at: http://www.ncbi.nlm.nih.gov/pubmed/11823453. Accessed February 18, 2014.

73. Ellinor PT, Nam EG, Shea M a, Milan DJ, Ruskin JN, MacRae C a. Cardiac sodium channel mutation in atrial fibrillation. *Heart Rhythm*. 2008;5(1):99–105. doi:10.1016/j.hrthm.2007.09.015.

74. Remme CA. Cardiac sodium channelopathy associated with *SCN5A* mutations: electrophysiological, molecular and genetic aspects. *J Physiol*. 2013. doi:10.1113/jphysiol.2013.256461.

75. Scheffer IE, Harkin LA, Grinton BE, et al. Temporal lobe epilepsy and GEFS+ phenotypes associated with *SCN1B* mutations. *Brain*. 2007;130(Pt 1):100–9. doi:10.1093/brain/awl272.

76. Nattel S. New ideas about atrial fibrillation 50 years on. *Nature*. 2002;415(6868):219–26. doi:10.1038/415219a.

77. Brackenbury WJ, Yuan Y, O'Malley HA, Parent JM, Isom LL. Abnormal neuronal patterning occurs during early postnatal brain development of *Scn1b*-null mice and precedes hyperexcitability. *Proc Natl Acad Sci U S A*. 2013;110(3):1089–94. doi:10.1073/pnas.1208767110.

78. Wong H-K, Sakurai T, Oyama F, et al. β Subunits of voltage-gated sodium channels are novel substrates of β-site amyloid precursor protein-cleaving enzyme (BACE1) and gamma-secretase. *J Biol Chem*. 2005;280(24):23009–17. doi:10.1074/jbc.M414648200.

79. Kim DY, Carey BW, Wang H, et al. BACE1 regulates voltage-gated sodium channels and neuronal activity. *Nat Cell Biol*. 2007;9(7):755–764. doi:http://www.nature.com/ncb/journal/v9/n7/suppinfo/ncb1602_S1.html.

80. Ishikawa T, Takahashi N, Ohno S, et al. Novel *SCN3B* Mutation Associated With Brugada Syndrome Affects Intracellular Trafficking and Function of $Na_v1.5$. *Circ J*. 2013;77(4):959–967. doi:10.1253/circj.CJ-12-0995.

81. Kurakami K, Ishii K. Is a Novel *SCN3B* Mutation Commonly Found in *SCN5A*-Negative Brugada Syndrome Patients? *Circ J*. 2013;77(4):900–901. doi:10.1253/circj.CJ-13-0242.

82. Marcus FI, Zareba W. The electrocardiogram in right ventricular cardiomyopathy/dysplasia. How can the electrocardiogram assist in understanding the pathologic and functional changes of the heart in this disease? *J Electrocardiol*. 42(2):136.e1–5. doi:10.1016/j.jelectrocard.2008.12.011.

83. Cox MGPJ, van der Zwaag PA, van der Werf C, et al. Arrhythmogenic right ventricular dysplasia/cardiomyopathy: pathogenic desmosome mutations in index-patients predict outcome of family screening: Dutch arrhythmogenic right ventricular dysplasia/cardiomyopathy genotype-phenotype follow-up study. *Circulation*. 2011;123(23):2690–700. doi:10.1161/CIRCULATIONAHA.110.988287.

84. Marcus FI, Zareba W, Calkins H, et al. Arrhythmogenic right ventricular cardiomyopathy/dysplasia clinical presentation and diagnostic evaluation: results from the North American Multidisciplinary Study. *Heart Rhythm*. 2009;6(7):984–92. doi:10.1016/j.hrthm.2009.03.013.

85. Namadurai S, Balasuriya D, Rajappa R, et al. Crystal Structure and Molecular Imaging of the Na_v Channel β3 Subunit Indicates a Trimeric Assembly. *J Biol Chem*. 2014. doi:10.1074/jbc.M113.527994.

86. McEwen DP, Chen C, Meadows LS, Lopez-Santiago L, Isom LL. The voltage-gated Na^+ channel β3 subunit does not mediate trans homophilic cell adhesion or associate with the cell adhesion molecule contactin. *Neurosci Lett*. 2009;462(3):272–275. doi:10.1016/j.neulet.2009.07.020.

87. Yereddi NR, Cusdin FS, Namadurai S, et al. The immunoglobulin domain of the sodium channel β3 subunit contains a surface-localized disulfide bond that is required for homophilic binding. *FASEB J*. 2013;27(2):568–80. doi:10.1096/fj.12-209445.

88. Wang DW, Yazawa K, George AL, Bennett PB. Characterization of human cardiac Na^+ channel mutations in the congenital long QT syndrome. *Proc Natl Acad Sci U S A*. 1996;93(23):13200–5. Available at: http://www.pubmedcentral.nih.gov/articlerender.fcgi?artid=24070&tool=pmcentrez&rendertype=abstract. Accessed February 21, 2014.

89. Yan GX, Wu Y, Liu T, Wang J, Marinchak RA, Kowey PR. Phase 2 early afterdepolarization as a trigger of polymorphic ventricular tachycardia in acquired long-QT syndrome : direct evidence from intracellular recordings in the intact left ventricular wall. *Circulation*. 2001;103(23):2851–6. Available at: http://www.ncbi.nlm.nih.gov/pubmed/11401944. Accessed February 15, 2014.

90. Trippel DL, Parsons MK, Gillette PC. Infants with long-QT syndrome and 2:1 atrioventricular block. *Am Heart J*. 1995;130(5):1130–4. Available at: http://www.ncbi.nlm.nih.gov/pubmed/7484750. Accessed February 21, 2014.

91. Gorgels AP, Al Fadley F, Zaman L, Kantoch MJ, Al Halees Z. The long QT syndrome with impaired atrioventricular conduction: a malignant variant in infants. *J Cardiovasc Electrophysiol*. 1998;9(11):1225–32. Available at: http://www.ncbi.nlm.nih.gov/pubmed/9835268. Accessed February 21, 2014.

92. Remme CA, Scicluna BP, Verkerk AO, et al. Genetically Determined Differences in Sodium Current Characteristics Modulate Conduction Disease Severity in Mice With Cardiac Sodium Channelopathy. *Circ Res*. 2009;104(11):1283–1292. doi:10.1161/circresaha.109.194423.

93. Gilchrist J, Das S, Van Petegem F, Bosmans F. Crystallographic insights into sodium-channel modulation by the β4 subunit. *Proc Natl Acad Sci U S A*. 2013;110(51):E5016–24. doi:10.1073/pnas.1314557110.

94. Møller DV, Andersen PS, Hedley P, et al. The role of sarcomere gene mutations in patients with idiopathic dilated cardiomyopathy. *Eur J Hum Genet*. 2009;17(10):1241–9. doi:10.1038/ejhg.2009.34.

95. An RH, Wang XL, Kerem B, et al. Novel LQT-3 Mutation Affects Na^+ Channel Activity Through Interactions Between - and 1-Subunits. *Circ Res*. 1998;83(2):141–146. doi:10.1161/01.RES.83.2.141.

96. Makita N, Shirai N, Wang DW, et al. Cardiac Na^+ Channel Dysfunction in Brugada Syndrome Is Aggravated by 1-Subunit. *Circulation*. 2000;101(1):54–60. doi:10.1161/01.CIR.101.1.54.

97. Mercier A, Clément R, Harnois T, et al. The β1-subunit of Na(v)1.5 cardiac sodium channel is required for a dominant negative effect through α-α interaction. *PLoS One*. 2012;7(11):e48690. doi:10.1371/journal.pone.0048690.

98. Du Y, Huang X, Wang T, et al. Downregulation of neuronal sodium channel subunits $Na_V1.1$ and $Na_V1.6$ in the sinoatrial node from volume-overloaded heart failure rat. *Pflugers Arch*. 2007;454(3):451–9. doi:10.1007/s00424-007-0216-4.

99. Maier SK, Westenbroek RE, Schenkman KA, Feigl EO, Scheuer T, Catterall WA. An unexpected role for brain-type sodium channels in coupling of cell surface depolarization to contraction in the heart. *Proc Natl Acad Sci U S A*. 2002;99(6):4073–4078. doi:10.1073/pnas.261705699.

100. Torres NS, Larbig R, Rock A, Goldhaber JI, Bridge JHB. Na^+ currents are required for efficient excitation-contraction coupling in rabbit ventricular myocytes: a possible contribution of neuronal Na^+ channels. *J Physiol*. 2010;588(Pt 21):4249–60. doi:10.1113/jphysiol.2010.194688.

101. Noujaim SF, Kaur K, Milstein M, et al. A null mutation of the neuronal sodium channel $Na_V1.6$ disrupts action potential propagation and excitation-contraction coupling in the mouse heart. *FASEB J*. 2012;26(1):63–72. doi:10.1096/fj.10-179770.

102. Aman TK, Grieco-Calub TM, Chen C, et al. Regulation of Persistent Na Current by Interactions between β Subunits of Voltage-Gated Na Channels. *J Neurosci*. 2009;29(7):2027–2042. doi:10.1523/jneurosci.4531-08.2009.

103. Lopez-Santiago LF, Brackenbury WJ, Chen C, Isom LL. Na^+ channel *Scn1b* gene regulates dorsal root ganglion nociceptor excitability in vivo. *J Biol Chem*. 2011;286(26):22913–23. doi:10.1074/jbc.M111.242370.

104. Chen C, Bharucha V, Chen Y, et al. Reduced sodium channel density, altered voltage dependence of inactivation, and increased susceptibility to seizures in mice lacking sodium channel β2-subunits. *Proc Natl Acad Sci U S A*. 2002;99(26):17072–17077. doi:10.1073/pnas.212638099.

105. Lopez-Santiago LF, Pertin M, Morisod X, et al. Sodium Channel β2 Subunits Regulate Tetrodotoxin-Sensitive Sodium Channels in Small Dorsal Root Ganglion Neurons and Modulate the Response to Pain. *J Neurosci*. 2006;26(30):7984–7994. doi:10.1523/jneurosci.2211-06.2006.

106. Chambers JC, Zhao J, Terracciano CMN, et al. Genetic variation in *SCN10A* influences cardiac conduction. *Nat Genet*. 2010;42(2):149–52. doi:10.1038/ng.516.

107. Zhao J, O'Leary ME, Chahine M. Regulation of $Na_v1.6$ and $Na_v1.8$ peripheral nerve Na^+ channels by auxiliary β-subunits. *J Neurophysiol*. 2011;106(2):608–19. doi:10.1152/jn.00107.2011.

108. Verkerk AO, Remme CA, Schumacher CA, et al. Functional $Na_v1.8$ channels in intracardiac neurons: the link between *SCN10A* and cardiac electrophysiology. *Circ Res*. 2012;111(3):333–43. doi:10.1161/CIRCRESAHA.112.274035.

109. Vijayaragavan K, Powell AJ, Kinghorn IJ, Chahine M. Role of auxiliary β1-, β2-, and β3-subunits and their interaction with $Na_V1.8$ voltage-gated sodium channel. *Biochem Biophys Res Commun*. 2004;319(2):531–40. doi:10.1016/j.bbrc.2004.05.026.

110. Marionneau C, Carrasquillo Y, Norris AJ, et al. The Sodium Channel Accessory Subunit Na_v β1 Regulates Neuronal Excitability through Modulation of Repolarizing Voltage-Gated K^+ Channels. *J Neurosci*. 2012;32(17):5716–5727. doi:10.1523/jneurosci.6450-11.2012.

111. Nerbonne JM, Kass RS. Molecular physiology of cardiac repolarization. *Physiol Rev*. 2005;85(4):1205–53. doi:10.1152/physrev.00002.2005.

112. Makielski JC, Limberis JT, Chang SY, Fan Z, Kyle JW. Coexpression of β1 with cardiac sodium channel alpha subunits in oocytes decreases lidocaine block. *Mol Pharmacol*. 1996;49(1):30–9. Available at: http://www.ncbi.nlm.nih.gov/pubmed/8569709. Accessed February 9, 2014.

113. Brugada R, Brugada J, Antzelevitch C, et al. Sodium channel blockers identify risk for sudden death in patients with ST-segment elevation and right bundle branch block but structurally normal hearts. *Circulation*. 2000;101(5):510–5. Available at: http://www.ncbi.nlm.nih.gov/pubmed/10662748. Accessed February 19, 2014.

114. Windle JR, Geletka RC, Moss AJ, Zareba W, Atkins DL. Normalization of ventricular repolarization with flecainide in long QT syndrome patients with *SCN5A*:DeltaKPQ mutation. *Ann Noninvasive Electrocardiol*. 2001;6(2):153–8. Available at: http://www.ncbi.nlm.nih.gov/pubmed/11333173. Accessed February 19, 2014.

115. Belhassen B, Glick A, Viskin S. Efficacy of quinidine in high-risk patients with Brugada syndrome. *Circulation*. 2004;110(13):1731–7. doi:10.1161/01.CIR.0000143159.30585.90.

116. Zipes DP, Camm a J, Borggrefe M, et al. *ACC/AHA/ESC 2006 Guidelines for Management of Patients With Ventricular Arrhythmias and the Prevention of Sudden Cardiac Death: a report of the American College of Cardiology/American Heart Association Task Force and the European Society of Cardiology Com*.; 2006. doi:10.1161/CIRCULATIONAHA.106.178233.

117. Stokoe KS, Balasubramaniam R, Goddard C a, Colledge WH, Grace A a, Huang CL-H. Effects of flecainide and quinidine on arrhythmogenic properties of *Scn5a*$^{+/-}$ murine hearts modelling the Brugada syndrome. *J Physiol*. 2007;581(Pt 1):255–75. doi:10.1113/jphysiol.2007.128785.

118. Hakim P, Thresher R, Grace AA, Huang CL-H. Effects of flecainide and quinidine on action potential and ventricular arrhythmogenic properties in Scn3b knockout mice. *Clin Exp Pharmacol Physiol*. 2010;37(8):782–9. doi:10.1111/j.1440-1681.2010.05369.x.

119. Uebachs M, Albus C, Opitz T, et al. Loss of β1 accessory Na^+ channel subunits causes failure of carbamazepine, but not of lacosamide, in blocking high-frequency firing via differential effects on persistent Na^+ currents. *Epilepsia*. 2012;53(11):1959–67. doi:10.1111/j.1528-1167.2012.03675.x.

120. Undrovinas AI, Belardinelli L, Undrovinas NA, Sabbah HN. Ranolazine improves abnormal repolarization and contraction in left ventricular myocytes of dogs with heart failure by inhibiting late sodium current. *J Cardiovasc Electrophysiol*. 2006;17 Suppl 1:S169–S177. doi:10.1111/j.1540-8167.2006.00401.x.

121. Mishra S, Undrovinas N a, Maltsev V a, Reznikov V, Sabbah HN, Undrovinas A. Post-transcriptional silencing of *SCN1B* and *SCN2B* genes modulates late sodium current in cardiac myocytes from normal dogs and dogs with chronic heart failure. *Am J Physiol Heart Circ Physiol*. 2011;301(4):H1596–605. doi:10.1152/ajpheart.00948.2009.

122. Viswanathan PC, Benson DW, Balser JR. A common *SCN5A* polymorphism modulates the biophysical effects of an *SCN5A* mutation. *J Clin Invest*. 2003;111(3):341–6. doi:10.1172/JCI16879.

123. Ye B, Valdivia CR, Ackerman MJ, Makielski JC. A common human *SCN5A* polymorphism modifies expression of an arrhythmia causing mutation. *Physiol Genomics*. 2003;12(3):187–93. doi:10.1152/physiolgenomics.00117.2002.

124. Schwartz PJ, Priori SG, Napolitano C. How really rare are rare diseases?: the intriguing case of independent compound mutations in the long QT syndrome. *J Cardiovasc Electrophysiol*. 2003;14(10):1120–1. Available at: http://www.ncbi.nlm.nih.gov/pubmed/14521668. Accessed February 21, 2014.

125. Killeen MJ, Thomas G, Sabir IN, Grace a a, Huang CL-H. Mouse models of human arrhythmia syndromes. *Acta Physiol (Oxf)*. 2008;192(4):455–69. doi:10.1111/j.1748-1716.2007.01822.x.

126. Olesen MS, Nielsen MW, Haunsø S, Svendsen JH. Atrial fibrillation: the role of common and rare genetic variants. *Eur J Hum Genet*. 2014;22(3):297–306. doi:10.1038/ejhg.2013.139.

127. Moretti A, Laugwitz K-L, Dorn T, Sinnecker D, Mummery C. Pluripotent stem cell models of human heart disease. *Cold Spring Harb Perspect Biol*. 2013;5(11). doi:10.1101/cshperspect.a014027.

128. Sarić T, Halbach M, Khalil M, Er F. Induced pluripotent stem cells as cardiac arrhythmic in vitro models and the impact for drug discovery. *Expert Opin Drug Discov*. 2014;9(1):55–76. doi:10.1517/17460441.2014.863275.

129. Bao Y, Isom LL. $Na_V1.5$ and Regulatory β Subunits in Cardiac Sodium Channelopathies. *Card Electrophysiol Clin*. 2014;6(4):679–694. doi:10.1016/j.ccep.2014.07.002.

130. Riuró H, Beltran-Alvarez P, Tarradas A, et al. A Missense Mutation in the Sodium Channel β2 Subunit Reveals *SCN2B* as a New Candidate Gene for Brugada Syndrome. *Hum Mutat*. 2013. doi:10.1002/humu.22328.

131. Maier SK, Westenbroek RE, McCormick KA, Curtis R, Scheuer T, Catterall WA. Distinct subcellular localization of different sodium channel alpha and β subunits in single ventricular myocytes from mouse heart. *Circulation*. 2004;109(11):1421–1427. doi:10.1161/01.CIR.0000121421.61896.24.

132. Bhargava A, Lin X, Novak P, et al. Super-resolution scanning patch clamp reveals clustering of functional ion channels in adult ventricular myocyte. *Circ Res*. 2013;112(8):1112–20. doi:10.1161/CIRCRESAHA.111.300445.

133. Bhargava A, Lin X, Novak P, et al. Super-resolution scanning patch clamp reveals clustering of functional ion channels in adult ventricular myocyte. *Circ Res*. 2013;112(8):1112–20. doi:10.1161/CIRCRESAHA.111.300445.

134. Wu J, Wu J, Zipes DP. Early afterdepolarizations, U waves, and torsades de pointes. *Circulation*. 2002;105(6):675–676. doi:10.1161/hc0602.104458.

135. Cerrone M, Noujaim SF, Tolkacheva EG, et al. Arrhythmogenic Mechanisms in a Mouse Model of Catecholaminergic Polymorphic Ventricular Tachycardia. *Circ Res*. 2007;101(10):1039–1048. doi:10.1161/circresaha.107.148064.

136. Antzelevitch C, Brugada P, Borggrefe M, et al. Brugada syndrome: report of the second consensus conference: endorsed by the Heart Rhythm Society and the European Heart Rhythm Association. *Circulation*. 2005;111(5):659–70. doi:10.1161/01.CIR.0000152479.54298.51.

137. Brugada P, Brugada J. Right bundle branch block, persistent ST segment elevation and sudden cardiac death: a distinct clinical and electrocardiographic syndrome. A multicenter report. *J Am Coll Cardiol*. 1992;20(6):1391–1396. doi:0735-1097(92)90253-J [pii].

138. Sarquella-Brugada G, Campuzano O, Arbelo E, Brugada J, Brugada R. Brugada syndrome: clinical and genetic findings. *Genet Med*. 2015;(April):1–10. doi:10.1038/gim.2015.35.

139. Zhang J, Sacher F, Hoffmayer K, et al. Cardiac Electrophysiologic Substrate Underlying the ECG Phenotype and Electrogram Abnormalities in Brugada Syndrome Patients. 2015. doi:10.1161/CIRCULATIONAHA.114.013698.

140. Chen Q, Kirsch GE, Zhang D, et al. Genetic basis and molecular mechanism for idiopathic ventricular fibrillation. *Nature*. 1998;392(6673):293–296. doi:10.1038/32675.

141. Postema PG, van Dessel PFHM, de Bakker JMT, et al. Slow and discontinuous conduction conspire in Brugada syndrome: a right ventricular mapping and stimulation study. *Circ Arrhythm Electrophysiol*. 2008;1(5):379–86. doi:10.1161/CIRCEP.108.790543.

142. Lambiase PD, Ahmed a. K, Ciaccio EJ, et al. High-density substrate mapping in brugada syndrome: Combined role of conduction and repolarization heterogeneities in arrhythmogenesis. *Circulation*. 2009;120(2):106–117. doi:10.1161/CIRCULATIONAHA.108.771401.

143. Nademanee K, Veerakul G, Chandanamattha P, et al. Prevention of ventricular fibrillation episodes in brugada syndrome by catheter ablation over the anterior right ventricular outflow tract epicardium. *Circulation*. 2011;123(12):1270–1279. doi:10.1161/CIRCULATIONAHA.110.972612.

144. Nagase S, Kusano KF, Morita H, et al. Epicardial electrogram of the right ventricular outflow tract in patients with the brugada syndrome. *J Am Coll Cardiol*. 2002;39(12):1992–1995. doi:10.1016/S0735-1097(02)01888-0.

145. Kurita T, Shimizu W, Inagaki M, et al. The electrophysiologic mechanism of ST-segment elevation in Brugada syndrome. *J Am Coll Cardiol*. 2002;40(2):330–334. doi:10.1016/S0735-1097(02)01964-2.

146. Nagase S, Kusano KF, Morita H, et al. Longer repolarization in the epicardium at the right ventricular outflow tract causes type 1 electrocardiogram in patients with Brugada syndrome. *J Am Coll Cardiol*. 2008;51(12):1154–61. doi:10.1016/j.jacc.2007.10.059.

147. Pitzalis MV, Anaclerio M, Iacoviello M, et al. QT-Interval Prolongation in Right Precordial Leads: An Additional Electrocardiographic Hallmark of Brugada Syndrome. *J Am Coll Cardiol*. 2003;42(9):1632–1637. doi:10.1016/j.jacc.2003.07.005.

148. Krishnan SC, Antzelevitch C. Flecainide-induced arrhythmia in canine ventricular epicardium. Phase 2 reentry? *Circulation*. 1993;87(2):562–572. doi:10.1161/01.CIR.87.2.562.

149. Krishnan SC, Antzelevitch C. Sodium channel block produces opposite electrophysiological effects in canine ventricular epicardium and endocardium. *Circ Res*. 1991;69(2):277–291. doi:10.1161/01.RES.69.2.277.

150. Nerbonne JM. Mouse models of arrhythmogenic cardiovascular disease: challenges and opportunities. *Curr Opin Pharmacol*. 2014;15C(Figure 1):107–114. doi:10.1016/j.coph.2014.02.003.

151. Martin C a, Zhang Y, Grace A a, Huang CL-H. Increased right ventricular repolarization gradients promote arrhythmogenesis in a murine model of Brugada syndrome. *J Cardiovasc Electrophysiol*. 2010;21(10):1153–9. doi:10.1111/j.1540-8167.2010.01767.x.

152. Milstein ML, Musa H, Balbuena DP, et al. Dynamic reciprocity of sodium and potassium channel expression in a macromolecular complex controls cardiac excitability and arrhythmia. *Proc Natl Acad Sci*. 2012. doi:10.1073/pnas.1109370109.

153. Haïssaguerre M, Extramiana F, Hocini M, et al. Mapping and ablation of ventricular fibrillation associated with long-QT and Brugada syndromes. *Circulation*. 2003;108(8):925–8. doi:10.1161/01.CIR.0000088781.99943.95.

154. Aiba T, Shimizu W, Hidaka I, et al. Cellular basis for trigger and maintenance of ventricular fibrillation in the Brugada syndrome model: high-resolution optical mapping study. *J Am Coll Cardiol*. 2006;47(10):2074–85. doi:10.1016/j.jacc.2005.12.064.

155. Morita H, Fukushima-Kusano K, Nagase S, et al. Site-specific arrhythmogenesis in patients with Brugada syndrome. *J Cardiovasc Electrophysiol*. 2003;14(4):373–379. doi:10.1046/j.1540-8167.2003.02365.x.

156. Kakishita M, Kurita T, Matsuo K, et al. Mode of onset of ventricular fibrillation in patients with Brugada syndrome detected by implantable cardioverter defibrillator therapy. *J Am Coll Cardiol*. 2000;36(5):1646–1653. doi:10.1016/S0735-1097(00)00932-3.

157. Nam GB, Ko KH, Kim J, et al. Mode of onset of ventricular fibrillation in patients with early repolarization pattern vs. Brugada syndrome. *Eur Heart J*. 2010;31(3):330–339. doi:10.1093/eurheartj/ehp423.

158. Morita H, Nagase S, Miura D, et al. Differential effects of cardiac sodium channel mutations on initiation of ventricular arrhythmias in patients with Brugada syndrome. *Hear Rhythm*. 2009;6(4):487–492. doi:10.1016/j.hrthm.2009.01.031.

159. Martin C a, Guzadhur L, Grace A a, Lei M, Huang CL-H. Mapping of reentrant spontaneous polymorphic ventricular tachycardia in a *Scn5a*$^{+/-}$ mouse model. *Am J Physiol Heart Circ Physiol*. 2011;300(5):H1853–62. doi:10.1152/ajpheart.00034.2011.

160. Dobrzynski H, Anderson RH, Atkinson A, et al. Structure, function and clinical relevance of the cardiac conduction system, including the atrioventricular ring and outflow tract tissues. *Pharmacol Ther*. 2013;139(2):260–288. doi:10.1016/j.pharmthera.2013.04.010.

161. Baruteau A-E, Probst V, Abriel H. Inherited progressive cardiac conduction disorders. *Curr Opin Cardiol*. 2014. doi:10.1097/HCO.0000000000000134.

162. Benson DW, Wang DW, Dyment M, et al. Congenital sick sinus syndrome caused by recessive mutations in the cardiac sodium channel gene (*SCN5A*). *J Clin Invest*. 2003;112(7):1019–28. doi:10.1172/JCI18062.

163. Monfredi O, Dobrzynski H, Mondal T, Boyett MR, Morris GM. The anatomy and physiology of the sinoatrial node--a contemporary review. *Pacing Clin Electrophysiol*. 2010;33(11):1392–406. doi:10.1111/j.1540-8159.2010.02838.x.

164. Zimmer T, Surber R. *SCN5A* channelopathies - An update on mutations and mechanisms. *Prog Biophys Mol Biol*. 2008;98(2-3):120–136. doi:10.1016/j.pbiomolbio.2008.10.005.

165. Probst V, Kyndt F, Potet F, et al. Haploinsufficiency in combination with aging causes *SCN5A*-linked hereditary lenègre disease. *J Am Coll Cardiol*. 2003;41(4):643–652. doi:10.1016/S0735-1097(02)02864-4.

166. Papadatos GA, Wallerstein PMR, Head CEG, et al. Slowed conduction and ventricular tachycardia after targeted disruption of the cardiac sodium channel gene *Scn5a*. *Proc Natl Acad Sci U S A*. 2002;99(9):6210–5. doi:10.1073/pnas.082121299.

167. Royer A, Van Veen T a B, Le Bouter S, et al. Mouse model of *SCN5A*-linked hereditary Lenègre's: Disease age-related conduction slowing and myocardial fibrosis. *Circulation*. 2005;111(14):1738–1746. doi:10.1161/01.CIR.0000160853.19867.61.

168. Van Veen T a B, Stein M, Royer A, et al. Impaired impulse propagation in *Scn5a*-knockout mice: Combined contribution of excitability, connexin expression, and tissue architecture in relation to aging. *Circulation*. 2005;112(13):1927–1935. doi:10.1161/CIRCULATIONAHA.105.539072.

169. O'Malley HA, Shreiner AB, Chen G-H, Huffnagle GB, Isom LL. Loss of Na^+ channel β2 subunits is neuroprotective in a mouse model of multiple sclerosis. *Mol Cell Neurosci*. 2009;40(2):143–155. doi:10.1016/j.mcn.2008.10.001.

170. Friberg L, Bergfeldt L. Atrial fibrillation prevalence revisited. *J Intern Med*. 2013;274(5):461–468. doi:10.1111/joim.12114.

171. Hong K, Xiong Q. Genetic basis of atrial fibrillation. *Curr Opin Cardiol*. 2014. doi:10.1097/HCO.0000000000000051.

172. Savio-Galimberti E, Darbar D. Atrial Fibrillation and *SCN5A* Variants. *Card Electrophysiol Clin*. 2014;6(4):741–748. doi:10.1016/j.ccep.2014.07.006.

173. Amin A, Asghari-Roodsari A, Tan H. Cardiac sodium channelopathies. *Pflügers Arch Eur J Physiol*. 2010;460(2):223–237. doi:10.1007/s00424-009-0761-0.

174. Van Veen T a B, Stein M, Royer A, et al. Impaired impulse propagation in *Scn5a*-knockout mice: Combined contribution of excitability, connexin expression, and tissue architecture in relation to aging. *Circulation*. 2005;112:1927–1935. doi:10.1161/CIRCULATIONAHA.105.539072.

175. Royer A, Van Veen T a B, Le Bouter S, et al. Mouse model of SCN5A-linked hereditary Lenègre's: Disease age-related conduction slowing and myocardial fibrosis. *Circulation*. 2005;111:1738–1746. doi:10.1161/01.CIR.0000160853.19867.61.

176. Hao X, Zhang Y, Zhang X, et al. TGF-β1-mediated fibrosis and ion channel remodeling are key mechanisms in producing the sinus node dysfunction associated with *SCN5A* deficiency and aging. *Circ Arrhythmia Electrophysiol*. 2011;4(3):397–406. doi:10.1161/CIRCEP.110.960807.

177. Andrade J, Khairy P, Dobrev D, Nattel S. The Clinical Profile and Pathophysiology of Atrial Fibrillation: Relationships Among Clinical Features, Epidemiology, and Mechanisms. *Circ Res*. 2014;114(9):1453–1468. doi:10.1161/CIRCRESAHA.114.303211.

178. Rodríguez-Mañero M, Namdar M, Sarkozy A, et al. Prevalence, clinical characteristics and management of atrial fibrillation in patients with Brugada syndrome. *Am J Cardiol*. 2013;111(3):362–7. doi:10.1016/j.amjcard.2012.10.012.

179. Bigi MAB, Aslani A, Shahrzad S. Clinical predictors of atrial fibrillation in Brugada syndrome. *Europace*. 2007;9(10):947–950. doi:10.1093/europace/eum110.

180. Morita H, Kusano-Fukushima K, Nagase S, et al. Atrial fibrillation and atrial vulnerability in patients with Brugada syndrome. *J Am Coll Cardiol*. 2002;40(8):1437–1444. doi:10.1016/S0735-1097(02)02167-8.

181. Toh N, Morita H, Nagase S, et al. Atrial electrophysiological and structural remodeling in high-risk patients with Brugada syndrome: Assessment with electrophysiology and echocardiography. *Hear Rhythm*. 2010;7(2):218–224. doi:10.1016/j.hrthm.2009.10.035.

182. Kusano KF, Taniyama M, Nakamura K, et al. Atrial fibrillation in patients with Brugada syndrome relationships of gene mutation, electrophysiology, and clinical backgrounds. *J Am Coll Cardiol*. 2008;51(12):1169–75. doi:10.1016/j.jacc.2007.10.060.

183. Amin AS, Boink GJJ, Atrafi F, et al. Facilitatory and inhibitory effects of *SCN5A* mutations on atrial fibrillation in Brugada syndrome. *Europace*. 2011;13(7):968–975. doi:10.1093/europace/eur011.

184. Verheule S, Sato T, Everett T, et al. Increased vulnerability to atrial fibrillation in transgenic mice with selective atrial fibrosis caused by overexpression of TGF-β1. *Circ Res*. 2004;94(11):1458–65. doi:10.1161/01.RES.0000129579.59664.9d.

185. Elliott P, Andersson B, Arbustini E, et al. Classification of the cardiomyopathies: a position statement from the european society of cardiology working group on myocardial and pericardial diseases. *Eur Heart J*. 2007;29(2):270–276. doi:10.1093/eurheartj/ehm342.

186. Aldhoon B, Melenovský V, Peichl P, Kautzner J. New insights into mechanisms of atrial fibrillation. *Physiol Res*. 2010;59(1):1–12. doi:1651 [pii].

187. Nattel S, Harada M. Atrial remodeling and atrial fibrillation: Recent advances and translational perspectives. *J Am Coll Cardiol*. 2014;63(22):2335–2345. doi:10.1016/j.jacc.2014.02.555.

188. Jalife J. Novel Upstream Approaches to Prevent Atrial Fibrillation Perpetuation. *Cardiol Clin*. 2014;32(4):637–650. doi:10.1016/j.ccl.2014.07.004.

189. Shen MJ, Zipes DP. Role of the autonomic nervous system in modulating cardiac arrhythmias. *Circ Res*. 2014;114(6):1004–21. doi:10.1161/CIRCRESAHA.113.302549.

190. Boukens BJ, Hoogendijk MG, Verkerk AO, et al. Early repolarization in mice causes overestimation of ventricular activation time by the QRS duration. *Cardiovasc Res*. 2013;97(1):182–91. doi:10.1093/cvr/cvs299.

191. Terentyev D, Rees CM, Li W, et al. *Hyperphosphorylation of RyRs Underlies Triggered Activity in Transgenic Rabbit Model of LQT2 Syndrome.*; 2014. doi:10.1161/CIRCRESAHA.115.305146.

192. Park DS, Cerrone M, Morley G, et al. Genetically engineered *SCN5A* mutant pig hearts exhibit conduction defects and arrhythmias. 2015;125(1):403–412. doi:10.1172/JCI76919DS1.

193. Priori SG, Wilde A a, Horie M, et al. Executive summary: HRS/EHRA/APHRS expert consensus statement on the diagnosis and

management of patients with inherited primary arrhythmia syndromes. *Europace*. 2013;15(10):1389–406. doi:10.1093/europace/eut272.

194. Pinsk V, Levy J, Moser A, Yerushalmi B, Kapelushnik J. Original Articles. *Children*. 2008;10(May):335–338. doi:10.1080/1366271032000141652.

195. Sacher F, Probst V, Iesaka Y, et al. Outcome After Implantation of a Cardioverter-Defibrillator in Patients With Brugada Syndrome: A Multicenter Study. *Circulation*. 2006;114(22):2317–2324. doi:10.1161/CIRCULATIONAHA.106.628537.

196. Sarkozy A, Boussy T, Kourgiannides G, et al. Long-term follow-up of primary prophylactic implantable cardioverter-defibrillator therapy in Brugada syndrome. *Eur Heart J*. 2007;28(3):334–344. doi:10.1093/eurheartj/ehl450.

197. Bordachar P, Reuter S, Garrigue S, et al. Incidence, clinical implications and prognosis of atrial arrhythmias in Brugada syndrome. *Eur Heart J*. 2004;25(10):879–884. doi:10.1016/j.ehj.2004.01.004.

198. Sears SF, Todaro JF, Lewis TS, Sotile W, Conti JB. Examining the Psychosocial Impact of Implantable Cardioverter Defibrillators : A Literature Review. *Clin Cardiol*. 1999;22:481–489.

199. Denegri M, Bongianino R, Lodola F, et al. Single Delivery of an Adeno-Associated Viral Construct to Transfer the CASQ2 Gene to Knock-In Mice Affected by Catecholaminergic Polymorphic Ventricular Tachycardia Is Able to Cure the Disease From Birth to Advanced Age. *Circulation*. 2014;129(25):2673–81. doi:10.1161/CIRCULATIONAHA.113.006901.

200. Auerbach DS, Jones J, Clawson BC, et al. Altered cardiac electrophysiology and SUDEP in a model of Dravet syndrome. *PLoS One*. 2013;8(10):e77843. doi:10.1371/journal.pone.0077843.

201. Sarmast F, Kolli A, Zaitsev A, et al. Cholinergic atrial fibrillation: IK,ACh gradients determine unequal left/right atrial frequencies and rotor dynamics. *Cardiovasc Res*. 2003;59(4):863–873. doi:10.1016/S0008-6363(03)00540-6.